# A STUDY ON ADHESION OF ADHESIVE RESIN TO DENTAL ALLOYS

（歯科用合金と接着性注入高分子材料との接着に関する研究）

March 2005

[illegible]

A Dissertation

Submitted to the Yokohama National University

Graduate School of Engineering

# A STUDY ON ADHESION OF ADHESIVE RESIN TO DENTAL ALLOYS

March 2006

Health Sciences University of Hokkaido
School of Dentistry
Department of Dental Materials Science

HIROKI OHNO

CONTENTS

# Chapter 1

# INTRODUCTION

# INTRODUCTION

Adhesion techniques are widely utilized in aircraft, automobiles, rolling stock, electrical appliances, architecture, and so on. However, the adhesion techniques used in dentistry are less developed than those used in industry, though there has considerable progress over the past 25 years.

There are many factors that hinder the development of adhesion techniques in dentistry:

(1) A wide variety of dental materials are used as adherend, including metals, polymers, and ceramics.

(2) Teeth are composed of a mixture of inorganic (hydroxyapatite) and organic (e.g., collagen) compounds including water.

(3) Adhesive structures must function in environments with oral fluids such as saliva at 37℃ or foods and drinks from 0°C to 70°C.

(4) Cyclic stress is imposed on adhesive structures by mastication loads.

(5) The acidity of oral fluids varies widely (pH 3-11) in foods and drinks.

(6) Adhesives must be handled in the narrow confines of the oral cavity, which is a humid environment.

(7) Adhesives must be non-toxic and non-irritant, have no carcinogenic or allergic potential, and have no harmful effects on the human body.

Although many efforts had been made to use industrial adhesives such as epoxy resins and cyanoacrylate as dental adhesives, adequate adhesion was not achieved under the extreme conditions of the oral cavity. Much effort has been expended to achieve adhesion between artificial compounds and tooth substances. In 1978, Nakabayashi et al. [1] synthesized a new dental adhesive that meets the requirements stated above. The dental adhesive contained 4-methacryloxyethyl trimellitate anhydride (4-META) as an adhesive monomer with methylmethacrylate (MMA). In 1983, Omura[2] synthesized an adhesive containing a dimethacrylate monomer (Bis-GMA) and phosphate monomers.

4-META is an ethyl anhydride of trimellitate acid and hydroxyethyl methacrylate and has both hydrophilic and hydrophobic groups as shown in Fig. 1-1. In the 4-META adhesive, tributyl borane (TBB) is used as the initiator for polymerization of MMA. TBB reacts with oxygen in air, resulting in the formation of peroxide, which is decomposed to free radicals. MMA containing TBB can also be polymerized by water that may be present. This characteristic is different from benzoyl peroxide (BPO) and the tri-amine polymerization system of MMA.

One of the main problems in dental adhesion techniques is that bonds between adhesives and metals that are strong in a dry environment weaken in a wet environment. For example, there are clinical reports of dental adhesion bridges breaking off from teeth after extended use, and this has led to a loss of confidence in dental adhesion techniques. Hence, a major problem awaiting solution in dentistry is the durability of bonding joints exposed to water.

In the present study, adhesion of 4-META/MMA-TBB adhesive resin (Super-Bond C&B, Sun Medical Co. Ltd., Kyoto, Japan; called 4-META resin) to the dental base metal alloys and precious metal alloys listed in Table 1-1 was investigated in relation to the surface structures of the alloys. The surface

structures of the alloys were mainly analyzed by electron spectroscopy for chemical analysis (ESCA). In chapter 2, the bonding ability of 4-META resin to base metal alloys (Co-Cr and Ni-Cr) covered with passive films and oxide layers formed by high-temperature oxidation is discussed. Resin-passive surface bonds were stronger than resin-oxidized surface bonds. Excellent adhesion to Ni-Cr alloys, comparable to the adhesion to Co-Cr alloys, was obtained by treating the as-polished surface with concentrated $HNO_3$ solution. The relationship between the adhesive ability and alloy surface structure was investigated by ESCA. The presence of adsorbed water several molecules thick between the surface oxidized at high temperature and the 4-META side chain was thought to be the reason why adhesion to the oxidized surface was inferior to adhesion to an as-polished surface. This speculation was supported by the results of an experiment demonstrating excellent bonding ability after removal of the adsorbed water on the oxidized surface. Adhesion of 4-META resin to a cleaned metal surface obtained by hydrogen gas reduction was also investigated to understand the roles of the adsorbed water layer, the oxides, and the passive film on the adherend metal surface.

In chapter 3, the mechanisms of destruction of metal-resin adhesion due to water are discussed from the viewpoint of the surface structures of alloys. The water content at the adhesion interface was calculated from the solution to Fick's second equation to discuss the degradation at the interface with respect to the water content. Water durability at the adhesion interface was investigated by separating tests of resin film using liquid nitrogen. Thermal stress induced by thermal shock was calculated by the three-dimensional finite element method. The relationship between degradation and the water concentration at the adhesion interface is discussed. The mechanism of degradation due to water molecules penetrating at the adhesion interface is discussed with changes in the interface structure on the metal side.

Adhesive resin bonding to dental precious metal alloys is inferior to that to dental base metal alloys such as Co-Cr alloy, Ni-Cr alloy, and stainless steel. Several methods for surface modification of precious metal alloys have been developed. However, these methods have a number of drawbacks. A new method (Ga-Sn modification) for promoting adhesion between precious metal alloys and 4-META resin was developed and it is described in chapter 4. Gold-based and silver-based alloys modified by a Ga-Sn liquid alloy showed not only high bond strengths but also excellent water durability at the adhesion interface. The surfaces of the alloys modified by the new method were analyzed by ESCA to determine the effect of the modification.

The adhesion procedures would be simplified if dental adhesive resins could bond strongly to dental precious metal alloys without surface modification. In the study described in chapter 5, base metals were added to a dental precious metal alloy in an attempt to develop alloys that adhere strongly to dental adhesive resins without surface modification. The idea for the present study was derived from the experimental finding that 4-META resin bonds strongly to dental precious metal alloys modified by Ga-Sn alloy and to silver-based alloys (Ag-In-Sn and Ag-Sn-Zn). As the oxides on the alloy surface play a very important role in the adhesion with 4-META, it was assumed that alloying base metals such as Sn, In and Zn to precious metal alloys could improve the adhesive ability of the dental precious metal alloys without

surface modification. New dental precious metal alloys for resin bonding without alloy surface modification were developed by adding base metals (In, Zn or Sn). The alloy surfaces were analyzed by ESCA and the results of analysis showed that oxides such as $In_2O_3$, ZnO, and SnO played an important role in improving the adhesive ability of the alloys.

For dental precious metal alloys containing Cu, external and internal oxidation zones composed of Cu oxides were formed on the surface when the alloy was heated at a high temperature in air. A sponge-like structure was formed on the alloy surface after removal of the internal oxidation particles with an acid solution. The bonding strength of 4-META resin to the porous alloy surface is discussed in chapter 6. It was found that high bonding strength was obtained when 4-META resin was bonded to a porous 14K gold alloy surface treated with a thiophosphate-type metal primer.

## REFERENCES

1) Takeyama M, Kashibuti S, Nakabayashi N, Masuhara E: Studies on dental self-curing resins (17) - Adhesion of PMMA with bovine enamel or dental alloys -. *J Jpn Soc Dent Appar Mat*, **19**: 179-185, 1978.

2) Omura I, Yamauchi J, Nagase Y, Uemura F: *Jpn Published Unexamined Patent Application*, 58-21607, 1983.

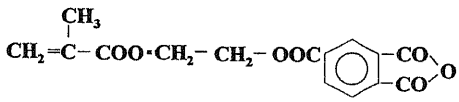

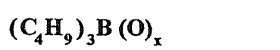

Fig. 1-1 4-methacryloxyethyl trimellitate anhydride (4-META) and tri-butyl borane (TBB).

Table 1-1 Compositions of dental alloys.

| | Au | Pt | Pd | Ag | Cu | Zn | Sn | In | Cr | Ni | Co | Fe | other |
|---|---|---|---|---|---|---|---|---|---|---|---|---|---|
| Type IV* | 70 | 3 | 3 | 10 | 14 | - | - | - | - | - | - | - | - |
| 14 K† | 58.33 | - | 3 | 13.7 | 23.97 | 1 | - | - | - | - | - | - | - |
| Ag-Pd‡ | 12 | - | 20 | 55 | 10 | - | - | - | - | - | - | - | 3 |
| Ag-Cu§ | - | - | - | 70 | 27 | - | - | - | - | - | - | - | 3 |
| Ag-Sn‖ | - | - | - | 65 | - | 13 | 22 | - | - | - | - | - | - |
| Ag-In¶ | - | - | 1 | 68 | - | 6 | - | 24 | - | - | - | - | 1 |
| SUS | - | - | - | - | - | - | - | - | 18 | 8 | - | 65 | 9 |
| Co-Cr | - | - | - | - | - | - | - | - | 23 | 5 | 57 | - | 15 |
| Ni-Cr** | - | - | - | - | - | - | - | - | 15 | 59 | 15 | - | 11 |

*Casting Gold IV M.S, GC, Tokyo, Japan; †K.14 M.C. Gold Alloy, GC, Tokyo, Japan; ‡New Palla Gold, Tokuriki, Tokyo, Japan; §Yatagin, Yata, Osaka, Japan; ‖Miro Silver, GC, Tokyo, Japan; ¶Salivan, Nippon, Shiken, Tokyo, Japan; **Suncolium, Sankin, Osaka, Japan; *Sunilium, Sankin, Osaka, Japan.

# Chapter 2

# RELATIONSHIP OF BONDING STRENGTH AND ALLOY SURFACE STRUCTURE

## 2.1 Adhesion of 4-META Adhesive Resin to Base Metal Alloys (Co-Cr and Ni-Cr)

### 2.1-1 Introduction

There are numerous studies that have been made on the adhesion to dental alloys; pioneering work by Tanaka on Ni-Cr alloys[1-3] and gold alloys[4]; studies on Ni-Cr alloys[5-9], Co-Cr alloys[5, 9-16], and precious metal alloys[8, 9, 17-22]. There are several surface pre-treatment methods for Ni-Cr alloys: immersion in concentrated $HNO_3$ solution after etching with HCl[3]; immersion in solutions containing an oxidizing agent after sand-blasting[5, 7]; etching and passivating by an electrochemical method[6]; and spraying of molten metal on the alloy surface[7]. These methods increase bond strength by increasing the mechanical retention and chemical affinity between the adhesive and alloys. However, it is necessary to distinguish the contribution of these two effects, mechanical and chemical, to evaluate how the alloy surface structure improves the resin adhesion.

The present study reports the adherence of the 4-META resin to the alloy with three different surface conditions, as-polished, concentrated $HNO_3$ treated, and oxidized at high temperatures to evaluate the bonding strength without mechanical retention.

The bonding strength of the 4-META resin to the base metal alloys was measured by a tensile test after the bonded specimens had been subjected to thermal stress by the thermal cycle method using liquid nitrogen. The evaluation of the adhesive ability was made on the basis of the bonding strength and observation of fracture appearances.

### 2.1-2 Materials and Methods

A 70 mass%Co-Cr alloy and a 70 mass%Ni-30%Cr alloy were used. The alloys were prepared by melting pure metals of purity better than 99.99% in an alumina Tammann tube under an argon atmosphere using a high frequency induction furnace. The alloys were cut into small chips and the chips were soldered to an 18-8 stainless steel rod as shown in Fig. 2.1-1.

The Co-Cr alloy specimens were polished metallographically to eliminate mechanical factors affecting the bonding strength and the specimens were subjected three surface treatments: polished, oxidized for 5 min in air at 300°C, and 500°C. There were three different surface states for the Ni-Cr alloy: as-polished, concentrated $HNO_3$ treated, and oxidized for 5 min at 300°C in air. The concentrated $HNO_3$ treated surface was obtained by immersing the specimen for 15 min in concentrated $HNO_3$ solution at room temperature. The specimens were stored in a desiccator with silica gel before the adhesion experiments.

The alloy specimen and a 5 mm$^{\phi}$ 18-8 stainless steel block were attached with the 4-META resin for tensile tests to measure the bonding strength as shown in Fig. 2.1-1. Figure 2.1-2 shows the adhesion apparatus with a micrometer, which was used for two purposes: to attach the stainless steel rod vertically to the stainless steel disk surface and to maintain a constant 50-μm thick resin layer. The effect of the excess resin at the point of adhesion on the bonding strength can be eliminated by Scotch Tape on the stainless steel disk.

The tensile test for the bonding strength measurements was carried out after keeping the specimens at room temperature for 24 hr after the adhesion treatment. The test was performed on a testing machine with a cross head speed of 2 mm/min, after inserting a U shaped piece in the groove of the stainless steel rod (Fig. 2.1-1) and placing the test piece in the jig of the tensile test shown in Fig. 2.1-3. Before testing, the specimen was subjected to 20 thermal cycles from liquid nitrogen (-196°C) to water (40°C) alternately for 1 min each. The fractured area was observed by a profile projector after the test.

### 2.1-3 Results

*Failure Types and Bonding Strength of Co-Cr Alloy*

Figures 2.1-4, 2.1-5, and 2.1-6 are the measured bonding strengths for the tensile test obtained from three surface states of Co-Cr alloy, the as-polished surface, and the surfaces oxidized for 5 min in air at 300°C and 500°C, respectively. The values in the left and right halves of each figure are the bonding strengths without (no-thermal cycle) and with the thermal cycles. The horizontal lines in the figures indicate the average of the repeated values. The fracture appearance was classified as shown in Table 2.1-1: Type I is a failure in the resin (cohesive failure); Type II is partly a cohesive failure and partly an interface failure at the alloy surface; Type III is a cohesive failure and interface failure at the periphery of the adhesion to the alloy surface; Type IV is a mixture of Types II and III and Type V is total interface failure.

The bonding strength for the as-polished surface (Fig. 2.1-4) is similar for both the no-thermal and thermal cycle specimens. Without the thermal cycles, the specimens show only Type I failure, while with the thermal cycles there are 5 Type III failures in addition to the Type I failure. On oxidized specimens at 300°C and 500°C, the bonding strengths without thermal cycles were similar to the specimens with as-polished surfaces and all the failures were of Type I except for a few cases of Type II and III failures. After the thermal cycle treatment, the bonding strength decreased significantly, there was a wide scattering of values, and all failures were of Type III.

Figure 2.1-7 shows the relationship between the bonding strength, $y$, and the area fraction, $x$, of interface failures at the periphery obtained from specimens subjected to the thermal cycles in Fig. 2.1-6. It is represented by equation (2.1-1):

$$y = -6x + 43.5 \text{ ---------- } (2.1\text{-}1)$$

*Failure Types and Bonding Strength of Ni-Cr Alloy*

Figure 2.1-8 is the bonding strength obtained from the Ni-Cr alloy specimens with as polished surfaces. Without the thermal cycles, the average bonding strength was 38.2 MPa and the observed failures are of Types I and II, while with the thermal cycles the specimens showed interface failure at the periphery (Types III and IV) with lower average bond strengths, 32.2 MPa. Figure 2.1-9 shows the bonding strength and failure types obtained from the Ni-Cr alloy specimens with surfaces treated by concentrated $HNO_3$ solution. The bonding strengths with and without the thermal cycles were 38.1 MPa and 40.2 MPa, here

were no statistically significant differences. Adhesive ability was excellent because the strength did not decrease with the thermal cycles and all failures are Type I. Figure 2.1-10 shows the results obtained from the Ni-Cr alloy specimens oxidized at 300°C. Without thermal cycles, the bonding strength was 33.8 MPa that was lower than as-polished and failures were of Type II in 12 of 18 tests. Further, after the thermal cycle treatment the strength decreased to 24.7 MPa and failures were of Type III and IV.

### 2.1-4 Discussion

*Adhesive Ability of 4-META Resin to Co-Cr Alloy*

The main factor affected on the bonding strength is not the strength of the covalent bond of PMMA but inter-molecular forces (hydrogen bonds and Van der Waals forces)[23]. However, when failure occurs in the resin, the bonding strength is not the full inter-molecular force of PMMA. There is factors[24] in the adhesive resin layer which reduce the bonding strength below the total intermolecular force of the resin. These include air bubbles, variation in the monomer-polymer ratio, impurities, and low molecular weight components. These factors are considered to cause the wide scattering in bond strength values for the Type I failure in Figs. 2.1-4 - 2.1-6.

In the adhesion tests, the different surface states were clearly shown by the thermal cycles. Without the thermal cycles there were no differences between the as-polished and oxidized surfaces. For the oxidized surfaces subjected to thermal cycles, interface failure occurred at the periphery of the adhesion (Type III), and bonding strength decreased with increasing area fraction of the interface failure as shown in Fig. 2.1-7. Even with the thermal cycles, the as-polished samples displayed no changes in bonding strength, showing that the as-polished surfaces were superior for adhesion.

In a butt joint as in the present study, thermal stress generated in an adhesive is considered to be a function of both diameter and thickness of the adhesive layer with the large stress at the periphery and zero at the center of adhesion[25]. Cracks at the resin/alloy interface propagate from the periphery to a point where the thermal stress balances with the adhesive force, resulting a Type III failure.

*Adhesive Ability of 4-META Resin to Ni-Cr Alloy*

In the case without thermal cycles, the as polished and $HNO_3$ treated specimens did not show clearly different bonding strengths, as shown in Figs. 2.1-8 and 2.1-9. Differences of surface states, however, appeared in the failure types because the failure type for the as-polished surface was Types I and II and only Type I for the concentrated $HNO_3$ treated surface. Further, the failure types clearly showed that the adhesive ability for the $HNO_3$ treated surface was superior to that for both the as-polished and oxidized surfaces. Observation of failure types is important to evaluate the adhesive ability because fracture types rather than the bonding strength sensitively reflects the state of the alloy surface.

*Comparisons between Adhesive Ability to Co-Cr and Ni-Cr Alloys*

Without the thermal cycles, there were only Type I failure in the Co-Cr alloy (Fig. 2.1-4) and both

Types I and II in the Ni-Cr alloy (Fig. 2.1-8). The appearance of Type II failures showed that the alloy surface of the Ni-Cr alloy was inferior to the Co-Cr alloy for resin adhesion. Differences in the alloy surface states were clearly shown by the failure types after the thermal cycles although the bonding strength was nearly equal. There are several reports on adhesion of 4-META resin to Co-Cr alloys showing two different results: one report that Ni-Cr alloys are superior to the Co-Cr alloy[5] and others report the opposite[17]. The present study, which examined only chemical and not mechanical factors in the adhesion, showed that the Co-Cr alloy was superior to the Ni-Cr alloy. The failure types and bonding strength indicated that the adhesive ability was lowered by oxidizing the Co-Cr and Ni-Cr alloys.

### 2.1-5 Conclusions

The adhesion of 4-META resin to Co-Cr and Ni-Cr alloys was examined by a tensile test with and without thermally induced stress. The resin bond to the as-polished surface of Co-Cr and Ni-Cr alloys is stronger than that to the oxidized surfaces. The thermal cycles caused clear differences in the surface states that affected the adhesion. The adhesive ability of 4-META resin to Ni-Cr alloy improved remarkably when the alloy surface was treated by concentrated $HNO_3$ solution. Adhesion to the alloy surfaces treated by concentrated $HNO_3$ was excellent, comparable with as-polished Co-Cr alloy, and was resistant to protects against thermal cycling using liquid nitrogen. The bonding strength of the 4-META resin to the Co-Cr and Ni-Cr alloys will be discussed on measured bonding strengths and details of the alloy surface structure in the next section.

## REFERENCES

1) Tanaka T, Nagata K, Nakabayashi N, Masuhara E: Application of 4-META on adhesive opaque resin (Part 1) Adhesive strength and the stability. *J Jpn Soc Dent Apparat Mater*, **20**: 79-84, 1979 (in Japanese).

2) Tanaka T, Nagata K, Nakabayashi N, Masuhara E: Application of 4-META on adhesive opaque resin (Part 2) Improvement of adhesive stability. *J Jpn Soc Dent Apparat Mater*, **20**: 221-227, 1979 (in Japanese).

3) Tanaka T, Nagata K, Takeyama M, Atsuta M, Nakabayashi N, Masuhara E: 4-META opaque resin - A new resin strongly adhesive to nickel-chromium alloy -. *J Dent Res*, **60**: 1697-1707, 1981.

4) Tanaka T, Nagata K, Takeyama M, Nakabayashi N, Masuhara E: Heat treatment of gold alloy to get adhesion with resin. *J Jpn Soc Dent Apparat Mat*, **21**: 95-102, 1980 (in Japanese).

5) Yamashita A, Yamami T: Procedures for applying adhesive resin (MMA-TBB) to crown and bridge restorations (Part 1) The influence of dental non-precious alloys and the treatment of inner surface of metal to adhesion. *J Jpn Prosthodont Dent*, **26**: 130-137, 1982 (in Japanese).

6) Yamashita A, Yamami T, Ishii M, Yamaguchi T, Uramoto T: Procedures for applying adhesive resin (MMA-TBB) to crown and bridge restorations (Part 3) The Ni-Cr alloys for adhesive resin and its adhesive strength and durability. *J Jpn Prosthodont Dent*, **26**: 22-31, 1982 (in Japanese).

7) Shinohara N, Tojinbara O, Akita H, Kakiuchi T, Jimi T: Studies on the adhesive strength between adhesive resin and each metal surface treated by wire explosion spray (Part 2) Adhesive shear strength between Ni-Cr alloy surface treated by wire explosion spray and adhesive resin (Super Bond C and B). *J Jpn Prosthodont Dent*, **28**: 165-169, 1984 (in Japanese).

8) Matsumura H: Adhesion of dental alloys, (Part 1) Effect of monomers with an acid anhydride group. *J J Dent Mater*, **4**: 421-429, 1985 (in Japanese).

9) Matsumura H: Adhesion of dental alloys (Part 2) Effect of monomers with an acid anhydride or a carboxylic group. *J J Dent Mater*, **5**: 65-70, 1986 (in Japanese).

10) Mogi T: Studies on adhesion of methacrylic resin to cobalt-chromium alloy for denture base - Effect of 4-methacryloxyethyl trimellitate anhydride monomer -. *J Jpn Prosthodont Dent*, **23**: 76-92, 1979 (in Japanese).

11) Yasuda N, Sasaki M, Mogi T, Matumoto M, Ai M: Interface between metal and resin on the finishing line of cobalt-chromium denture (Part 1) Effect of finishing line structure on the degree of dye penetration. *J Jpn Prosthodont Dent*, **22**: 15-18, 1978 (in Japanese).

12) Yasuda N, Sasaki M, Mogi T, Ai M, Nakabayashi N: Interface between metal and resin on the finishing line of cobalt-chromium denture (Part 2) Effect of 4-META on preventing dye penetration at the finishing line. *J Jpn Prosthodont Dent*, **22**: 19-25, 1978 (in Japanese).

13) Sasaki M, Yasuda N, Mogi T, Ai M: Interface between metal and resin on the finishing line of cobalt-chromium denture (Part 3) Studies on finishing line structure. *J Jpn Prosthodont Dent*, **23**: 162-166, 1979 (in Japanese).

14) Yasuda N, Sasaki M, Mogi T, Ai M: Interface between metal and resin on the finishing line of cobalt-chromium denture (Part 4) A clinical survey of cobalt-chromium dentures by 4-META coating system. *J Jpn Prosthodont Dent*, **23**: 167-172, 1979 (in Japanese).

15) Sasaki K, Yasuda N, Mogi T, Ai M: Interface between metal and resin on the finishing line of cobalt-chromium denture (Part 5) Changes of bonding strength caused by using adhesive resin. *J Jpn Prosthodont Dent*, **24**: 7-10, 1980 (in Japanese).

16) Yasuda N, Sasaki M, Ai M: Interface between metal and resin on the finishing line of cobalt-chromium denture (Part 6) A clinical survey of cobalt-chromium dentures by 4-META dough system. *J Jpn Prosthodont Dent*, **26**: 1-5, 1982 (in Japanese).

17) Takagi A, Fujiyama E, Shimizu H, Tanaka T, Atsuta M: Study on bond strength between adhesive resin and Au-Ag-Pd alloy. *J Jpn Prosthodont Dent*, **28**: 9-14, 1984 (in Japanese).

18) Yamashita A, Kondo Y, Fujita M: Adhesive strength of adhesive resin PANAVIA EX to dental alloys (Part 2) Adhesive strength of precious alloys. *J Jpn Prosthodont Dent*, **28**: 43-53, 1984 (in Japanese).

19) Etchu Y, Nakamura K, Ozonoe Y, Noguchi H: On oxidation treatment of alloy adherends for adhesion of dental cements. *J J Dent Mater*, **4**: 692-700, 1985 (in Japanese).

20) Varga J, Matsumura H, Tabata T, Masuhara E: Adhesive behavior of the alloys 'ALBABOND E' containing large percentage of Pd after various surface treatments. *Dent Mater J*, **4**: 181-190, 1985.

21) Shintani H, Futagami M, Yukihiro A, Satou J, Satou N, Kai M, Hayashihara H, Inoue T, Seo T: Bond strength and marginal closure of newly developed adhesive cements. *Dent Mater J*, **4**: 175-180, 1985.

22) Doi M: Tensile adhesive strength of dental resin cements to dental alloy surface - Adhesion to Type II dental gold alloy -. *Jpn J Conserv Dent*, **28**: 956-967, 1985 (in Japanese).

23) Imoto M (ed. by Inst. Jpn Adhesion), in "Adhesion handbook", (Nippon-Kougyo-Shinbun, 1976), p.7, (in Japanese).

24) Hata T, *ibid.* p. 67.

25) Obata Y, Inoue Y: Analysis of residual stress at adhesion layer. *J Chem Industry*, **61**: 39-42, 1958.

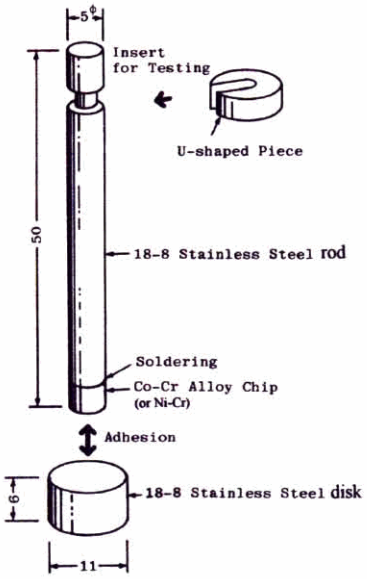


Fig. 2.1-1 Tensile test piece for bonding strength measurements. Alloy specimens were bonded with adhesive resin to an 18-8 stainless steel disk. The U shaped piece was applied to the groove in the stainless steel rod for the testing.

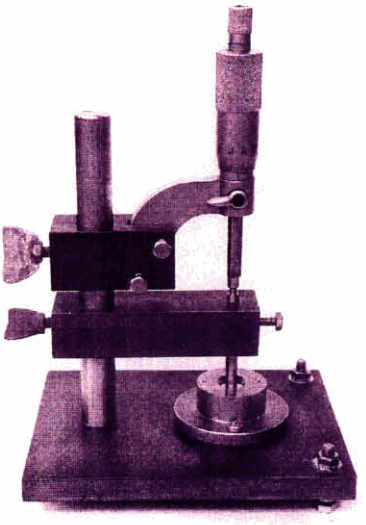

Fig. 2.1-2 Adhesion apparatus used to bond the stainless steel rod vertically to the alloy surface and to maintain a constant 50-μm thick resin layer.

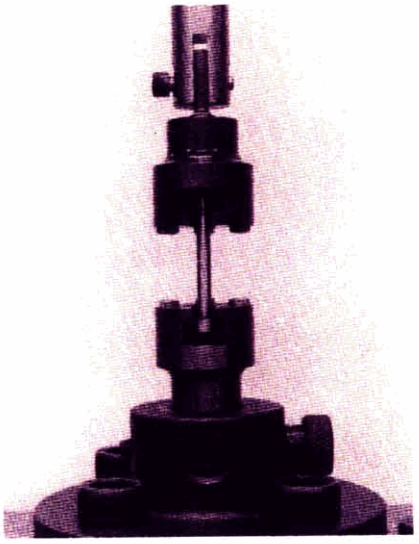

Fig. 2.1-3 Jig for the tensile test.

Table 2.1-1 Failure types and notation.

| Failure Type | Observed Figure | Notation |
|---|---|---|
| I | Resin | ● |
| II | Alloy Interface | ◉ |
| III | Alloy Inter-face, Resin | ◉ |
| IV | | ◉ |
| V | | ○ |

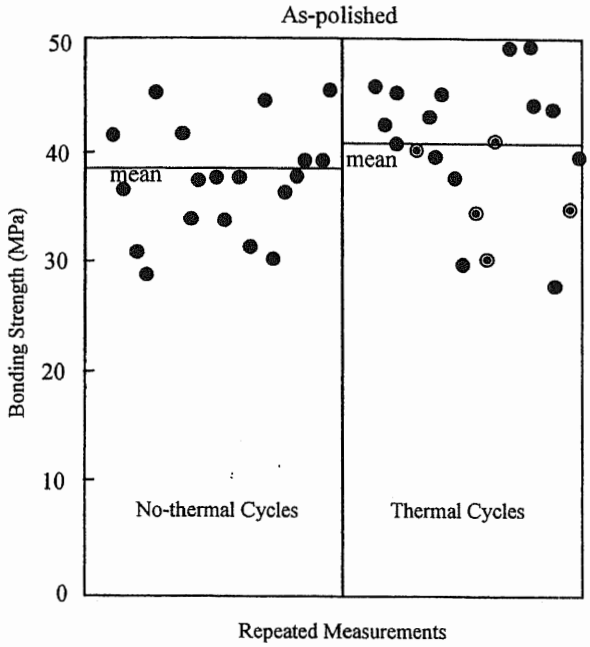


Fig. 2.1-4 Results of bonding strength measurement obtained from specimens bonded to the as-polished Co-Cr alloy surface. The left side shows the bonding strengths without thermal cycles (no-thermal cycles) and the right side are with the thermal cycles. The horizontal line shows the average of the repeated tests.

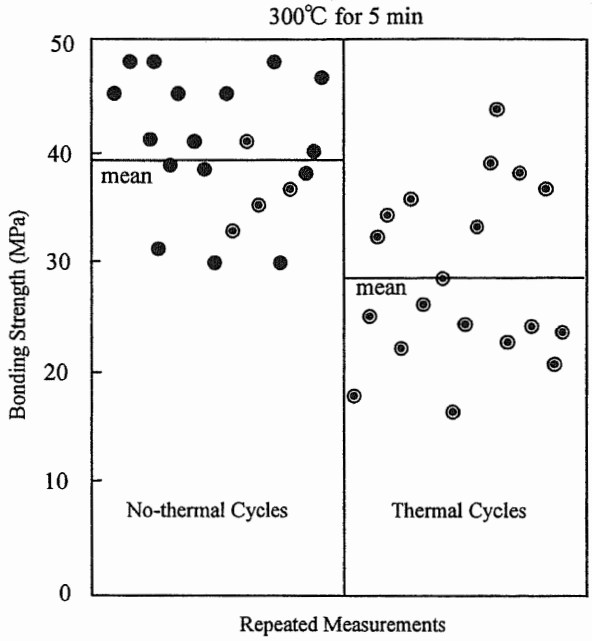


Fig. 2.1-5 Results of bonding strength measurements obtained for Co-Cr alloy specimens oxidized at 300℃.

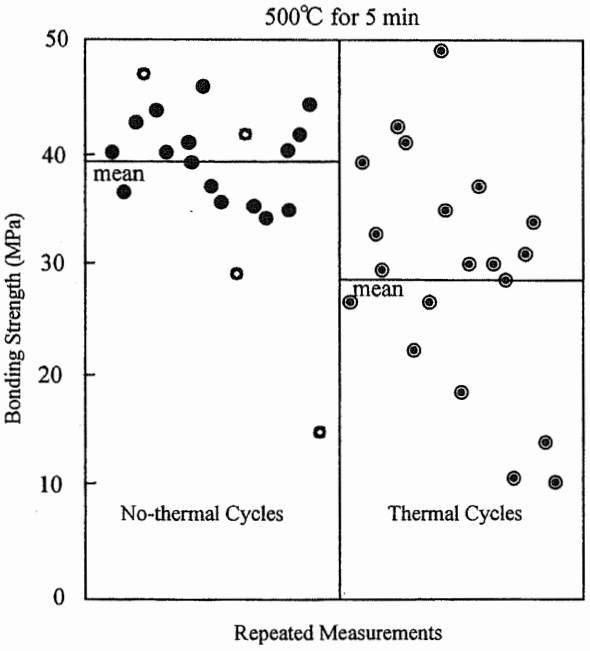


Fig. 2.1-6 Results of bonding strength measurements obtained from the Co-Cr alloy specimens oxidized at 500℃.

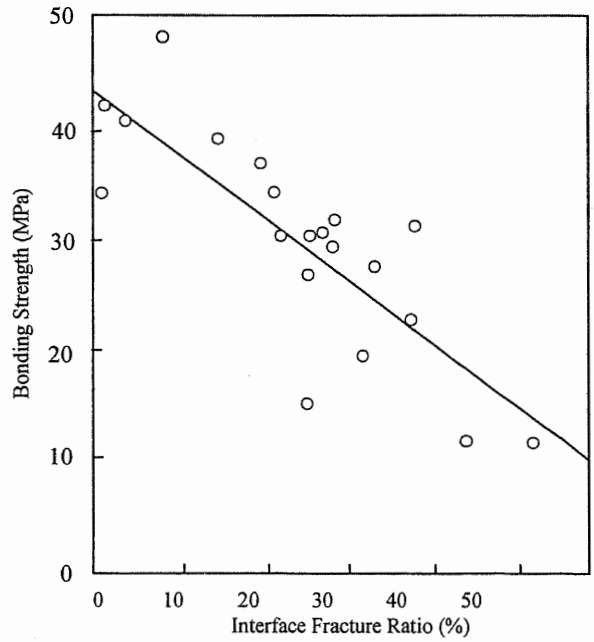


Fig. 2.1-7 Relationship between bonding strength and area fraction of interface failure at the periphery (Interface Fracture Ratio) from the tests of specimens subjected to thermal cycles in Fig. 2.1-6.

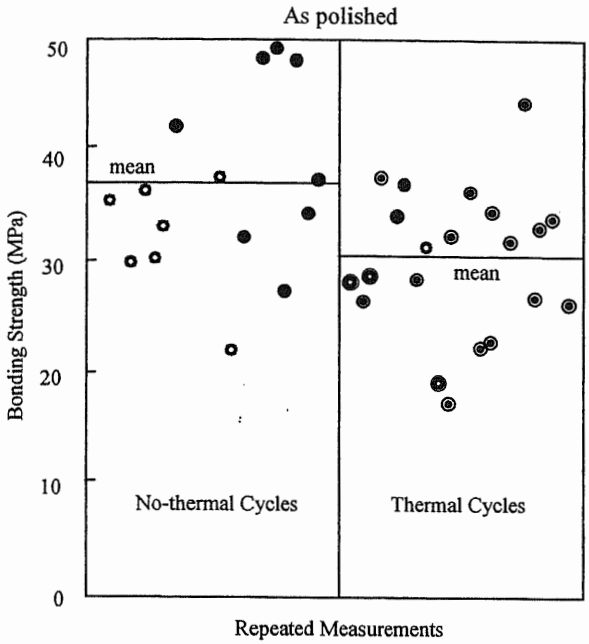


Fig. 2.1-8 Results of bonding strength measurements for specimens bonded to the as-polished Ni-Cr alloy surface.

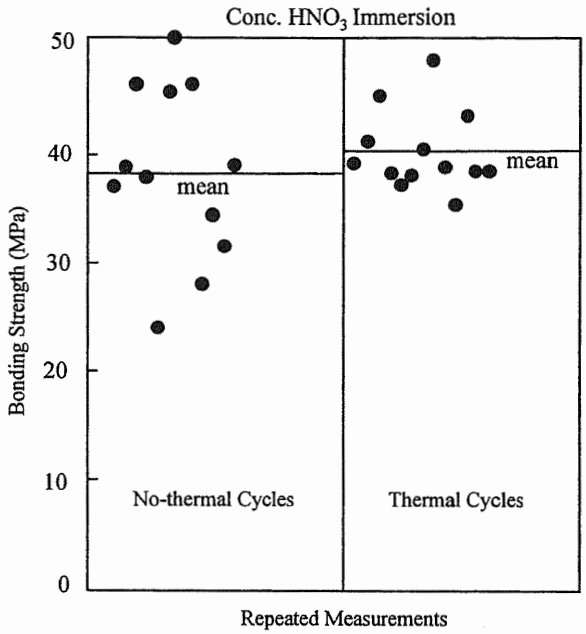


Fig. 2.1-9 Results of bonding strength measurements for the Ni-Cr alloy specimens treated with $HNO_3$ solution.

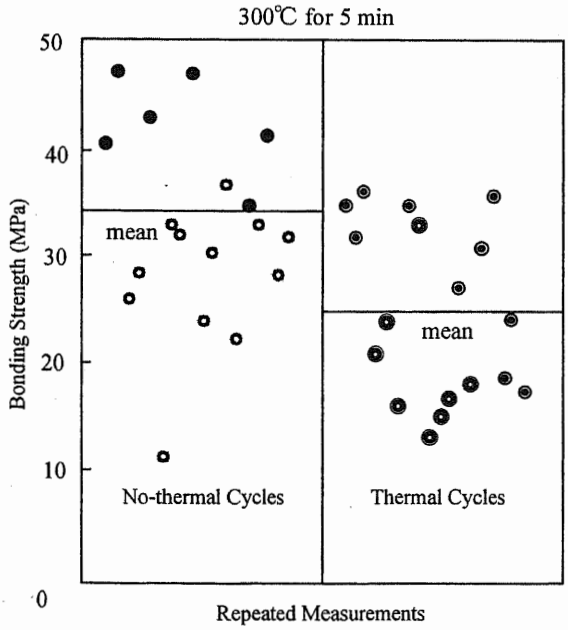


Fig. 2.1-10 Results of bonding strength measurements for Ni-Cr alloy specimens oxidized at 300℃.

## 2.2 Surface Structure of Base Metal Alloys (Co-Cr and Ni-Cr) and Bonding Strength

### 2.2-1 Introduction

A detailed understanding of the mechanism of adhesion would enable us to specify alloy surface structures which would ensure strong adhesion to the resin and also to establish guidelines for both the development of alloys and preparation of alloy surfaces to obtain strong bonds with the adhesive resin. To clarify the relationship between bonding strength and alloy surface structure, the alloy surface was characterized by reflection electron diffraction and ESCA. With ESCA the chemical state of the atoms can be determined in the top several 1 nm thick layer of a specimen, making ESCA suitable for investigating adhesion phenomena that are sensitive to the surface state of adherend. The adhesive abilities described section 2.1 are discussed on the basis of differences in the surface structure.

### 2.2-2 Materials and Methods

*Surface Treatment of Alloys*

The 70 mass%Co-30%Cr and 70 mass%Ni-30%Cr alloys specimens were polished metallographically and given three different surface treatments: polished only, oxidized for 5 min in air at 300°C, or 500°C. The $HNO_3$ treatment was performed by immersing the as-polished Ni-Cr specimen in concentrated $HNO_3$ (60%) solution for 15 min at room temperature. Both the as-polished and concentrated $HNO_3$ treated specimens were rinsed with distilled water.

*Reflection Electron Diffraction and ESCA Analysis*

The alloy specimens were kept in a silica gel desiccator for 2 hr before reflection electron diffraction and ESCA measurements. Reflection high-energy electron diffraction patterns were determined with an electron microscope with 100 kV accelerating voltage. The camera constant was calibrated with the transmission diffraction pattern of a gold film immediately before and after observing the reflection patterns. The compounds on the alloy surface were identified from the JCPDS card-index on the basis of the measured spacing.

The ESCA measurements of the three different surface states were performed using an electron spectrometer (Shimadzu ESCA-850) with Mg Kα radiation (1,253.6 eV). The binding energies of the measured photoelectron peaks were calibrated by the C 1s peak of hydrocarbon contamination at a binding energy of 285.0±0.2 eV. The alloy surface was subjected to argon ion etching at 2 kV and 20 mA under a pressure of $5\times10^{-4}$ Pa in the spectrometer. The etching rate was about 0.1 nm/sec under these etching conditions. The ESCA measurements and argon ion etching were performed alternately to determine both the amounts and chemical states of the elements in the depth direction. The chemical shift of the Cr and Ni spectra was measured on the basis of the peak position of metallic states after the argon ion etching. A standard sample of $Cr_2O_3$ was obtained by heating Cr of purity better than 99.99% at 300°C in air. A NiO standard sample was not used because NiO is reduced by the argon ion etching [1].

The amounts of Co, Cr, Ni and O were computed according to equation (2.2-1)[2]. The intensity of a photoelectron, $N$, which is ejected from a shell in an element, 'a', in a thick specimen is expressed by:

$$N = N_0 \cdot n_a \cdot \sigma \cdot \lambda \cdot S \text{ ---------- (2.2-1)}$$

where $N_0$ is a constant, $n_a$ the amount of atom '$a$' per unit volume, $\sigma$ the photoelectron cross section, $\lambda$ the mean-free path, and $S$ a spectrometer factor. In the present study, the photoelectron intensity of each element was measured from the peak areas of Co $2p_{3/2}$, Cr $2p_{1/2,3/2}$, O 1s, and C 1s. For example, the concentration of Cr, $C_{Cr}$, is expressed by equation (2.2-2):

$$C_{Cr} = n_{Cr}/(n_{Co} + n_{Cr} + n_O + n_C) \text{ ---------- (2.2-2)}$$

where $n_{Co}$, $n_{Cr}$, $n_O$, and $n_C$ are the amounts of Co, Cr, O, and C calculated from equation (2.2-1). The quantitative error in the calculations is estimated to be ±5-30%[2]. Quantitative values obtained from equation (2.2-2) were separated into the metallic and oxidation states of Co and Cr by subtracting the metallic state component from the measured spectrum.

## 2.2-3 Results

### 2.2-3.1 Co-Cr alloy

*Reflection Electron Diffraction*

Figures 2.2-1 (a) and (b) show the reflection electron diffraction patterns obtained from the surfaces of the as-polished and 500°C oxidized specimens. The pattern of the diffraction rings in the specimen oxidized at 300°C was similar to Fig. 2.2-1 (b) although more diffuse. There were no diffraction rings in (a), indicating that the as-polished surface was covered with an amorphous film. In Table 2.2-1, the observed lattice spacings and intensities of the diffraction rings in (b) are shown together with the data for $Co_3O_4$ from the JCPDS card-index, indicating that the oxidized specimens were covered with $Co_3O_4$. There was no identification lattice spacing at 'X' in the table, however, the diffraction intensity of the substance was very weak, indicating that there is only a small amount.

*ESCA Measurements*

Figure 2.2-2 shows the Co $2p_{3/2}$ spectrum (a) and the Cr $2p_{1/2,3/2}$ spectra (b) obtained at different depths of the as-polished specimen by varying the argon ion etching time. The 'surface' spectrum was obtained from the polished surface without argon ion etching and the 20 and 40 sec spectra were obtained after argon ion etching for 20 and 40 sec. In Fig. 2.2-2 (a), the binding energy of the Co $2p_{3/2}$ peaks at the 2 nm (20 sec) and 4 nm (40 sec) depth are 778.7 eV, which indicates metallic Co. The 'surface' spectrum showed a doublet with a separation of approximately 2.9 eV, showing that the surface contained two different chemical states: the lower binding energy peak was identified as metallic Co while the other was an

unknown state. Figure 2.2-2 (b) shows that there were no peaks except for the metallic Cr peak after etching for 40 sec. The spectra obtained from the unetched surface had a shoulder indicating the metallic state at 574.4 eV and the unknown state had a peak 2.8 eV higher than the shoulder of the metallic state. The unknown states of Co and Cr will be discussed later.

Figure 2.2-3 shows a set of spectra obtained from different depths of specimens oxidized at 300°C: (a) is for Co $2p_{3/2}$ spectrum and (b) is for Cr $2p_{1/2,3/2}$. In (a), metallic Co was obtained by etching for 120 sec, which removed the oxides on the alloy surface. The peak at the unetched surface was 1.7 eV higher than the metallic state, and may be attributed to Co-oxide. At longer etching time, the shoulder on the lower binding energy side of the peak at 40 sec developed to a well-shaped peak for the metallic state at 60 sec, showing a mixture of Co-oxide and metallic Co. In (b), the all-metallic state appeared by etching for 180 sec. The Cr $2p_{3/2}$ peak on the unetched oxidized surface lied 2.5 eV higher than that of the metallic state. Metallic and oxidized Cr were mixed in the 80 and 120 sec spectra.

Figure 2.2-4 shows the depth variation of Co, Cr, and O calculated with equation (2.2-2) for the as-polished specimen. The calculation was performed by including adsorbed carbon that is not shown in Fig. 2.2-4. The concentrations at etching time zero are those of the surface before etching. The Co and Cr concentrations became constant after etching 20 sec and oxygen decreased remarkably with increasing etching time. The concentrations of Co and Cr in Fig. 2.2-4 were obtained from the mixture of the metallic and unknown states shown in Fig. 2.2-2. The two states could be separated and their concentrations determined. For example, the spectra from the specimen in Fig. 2.2-3 (b) at 80 sec could be separated into the two spectra as shown in Fig. 2.2-5: metallic (fine solid line) and Cr-oxide (dotted line). The area fraction gives the concentration of the two states. The concentrations of Co and Cr in Fig. 2.2-4 could be separated into metallic and unknown states. Separated concentrations of Co and Cr show in Fig. 2.2-6 (a) and (b). The metallic and unknown states of Co and Cr were present at the surface (etching time zero). The concentration of the Co unknown state became zero at the depth reached after etching for 20 sec, when the unknown Cr state reached a maximum. The film thickness on the as-polished surface was 2-3 nm as the etching rate is about 0.1 nm/sec.

Figure 2.2-7 shows the concentrations of Co, Cr, and O in the depth direction, for specimens oxidized at 300℃. In the same manner as in Fig. 2.2-5, the concentrations in Fig. 2.2-7 can be separated into metallic and oxidized states as shown in Fig. 2.2-8 (a) for Co and in (b) for Cr. The Co-oxide was rich at the surface, while Cr-oxide reached a maximum at the depth equivalent to 60 sec etching. The oxide film was about 12 nm thick and contained metallic Co and Cr from 3-4 nm into the specimen.

### 2.2-3.2 Ni-Cr alloy

*Reflection Electron Diffraction*

Figure 2.2-9 (a) shows the reflection electron diffraction pattern obtained from the surface of the as-polished specimen. In Table 2.2-2, the observed lattice spacings and intensities of the diffraction ring are shown together with data obtained from the Ni-Cr alloy powder by the Debye-Scherrer method. Except for

weak 222 and 400 reflections, the observed lattice spacings and intensities coincided with the X-ray diffraction in the strong intensity reflections, showing that the electron diffraction pattern diffracted from the alloy substrate. Figure 2.2-9 (b) shows the reflection electron diffraction pattern obtained from the specimen oxidized at 300°C. It was impossible to precisely measure the lattice spacings from the very diffuse diffraction pattern which showed an extremely thin oxide layer formed on the alloy surface. The alloy specimen was heated for 5 min at 500°C in air to obtain the sharp diffraction pattern shown in Fig. 2.2-9 (c). Both the patterns in (b) and (c) were considered to be the same diffraction patterns from the coincidence of both the ring sizes and intensities. Table 2.2-3 shows the observed lattice spacings and intensities obtained from the oxidized specimen (Fig. 2.2-9 (c)) and JCPDS card index of NiO.

*ESCA Measurement*

Figure 2.2-10 shows (a) the Cr $2p_{1/2,3/2}$ spectra, (b) the O 1s spectra, and (c) the Ni $2p_{3/2}$ spectra obtained at different depths of the as-polished specimen, by varying the argon ion etching time (min). The 0 min spectrum was obtained from the polished surface without argon ion etching. In (a), the peaks of the binding energy at 574.3 eV, obtained by etching for 2.7 min, indicated Cr $2p_{3/2}$ from the metallic state. The Cr $2p_{3/2}$ spectrum obtained from the as-polished surface without etching (0 min) had a peak 3.0 eV higher than the metallic 574.3 eV peak and a shoulder at 574.3 eV, indicating that the surface contained two different chemical states of Cr: the lower binding energy shoulder was identified as metallic Cr while the other was an unknown state in a passive film which will be discussed later. The O 1s spectrum in (b) obtained from the unetched surface had a peak at 531.8 eV and a shoulder 1.5 eV lower than the peak, showing different chemical states of oxygen. By etching for 0.3 min, the peak at 531.8 eV disappeared rapidly and the shoulder on the lower binding energy side developed into a small peak. The O 1s spectrum disappeared by subsequent etching. Metallic Ni was indicated by the peak at 852.8 eV in all the spectra in (c). The unetched surface (0 min) had a peak at 852.8 eV of the metallic state and a shoulder 3.2 eV higher than the metallic one. The depth variation in the concentrations (at%) of Cr, O, and Ni for the as-polished specimen is shown in Fig. 2.2-11, where oxygen decreased sharply and Ni increases by etching for 0.3 min.

Figure 2.2-12 shows a set of spectra obtained from different depths of a specimen treated by concentrated $HNO_3$; (a) is the Cr $2p_{1/2,3/2}$ spectra, (b) the O 1s spectra, and (c) Ni $2p_{3/2}$ spectra. Compared with the as-polished spectra (Fig. 2.2-10 (a) and (b)), there were a difference in the intensity ratios at the unetched surface, for a peak at 577.3 eV or 576.8 eV and a shoulder at 574.3 eV in the Cr $2p_{3/2}$ spectrum; and for a peak at 530.1 eV and a shoulder at 531.6 eV in the O 1s spectrum. These differences will be discussed later. Figure 2.2-13 shows the concentration variations of Cr, O, and Ni in the depth direction for the specimen treated by concentrated $HNO_3$ solution. At the unetched surface (0 min), concentrations of Cr and Ni are 25% and 13% for the concentrated $HNO_3$ treated specimen versus the 17% and 21% for the as-polished specimens (Fig. 2.2-11). It indicated that Cr concentrated at the alloy surface by treatment with concentrated $HNO_3$ solution. With argon ion etching, the oxygen concentration in Fig. 2.2-13 decreased slower than in Fig. 2.2-11, indicating that a thicker passive film formed on the alloy surface after the

concentrated $HNO_3$ treatment.

### 2.2-4 Discussion

*Characterization of the Co-Cr Alloy Surface*

Table 2.2-4 shows the oxide chemical shifts, $\Delta E_B$ (with reference to the metallic state), of energy level ($2p_{3/2}$) which have been reported for Co and Cr. Table 2.2-5 shows the chemical shifts, $\Delta E_B$, for Co $2p_{3/2}$ and Cr $2p_{3/2}$, obtained in this study from the three alloy surfaces, as-polished, oxidized at 300°C and oxidized at 500°C all before argon ion etching. Comparing Tables 2.2-4 and 2.2-5, the oxidation states of the unknown peaks in Fig. 2.2-2 (as-polished surface) are identified as divalent (II) for Co and trivalent (III) for Cr. On the surface oxidized at 300°C, Co can not be identified as Co (III) or Co (II+III) from $\Delta E_B$ because both Co chemical states are very close [3, 4]. The chemical states on the surface oxidized at 500°C were the same as those oxidized at 300°C. Reflection electron diffraction identified an amorphous layer on the as-polished surface and $Co_3O_4$ + X (unidentified compound) on the oxidized surface. Table 2.2-6 shows the results obtained from ESCA and reflection electron diffraction.

The film on the as-polished surface of the Co-Cr alloy is a so-called passive film, which also forms on stainless steel, Ni base alloys, and Co base alloys containing Cr at a certain content. A number of studies have reported passive films on these alloys, and proposed formulas of $Cr_2O_3$-$CrO_3$[5], Cr(OH)-$CrO_4$[6], $Cr_2O_3$[7], $Cr(OH)_3$[8], 2CrO(OH)-$3H_2O$[9], and CrO(OH)-$H_2O$[10]. Hashimoto et al. have introduced a more general formula: $CrO_x(OH)_{3-2}$-$nH_2O$, hydrated chromium oxy-hydroxide[11, 12]. On stainless steel the film is amorphous and 3 to 6 nm thick[13]. Okada has proposed that the surface structure of chromium electroplating is a one molecule layer of the ol-compound coordinating six -OH around a central $Cr^{3+}$ [14]. By studying the films formed by chromium electroplating, Uchida et al. found OH stretching and HOH bending vibration by infrared absorption spectroscopy[9], and they also confirmed the vaporization of water in the film up to 240℃ by thermo-gravimetry and by the decrease in infrared absorption[15]. They concluded that the film structure is the ol-compound containing zeolitic water in addition to Okada's structure. Okamoto has proposed the structural mode of the passive film on stainless steel in Fig. 2.2-14, two dimensional inorganic polymers which coordinate $O^{2-}$, $OH^-$, and $H_2O$ around $Cr^{3+}$ (indicated as M)[16].

Thus the structure of the passive film on the as-polished surface of the Co-Cr alloy in this study was considered to have a structure which is somewhat more complicated than in Fig. 2.2-14. The film was amorphous, 2-3 nm thick, and the surface was rich in Co (Ⅱ). In the inner part of the film, Co(Ⅲ) decreased remarkably while Cr (Ⅲ) increased. The states of the –OH and $H_2O$ on the as-polished surface can be determined as follows: The oxygen concentration in the passive film, $C_{Ox(passive)}$, can be obtained by equation (2.2-3) from the Co and Cr concentrations, $C_{Co}$ and $C_{Cr}$, assuming six coordinating –OH and /or $H_2O$ around Co and Cr.

$$C_{Ox(passive)} = 3(C_{Co} + C_{Cr}) \quad \text{---------- (2.2-3)}$$

The concentrations, $C_{Co}$ and $C_{Cr}$, can be obtained from Fig. 2.2-6 (unknown state). The calculated

and measured (Fig. 2.2-4) oxygen concentrations are plotted in Fig. 2.2-15. The calculated values agree with those measured at the surface (etching time zero), showing that these metal ions have six coordinated -OH ions and $H_2O$ molecules. The discrepancies in the inner part show that the coordination number here is below six. Thus the structure of the passive film on the as-polished surface of the Co-Cr alloy in this study is considered to have a structure that is somewhat more complicated than in Fig. 2.2-14

On the oxidized specimens, the ESCA measurements could not establish the oxidation states of Co, Co (III), or Co (II+III), however, reflection electron diffraction revealed that $Co_3O_4$ was predominantly formed on the oxidized alloy surface. Though Co has a lower affinity for oxygen than Cr, Co was preferentially oxidized near the surface (Fig. 2.2-8) because of the high Co content. The $Co_3O_4$ has a normal spinel structure with $Co^{2+}$ ions at the tetrahedral sites, and $Co^{3+}$ ions at the octahedral sites [17], and the ESCA measurements could not be distinguish $Co_2O_3$ and $Co_3O_4$ by chemical shift which contain both $Co^{2+}$ and $Co^{3+}$. To increase the surface energy due to unsaturated bonds at the solid surface, the surface (decreasing free energy) is stabilized by arranging the atoms into particular positions and by adsorbing molecules. The oxide surface adsorbs mainly –OH ions or $H_2O$ molecules and is not directly exposed to air. Bolger proposed the oxide model shown in Fig. 2.2-16[18]: the oxide surface adsorbs -OH monolayer directly, then chemisorbed $H_2O$ molecules in the middle, and physisorbed $H_2O$ at the top of the adsorbed layer.

The thickness of these adsorbed layers on surface oxidized at 300°C can be measured from the ESCA data: when the concentrations of forming Co- and Cr-oxides, $C_{Co}$ and $C_{Cr}$ are known, the oxygen concentration in the oxides, $C_{Ox(oxide)}$, can be calculated from equation (2.2-4) assuming that the formed oxides are stoichiometric oxides of $Co_3O_4$ and $Cr_2O_3$.

$$C_{Ox(oxide)} = 1.33 \times C_{Co} + 1.5 \times C_{Cr} \quad \text{---------- (2.2-4)}$$

Both $C_{Co}$ and $C_{Cr}$ are shown in Fig. 2.2-8. The measured (Fig. 2.2-7) and calculated oxygen concentrations in the depth direction are plotted together in Fig. 2.2-17. At the top (unetched surface), the measured value was 17% higher than the calculated value. At 2 nm (20 sec) below the top layer, the measured value increased slightly and the calculated value decreased markedly. These increases and decreases in oxygen concentration are considered to be due to the adsorbed -OH and $H_2O$. Though sputtering yield by the ion etching and mean free path of ejected photoelectrons should be considered, it may be concluded that there is a 2 nm thick adsorbed layer on the Co-Cr alloy surface oxidized at 300°C. The thickness is equivalent to a 5-8 molecule layer of adsorbed water.

*Characterization of the Ni-Cr Alloy Surface*

To compare the chemical states of Cr, Fig. 2.2-18 shows a set of Cr 2p spectra from four specimens, the unetched surface of the as-polished specimen in Fig. 2.2-10 (a), the $HNO_3$ treated specimen in Fig. 2.2-12 (a), $Cr_2O_3$, and metallic Cr. A 2.5 eV chemical shift is observed between $Cr^{3+}$ and the metallic Cr state. The major peak of Cr $2p_{3/2}$ for the $HNO_3$ treated specimen coincides with the peak of the $Cr^{3+}$ state.

The Cr $2p_{3/2}$ spectrum obtained from the as-polished specimen has a peak of 0.5 eV higher binding energy than the $Cr^{3+}$ state, indicating a higher oxidation state than the $Cr^{3+}$ state. Both Cr $2p_{3/2}$ spectra of the as polished and $HNO_3$ treated specimens have a shoulder at the position of the metallic state. The intensity ratio for the as-polished specimen, the metallic/oxidation state, is larger than that for the $HNO_3$ treated specimen.

To clarify the changes in the oxygen chemical state, Fig. 2.2-19 shows a set of O 1s spectra obtained from the unetched surface of the as-polished specimen in Fig. 2.2-10 (b) and the $HNO_3$ treated specimen in Fig. 2.2-12 (b) with O 1s spectrum obtained from $Cr_2O_3$. For the $HNO_3$ treated surface the major peak position coincides with the peak of $Cr_2O_3$ and the shoulder agrees with the major peak of the as-polished specimen. The spectrum of the as-polished surface has a shoulder at the peak of $Cr_2O_3$. This shows different oxygen chemical states: one is $O^{2-}$ and the other is an unknown state.

Separation of oxygen states of the O 1s spectra was performed with the data analysis system in the ESCA spectrometer by assuming that the spectra are approximated by a Gaussian function. Figures 2.2-20 and 2.2-21 show the separated spectra of O 1s, obtained from the as-polished (Fig. 2.2-10 (b)) and $HNO_3$ treated specimen (Fig. 2.2-12 (b)). Both O 1s spectra can be separated into three components as indicated by the dotted line. The solid line, the observed spectra, agrees well with the dotted lines of the three components. Table 2.2-7 lists the peak positions and area fractions of the components. The peak positions show the chemical states of oxygen and the area fractions give the amount of each chemical state. The O 1s component I is the same chemical state as the oxygen in $Cr_2O_3$ as shown in Fig. 2.2-19. The oxygen of components II and III exist in the upper part of component I oxygen because these decrease remarkably with only limited argon ion etching as shown in Figs. 2.2-10 (b) and 2.2-12 (b).

From the above, the origins of the oxygen states are estimated as follows: Component I is due to oxygen bonded with chromium in the passive film, Cr-O-Cr; Component II is due to oxygen bonded with chromium and hydrogen in the passive film, Cr-OH---$OH_2$; Component III is due to oxygen in physisorbed water molecules on the passive film. The area fractions are in the order II > I > III for the as-polished surface and I > II > III for the $HNO_3$ treated surface, indicating that a firm passive structure is formed on the surface treated by $HNO_3$.

*Surface Structures and Adhesive Ability*

The reflection electron diffraction pattern obtained from the as-polished Co-Cr alloy surface showed no diffraction rings, indicating that the surface was covered with an amorphous film. The result coincided with reports of an amorphous passivated film on the alloy containing Cr. The passive film on the Ni-Cr alloy surface was not sufficiently thick as the diffraction pattern showed the substrate to have an alloy structure. The Ni content at the alloy surface decreased by eluting Ni to the $HNO_3$ solution, so that Cr which has good chemical affinity for the 4-META resin concentrated on the alloy surface, resulting in the formation of a firm, thick passive film. This leaded to an increase in the adhesive ability of the 4-META resin on the passive film.

Adhesion depends on the atomic interaction that is determined by atoms less than 1 nm from the top surface[19]. Here, it is necessary to describe the differences in adhesion between the as-polished and oxidized surfaces of the alloy on the basis of the adhesion mechanisms. The surface models in Figs. 2.2-14 and 2.2-16 help in understanding the mechanism of adhesion of adhesive resin to the alloy surface. For the adhesion mechanism of the 4-META resin on a metal surface, Masuhara has suggested the presence of hydrogen bonds between the 4-META and adsorbed –OH on the metal as in Fig. 2.2-22[20]. Figure 2.2-23 shows the possible adhesion mechanism models of the 4-META: Models (a), (b), (c) for the as-polished surface were made according to Fig. 2.2-14 and Models (d), (e), and (f) for the oxidized surface according to Fig. 2.2-16. Adhesion is the interaction of molecules through the interface between adhesive and substance. Model (a) shows the possibility of primary atomic bonds for 4-META with the metal existing in a 0.7-0.8 nm deep layer. Model (b) shows a hydrogen bond of the 4-META and –OH in the passive film. Model (c) is Van der Waals interaction between water molecule and metal ion with hydrogen bond of water molecule and the 4-META. Model (d) shows the hydrogen bond of 4-META with hydroxyl groups on the top surface of oxide layer. Model (e) includes one water molecule between the hydroxyl group and 4-META. Model (f) which includes several molecules of water is not part of the model for the adhesion mechanism on the as-polished surface because adsorption model of the as-polished surface coordinates six –OH and $H_2O$ around a metal ion and does not have several-molecules thick layer of adsorbed water. In these models the chemical bonds which have nearly equal bonding strengths are labeled by the same number at the bonding positions.

Differences in the adhesiveness to the as-polished and oxidized surfaces with the thermal cycles described in section 2.1, are as follow: (1) almost all cohesive failures in the resin are for the as-polished surfaces (Fig. 2.1-4), and (2) interface failures at the oxide/resin interface are at the periphery of adhesion for the oxidized surfaces (Fig. 2.1-5). These results and the adhesion model in Fig. 2.2-23 indicate that the strength at the adhesion interface decreases in the order interface formed from (a), (b), and (c) > resin > interface formed from (d), (e), and (f). The adhesive force depends on the strength of specific chemical bonds and the number of bonds. Models (b) and (c), for the as-polished surface are considered to be in agreement with Models (d) and (e) for the oxidized surface in the chemical states of the bonds. Therefore, Mode (a) and (f) are different for the two surfaces. Model (a) due to the primary atomic bond is stronger than Mode (f). Furthermore, the probability of the existence of Model (f) is not small as there is a several-molecule layer of adsorbed water on the oxidized surface. Thus the existence of the chemical bond (f) is a factor that lowers the adhesion to the oxidized surface.

### 2.2-6 Conclusions

The alloy surface structures were analyzed by reflection electron diffraction and ESCA. The relationship between the adhesion and the alloy surface structure was discussed by considering adhesion models, including hydrogen bonds with -OH and $H_2O$ molecule on the alloy surfaces.

The structure of the as-polished Co-Cr alloy surface was an amorphous 2-3 nm thick passive film, and

it was considered to be formed by up to six –OH ion and or $H_2O$ molecules coordinated around $Cr^{3+}$ and $Co^{2+}$ or $Co^{3+}$ metal ions. The $Co_3O_4$ was predominant on the surfaces oxidized at 300°C and 500°C. On the 300°C surface, a several molecule thick layer of water was adsorbed on the 2 nm thick oxide layer. The presence of chemical bonds including the several-molecule thick layer of adsorbed water between the oxidized surface and the 4-META side-chain was considered to be the reason why adhesion to the oxidized surface is inferior to that of the as-polished surface.

On the as-polished surface, the adhesive ability of the Ni-Cr alloy was inferior to the Co-Cr alloy. The adhesive ability of 4-META resin to Ni-Cr alloy improved remarkably when the alloy surface was treated with concentrated $HNO_3$. The Ni-Cr alloy displayed adhesive ability comparable with that of the Co-Cr alloy by treatment of the as-polished surface with concentrated $HNO_3$ solution. Both the as-polished and concentrated $HNO_3$ treated alloy surfaces were analyzed by ESCA to explain the superior adhesive ability of the alloy surface treated with $HNO_3$. The surface of the $HNO_3$ treated specimen contains 25 at%Cr and 13%Ni and the as-polished specimen contains 17%Cr and 21%Ni, showing that Cr, which has good chemical affinity for 4-META resin, was enriched on the alloy surface. A firm passive structure was formed on the surface treated by $HNO_3$ solution. This is the cause of the increase in the adhesive ability of the 4-META resin on the passive film.

## REFERENCES

1) Kim K S, Winograd N: X-ray photoelectron spectroscopic studies of nickel-oxygen surfaces using oxygen and argon ion bombardment. *Surface Sci*, **43**: 625-643, 1974.

2) Hirokawa K: Surface analysis by XPS, AS, and SIMS. *Bul Jpn Inst Met*, **21**: 885-890, 1982 (in Japanese).

3) Okamoto Y, Nakano H, Imanaka T, Teranishi S: X-ray photoelectron spectroscopic studies of catalysts. *Bul Chem Soc Jpn*, **48**: 1163-1168, 1975.

4) Haber J, Ungier L: On chemical shifts of ESCA and auger lines cobalt oxides. *ibid*, **12**: 305-312, 1977.

5) Sargent G J: Electrolytic chromium. *Trans Amer Electrochem Soc*, **37**: 479-497, 1920.

6) Muller E: Die Wirkung von Fremdanionen auf die Elektrolyse wassriger Chromsaure-Losungen. *Ztschr Elektrochem*, **50**: 172-186, 1944.

7) Weiner R, Schiele C: Elektronenbeugungsuntersuchungen an Kathodenfilmen bei der Elektrolytischen Reduktion der Chromsaure. *Z Phys Chem N F*, **26**: 248-268, 1960.

8) Solov'eva Z A, Vagramyan A T: Oscillographic investigation of film formation on the cathode surface in the electrolytic reduction of chromic acid. *J Phys Chem (USSR)*, **36**: 751-756, 1962.

9) Uchida H, Kado S, Yamada K, Ogasawara T: Structure of hydrated chromium oxide film on tin free steel. *J Jpn Inst Met*, **33**: 1295-1299, 1969 (in Japanese).

10) Kondo Y, Matsubayashi H: Structure of hydrated chromium oxide film formed by electrolytic reduction in chromic acid solution. *Kinzoku-Hiyoumen-Gijutsu*, **28**: 223-227, 1977 (in Japanese).

11) Asami K, Hashimoto K, Shimodaira S: An XPS study of the passivity of a series of iron-chromium

alloys in sulphuric acid. *Corro Sci*, **18**: 151-160, 1978.

12) Hashimoto K, Asami K, Naka M, Masumoto T: Surface films formed on amorphous Co-Cr alloys in 1 N HCl. *Boshoku Gijutsu*, **28**: 271-277, 1979.

13) Rhodin T N: Oxide films on stainless steels. *Corro NACE*, **12**: 41-53, 1956.

14) Okada H: Electrochemical study on chromium and nickel-plating. *Thesis of Hokkaido Univer (No. 4473)*, 1961 (in Japanese).

15) Uchida H, Kado S, Yamada K, Kato C: Dehydration of hydrated chromium oxide film on tin free steel. *J Jpn Inst Met*, **33**: 1290-1295, 1969 (in Japanese).

16) Okamoto G, Shibata T: Stability of passive stainless steel in relation to the potential of passivation treatment. *Corro Sci*, **10**: 371-378, 1970.

17) Kiriyama R, Kiriyama H: *Structural inorganic chemistry (I)*, Kyoritu-Suppan, 1975, p. 144 (in Japanese).

18) Bolger J C, Michaels A S: Molecular structure and electrostatic interactions at polymer solid interfaces. *Interface conversion for polymer coatings* (ed. By Wess P and Cheever GD), Elsevier Publishing Co, 1968, pp. 3-60.

19) Nishiyama Y: *Design of surface* (Modification of surface, ed. By Jpn Chemical Soc), Kagaku-Sousestu, No. 44, 1984, pp. 1-6 (in Japanese).

20) Masuhara E: *A dental adhesive and its clinical application*. Quintessence Books Co, 1982, pp. 11-68 (in Japanese).

21) Holm R, Storp S: ESCA studies of chemical shifts for metal oxides. *Applied Phys*, **9**: 217-222, 1976.

22) Bouyssoux G, Romand M: XPS and AES studies of anodic passive films grown on chromium electrodes in sulphuric acid baths. *J Electro Spectro and Related Phenom*, **11**: 185-196, 1997.

23) Asami K, Hashimoto K: The X-ray photo-electron spectra of several oxides of iron and chromium. *Corro Sci*, **17**: 559-570, 1977.

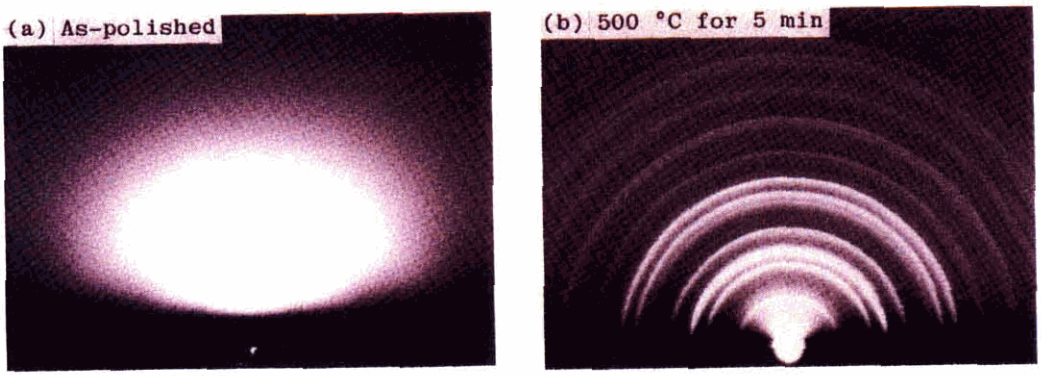


Fig. 2.2-1 Reflection electron diffraction patterns from the surfaces of the as-polished (a) and 500℃ oxidized Co-Cr alloy specimens (b).

Table 2.2-1 Lattice spacings and intensities observed from diffraction rings (in Fig. 2.2-1 (b)) with the data for $Co_3O_4$ from the JCPDS card-index. An 'X' indicates the absence of an identification lattice spacing.

| Observed values | | | Reference substance measured by X-ray | | |
|---|---|---|---|---|---|
| | | | JCPDS card | | |
| | | | $Co_3O_4$ | | |
| Ring No. | dÅ | I | dÅ | $I/I_1$ | hkl |
| 1 | 4.71 | m | 4.666 | 20 | 111 |
| 2 | 2.88 | s | 2.860 | 40 | 220 |
| 3 | 2.46 | vs | 2.438 | 100 | 311 |
| 4 | 2.33 | vw | 2.333 | 12 | 222 |
| 5 | 2.03 | s | 2.021 | 25 | 400 |
| 6 | 1.86 X | vw | | | |
| 7 | 1.65 | w | 1.6505 | 12 | 422 |
| 8 | 1.57 | s | 1.5559 | 35 | 511 |
| 9 | 1.44 | s | 1.4293 | 45 | 440 |
| 10 | 1.37 X | vw | | | |
| 11 | 1.29 | vw | 1.2788 | 6 | 620 |
| 12 | 1.24 | w | 1.2330 | 12 | 533 |
| | | | 1.2191 | 8 | 622 |
| 13 | 1.18 | vw | 1.1671 | 4 | 444 |
| 14 | 1.14 | vw | 1.1321 | 4 | 711 |
| 15 | 1.09 | w | 1.0803 | 8 | 642 |
| 16 | 1.06 | w | 1.0524 | 16 | 731 |

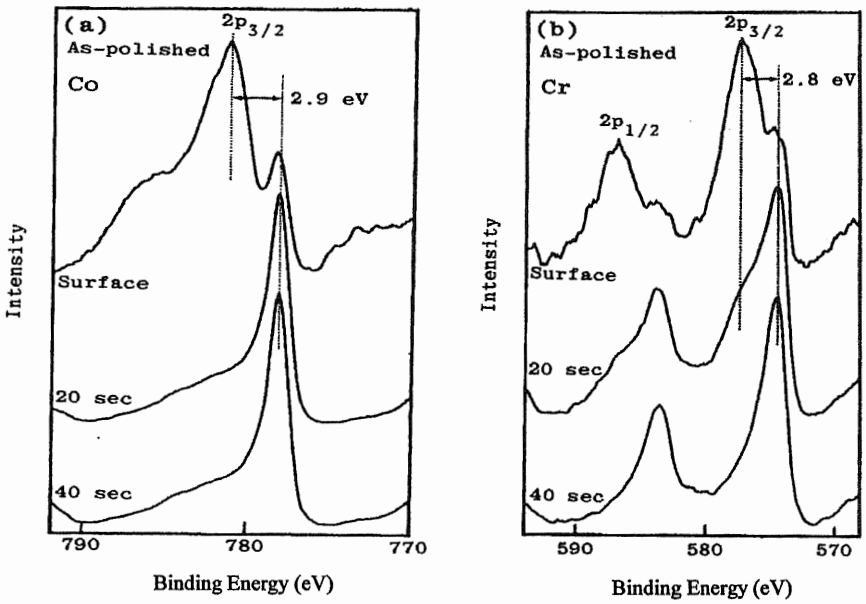


Fig. 2.2-2 ESCA spectra at different depths of the as-polished Co-Cr alloy specimens at varying argon ion etching times: (a) is the Co $2p_{3/2}$ spectrum and (b) is the Cr $2p_{1/2,3/2}$ spectra. The 'surface' spectra are from the surface without argon ion etching.

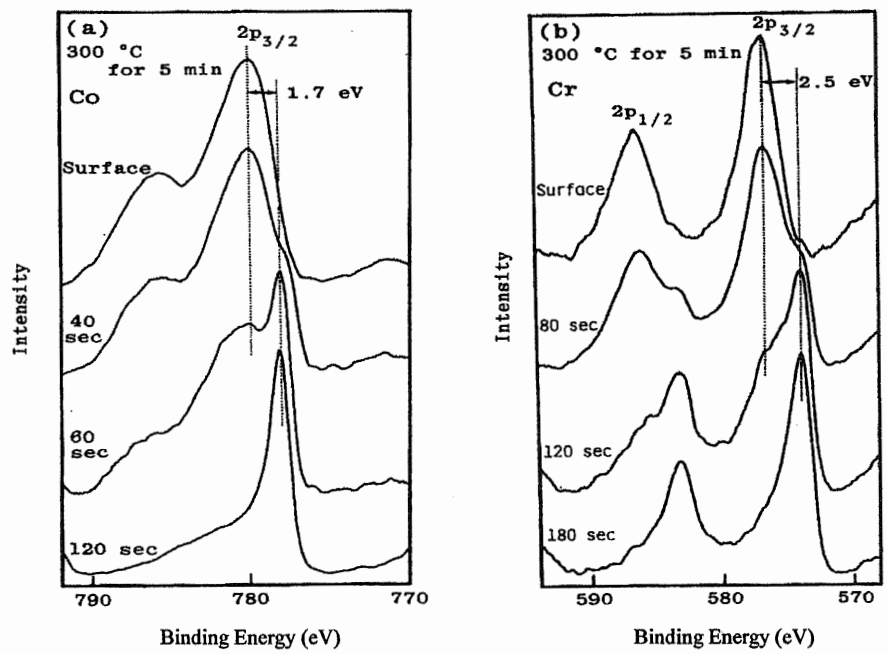


Fig. 2.2-3 ESCA spectra at different depths of the 300℃ oxidized Co-Cr alloy specimen.

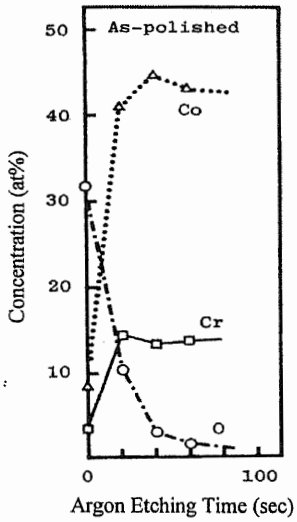


Fig. 2.2-4 Depth concentrations of Co, Cr, and O from the as-polished Co-Cr alloy specimen. One sec of etching time is equivalent about 0.1 nm etching.

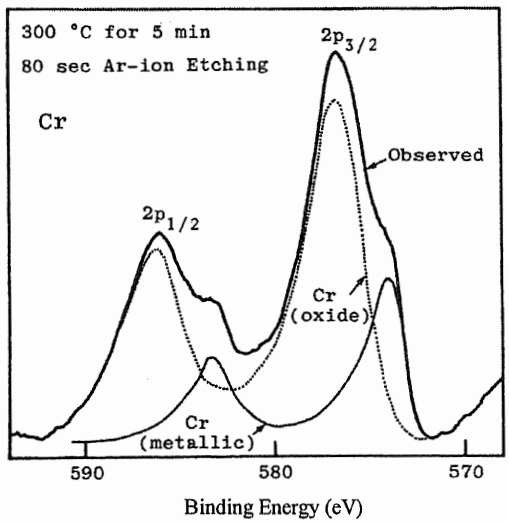


Fig. 2.2-5 The observed Cr $2p_{1/2,3/2}$ spectra (heavy solid line) after 80 sec argon ion etching of the Co-Cr alloy specimen oxidized at 300℃ resolved into the spectra for the metallic state (fine solid line) and Cr-oxide (dotted line). The area fractions of the spectra give the concentration of the two states.

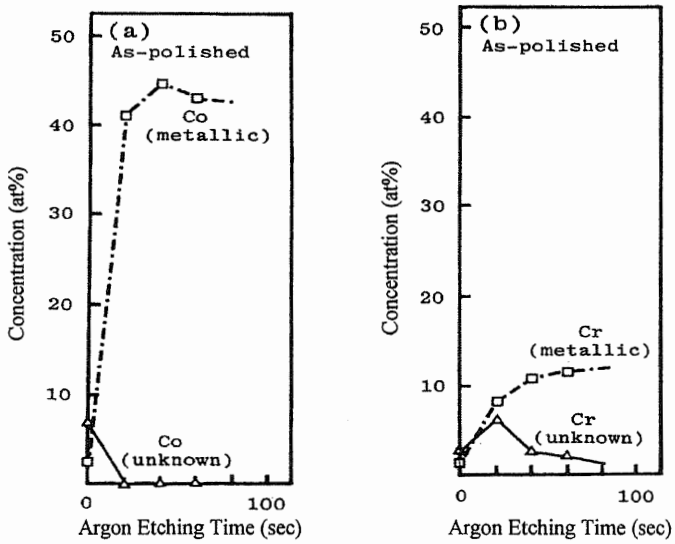


Fig. 2.2-6 Concentrations of the metallic and unknown states of Co (a) and Cr (b) in depth, obtained from the as-polished Co-Cr alloy surface (Fig. 2.2-4).

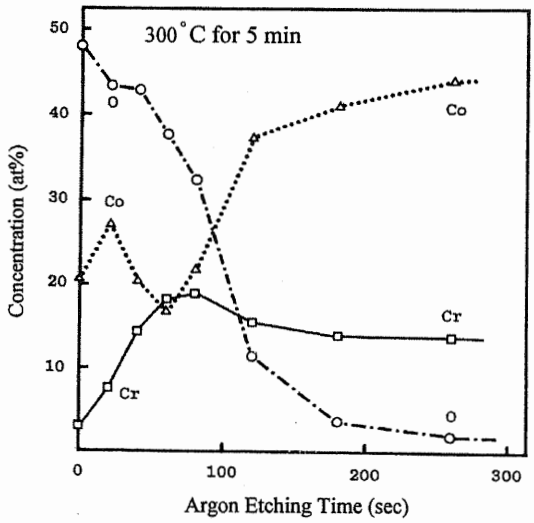


Fig. 2.2-7 Concentrations of Co, Cr, and O in depth, from the 300°C oxidized Co-Cr alloy specimen. One sec etching is equivalent to ca. 0.1 nm in depth.

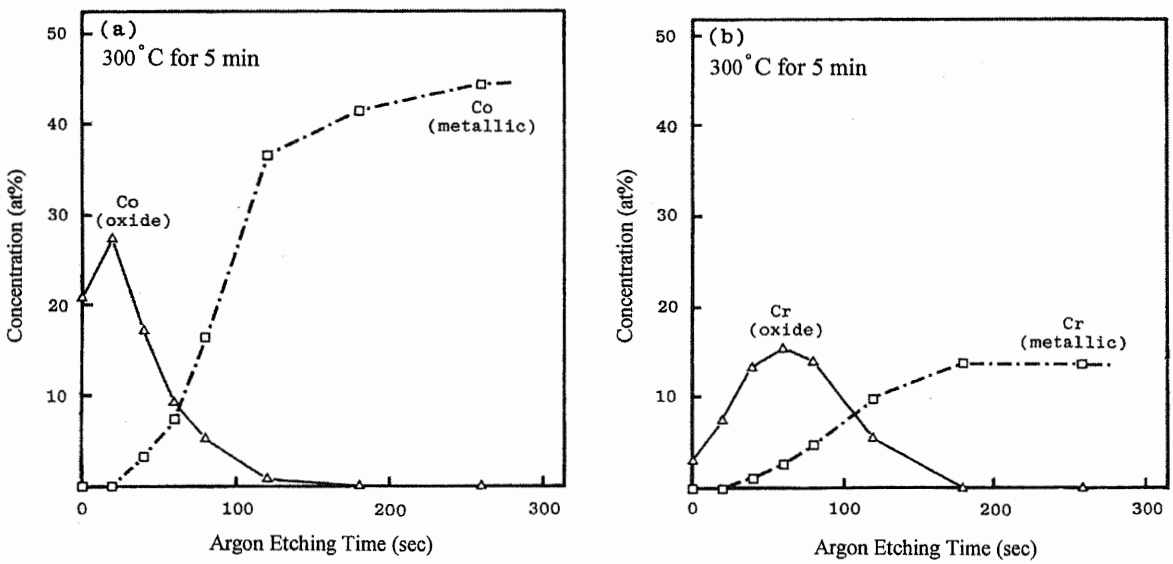


Fig. 2.2-8 Concentrations of the metallic and unknown states of Co (a) and Cr (b) in depth, obtained from the 300°C oxidized Co-Cr alloy surface (Fig. 2.2-5).

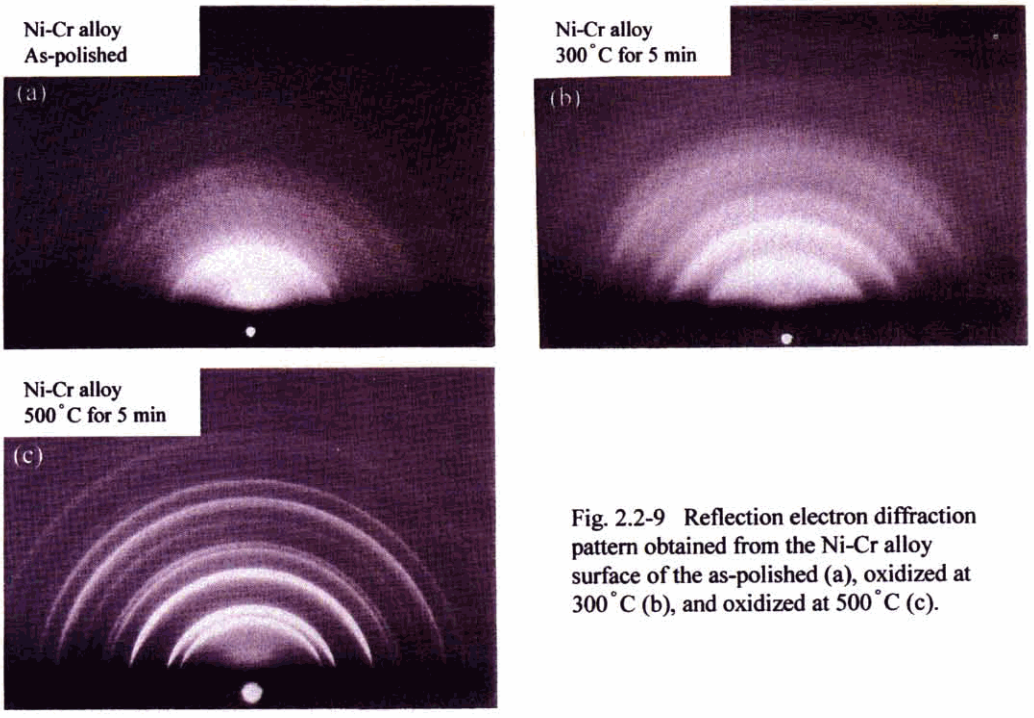


Fig. 2.2-9 Reflection electron diffraction pattern obtained from the Ni-Cr alloy surface of the as-polished (a), oxidized at 300°C (b), and oxidized at 500°C (c).

Table 2.2-2 Lattice spacings and intensities observed by reflection electron diffraction, obtained from the as-polished specimen (Fig. 2.2-9 (a)).

| Measured values by reflection electron diffraction (As-polished) | | Measured values by X-ray diffraction* | | |
|---|---|---|---|---|
| | | Alloy | | |
| dA | I | dA | I | hkl |
| 2.10 | s | 2.063 | vs | 111 |
| 1.80 | m | 1.782 | s | 200 |
| 1.28 | m | 1.259 | m | 220 |
| 1.08 | m | 1.076 | m | 311 |
| | | 1.030 | vw | 222 |
| | | 0.8929 | vw | 400 |
| 0.834 | w | 0.8197 | w | 331 |
| 0.813 | w | 0.7991 | w | 420 |

* Debye-Scherrer method

Table 2.2-3 Lattice spacings and intensities observed by reflection electron diffraction, obtained from the oxidized specimen (Fig. 2.2-9 (c)).

| Measured values by reflection electron diffraction (500°C for 5 min) | | Measured values by X-ray diffraction* | | |
|---|---|---|---|---|
| | | NiO | | |
| dA | I | dA | $I/I_1$ | hkl |
| 2.43 | s | 2.410 | 91 | 111 |
| 2.08 | vs | 2.088 | 100 | 200 |
| 1.48 | vs | 1.476 | 57 | 220 |
| 1.26 | m | 1.259 | 16 | 311 |
| 1.21 | m | 1.206 | 13 | 222 |
| 1.05 | w | 1.0441 | 8 | 400 |
| 0.960 | w | 0.9582 | 7 | 331 |
| 0.934 | m | 0.9338 | 21 | 420 |
| 0.851 | m | 0.8527 | 17 | 422 |
| 0.806 | vw | 0.8040 | 7 | 511 |

* JCPDS card

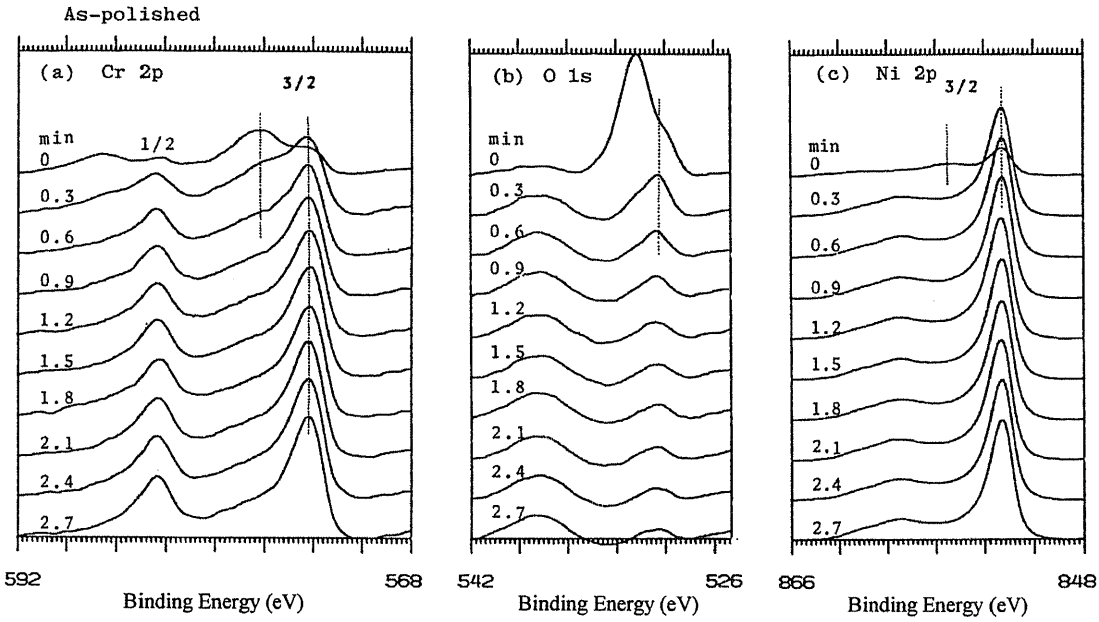


Fig. 2.2-10 Cr 2p (a), O 1s (b), and Ni 2p (c) spectra at different depths obtained from as-polished Ni-Cr alloy specimens, by varying the argon ion etching time (in min).

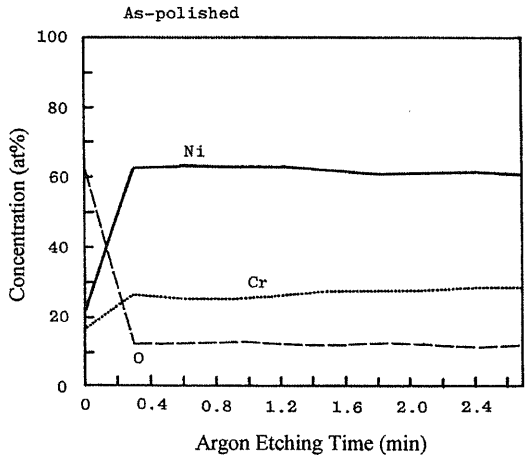


Fig. 2.2-11 Depth variation of concentrations (at%) of Cr, O, and Ni for as-polished Ni-Cr alloy specimens.

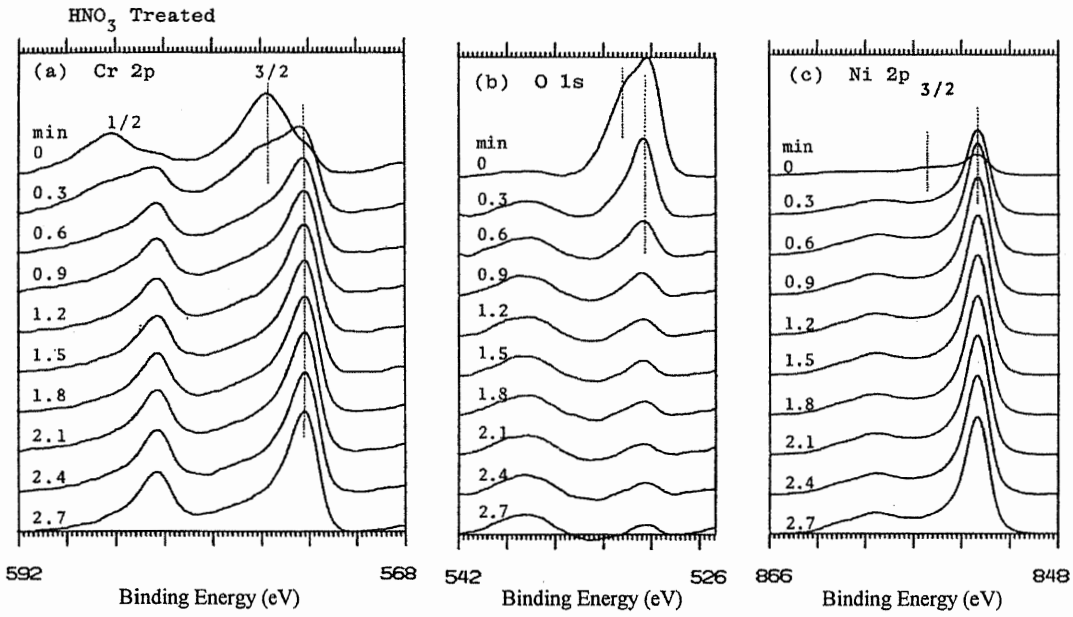


Fig. 2.2-12 Cr 2p (a), O 1s (b), and Ni 2p (c) spectra at different depths obtained from $HNO_3$ treated Ni-Cr alloy specimen by varying the argon ion etching time (in min).

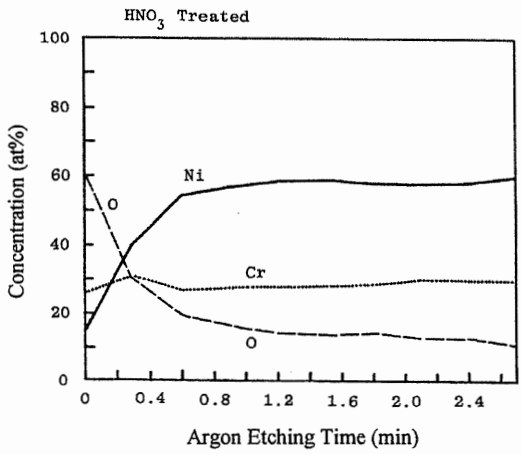


Fig. 2.2-13 Depth variation of concentrations (at%) of Cr, O, and Ni for $HNO_3$ treated Ni-Cr alloy specimens.

Table 2.2-4 Reported oxide chemical shifts $\Delta E_B$ (eV) with reference to the metallic state.

| Element | Oxides | Oxidation states | Energy level | $\Delta E_B$ (eV) Data taken from literature |
|---|---|---|---|---|
| Co | CoO | II | $2p_{3/2}$ | 2.9 [21], 2.2 [4], 2.5 [3], |
| | $Co_3O_4$ | II + III | | 1.8 [3], |
| | $Co_2O_3$ | III | | 1.6 [3], 1.1 [4] |
| Cr | $Cr_2O_3$ | III | $2p_{3/2}$ | 3.0 [21], 2.5 [22], 2.4 [23] |
| | $CrO_3$ | IV | | 4.5 [21], 4.9 [23] |

Table 2.2-5 Measured chemical shifts $\Delta E_B$ (eV) of the unknown peak obtained from the Co-Cr alloy surface before argon ion etching with reference to the metallic state.

| Surface pretreatment | Measured $\Delta E_B$ (eV) | |
|---|---|---|
| | Co $2p_{3/2}$ | Cr $2p_{3/2}$ |
| As−polished | 2.9 | 2.8 |
| 300°C | 1.7 | 2.5 |
| 500°C | 2.2 | 2.3 |

Table 2.2-6 Characterization of the as-polished and oxidized surfaces of the Co-Cr alloy. X: the unknown substance, ?: chemical state not determined by ESCA.

| Surface pretreatments | ESCA | Reflection electron diffraction |
|---|---|---|
| As−polished | Co(II)+Co(O), Cr(III)+Cr(O) | Amorphous |
| 300°C | Co(?), Cr(III) | $Co_3O_4$ + X |
| 500°C | Co(?), Cr(III) | $Co_3O_4$ + X |

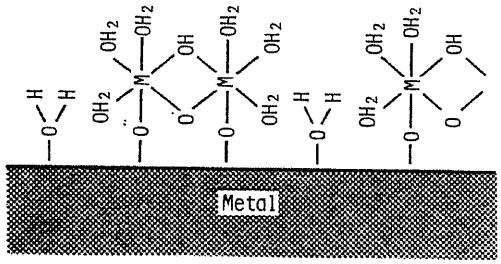


Fig. 2.2-14 Model of passivated surface on stainless steel (Okamoto) [16].

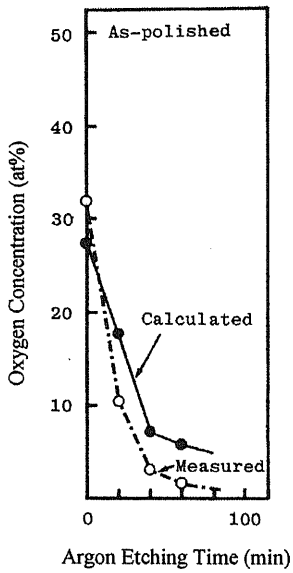


Fig. 2.2-15 Measured oxygen concentration (from Fig. 2.2-4) and calculated oxygen concentration for six coordinated -OH and/or $H_2O$ around the metal ions.

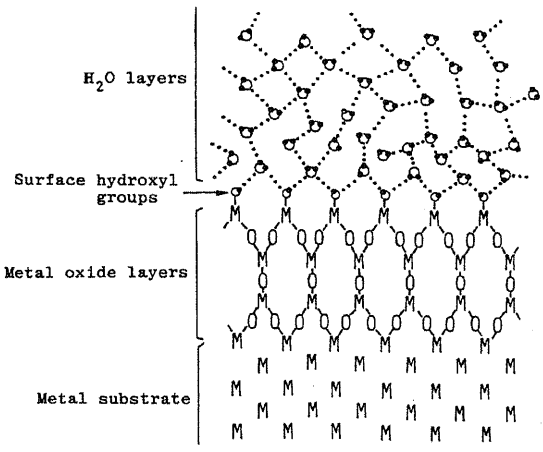


Fig. 2.2-16 Adsorbed -OH and $H_2O$ layer model for metal oxide (Bolger) [18].

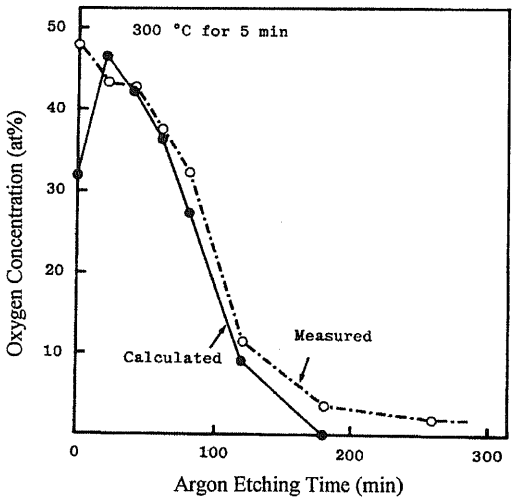


Fig. 2.2-17 Measured oxygen concentration (from Fig. 2.2-7) and oxygen concentration calculated to be necessary to form Co- and Cr-oxides.

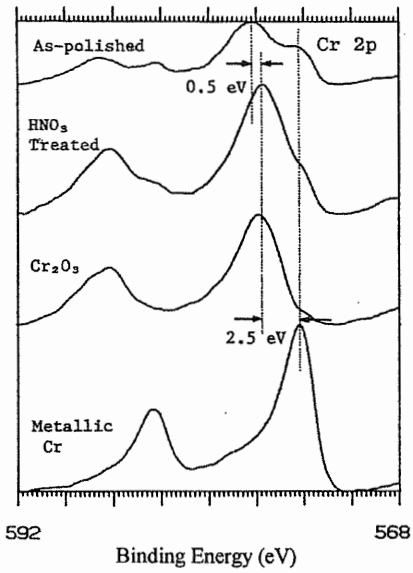


Fig. 2.2-18 The Cr 2p spectra obtained from four specimens: as-polished Ni-Cr alloy surface (unetched), $HNO_3$ treated Ni-Cr alloy surface (unetched), $Cr_2O_3$, and metallic Cr.

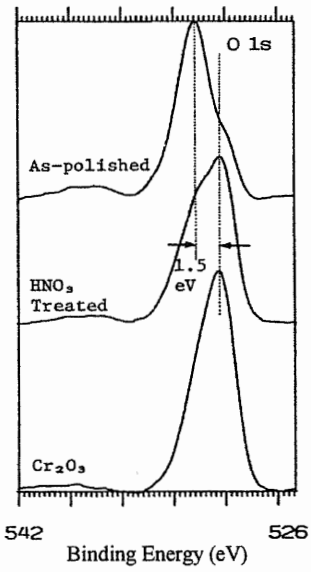


Fig. 2.2-19 The O 1s spectra obtained from three specimens: as-polished Ni-Cr alloy surface (unetched), $HNO_3$ treated Ni-Cr alloy surface (unetched), and $Cr_2O_3$.

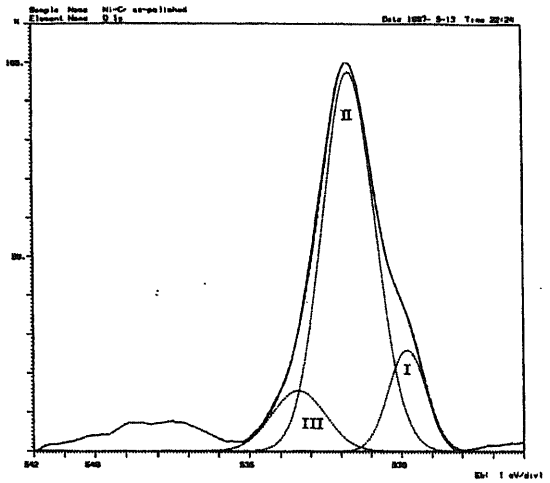


Fig. 2.2-20 The O 1s spectra obtained from as-polished Ni-Cr alloy specimens (unetched), separated into three components.

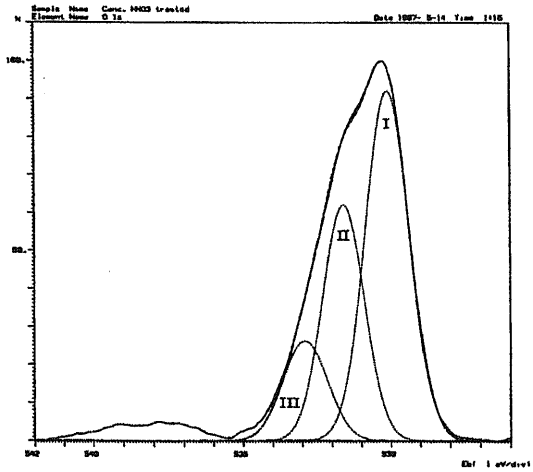


Fig. 2.2-21 The O 1s spectra obtained from $HNO_3$ treated Ni-Cr alloy specimens (unetched), separated into three components.

Table 2.2-7 Peak position and area fraction of the three components in the O 1s spectra in Figs. 2.2-20 and 2.2-21.

| | As-polished | | $HNO_3$ Treated | |
|---|---|---|---|---|
| Ols Spectra Component | Peak Position (eV) | Area (%) | Peak Position (eV) | Area (%) |
| I | 529.8 | 14 | 530.1 | 52 |
| II | 531.7 | 74 | 531.6 | 33 |
| III | 533.4 | 12 | 532.9 | 15 |

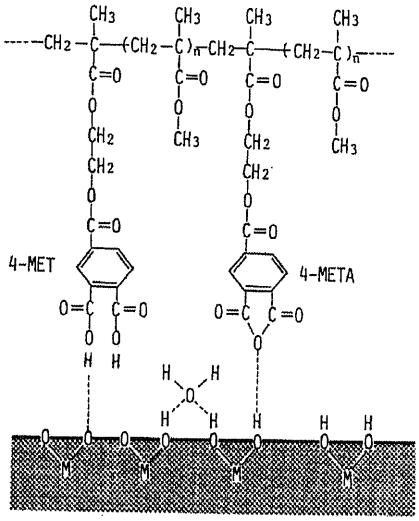


Fig. 2.2-22 Hydrogen bond model for the 4-META side-chain and adsorbed –OH on metal (Masuhara) [20]

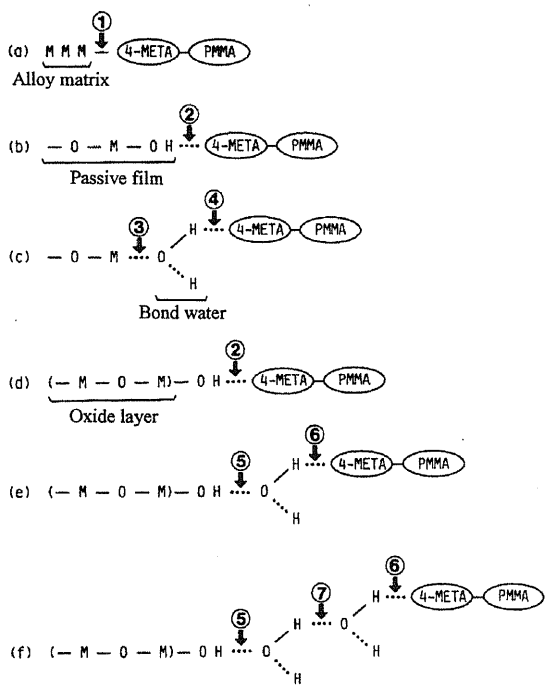


Fig. 2.2-23 Suggested adhesion model of PMMA resin containing 4-META on as polished (a, b, and c) and oxidized (d, e, and f) surface: M is the metal atom, --- hydrogen bond. The chemical bonds which are similar in bonding strength are labeled by the same number at the bonding positions.

## 2.3 Experimental Evidence of Deterioration in Bonding Ability due to Adsorbed Water on Oxide Layer

### 2.3- 1 Introduction

Section 2.2 investigated the bonding ability of 4-META resin to a Co-Cr alloy and showed that the bonding to the as-polished surface was superior to oxidized surfaces heated at 300°C or 500°C. To explain the differences in the two surface states and their influence of the boning ability, the alloy surfaces were analyzed by reflection electron diffraction and ESCA in the previous section. These analysis showed that: the structure of the as-polished surface was an amorphous 2-3 nm thick passive film formed by a mono-layer of six-OH ions and/or $H_2O$ molecules coordinated around $Cr^{3+}$ and $Co^{2+}$ or $Co^{3+}$ metal ions. On alloy surfaces oxidized at 300°C and 500°C, $Co_3O_4$ was predominantly formed and it was covered by a several-molecule thick layer of adsorbed water. It was most likely that the presence of adsorbed water in several molecule thicknesses between the surface oxidized at high temperature and the 4-META side chain was the reason why adhesion to oxidized surfaces was inferior to that to the as-polished surfaces.

The results suggest that good adherence between the 4-META side-chain and oxidized surface is possible when there is no adsorbed water layer on top of the surface oxidized at high temperatures. The hypothesis will be supported experimentally in the present section. In the experiments, the several-molecule thick layer of adsorbed water on the oxidized surface was removed and adhesion of the 4-META resin to the oxidized surface in an atmosphere containing no water vapor was evaluated.

### 2.3-2 Experimental Methods

*Materials*

A 70 mass%Co-30%Cr and 18-8 stainless steel were used. The adhesive was 4-META dental adhesive resin.

*High Temperature Oxidation of Alloy Surface and Dehydration of the Oxidized Surface*

The alloy specimens were soldered to the end of the specimen rod shown in Fig. 2.1-1. The polished alloy specimen was heated at 500°C for 5 min in air in an electric furnace and cooled in air. To dehydrate the adsorbed water on the oxidized surface, the specimen was placed in a silica glass tube of 9 mm$^{\phi}$ outer diameter and air pressure was reduced to $1\times10^{-4}$ Pa with a diffusion pump. The tube was heated at 700°C for 15 min in an electric furnace as shown in Fig. 2.3-1. After cooling, the specimen was sealed in the silica glass tube by an oxygen-propane gas burner under a vacuum of $1\times10^{-4}$ Pa. Figure 2.3-2 shows specimens enclosed in silica glass tubes.

*Adhesion Procedures*

Monomer and polymer of an adhesive resin was dried to eliminate trace amounts of water: the monomer was stored with a drying agent, well-dried anhydrous magnesium sulfate. The polymer was also

dried in a drying furnace at 80°C for 60 min and then stored in a desiccator with silica gel. To prevent adsorption of water molecules on the anhydrous oxidized surface, adhesion procedures were performed in a polyethylene chamber with gloves filled with ultra-high purity argon gas (purity 99.999%; oxygen content below 0.2 ppm; dew point below -70°C) as shown in Fig. 2.3-3. The silica glass tube with the dehydrated alloy specimen was broken in the polyethylene chamber.

Before adhesion, the monomer must be in contact with oxygen to produce TBB peroxide immediately after the addition of TBB to the monomer. To enable this, the preparation was performed in a chamber filled with ultra-dried air (dew point below -60°C) by a dried dish and spatula to avoid contamination with water vapor during mixing. After mixing, the monomer dish was immediately transferred to the argon gas filled chamber. The argon gas pressure was raised so as not to introduce air to the chamber. No-dehydrated specimens (as heated at 500°C) were also bonded in this manner.

*Measurement of Bonding Strength*

All bonded specimens were stored at 37°C for one day in a dry atmosphere after the adhesion treatment and subjected to 20 thermal cycles from liquid nitrogen (-196°C) to water (40°C), alternately for 1 min each before the tensile test. The tensile test was performed on a testing machine with a cross head speed of 2 mm/min as described in section 2.1.

### 2.3-3 Results and Discussion

Figures 2.3-4 and 2.3-5 are the measured bonding strengths obtained from the Co-Cr alloy and 18-8 stainless steel: the results of (a) and (b) were obtained from the as-heated specimens at 500°C in air and from the specimens dehydrated at 700°C in $1\times10^{-4}$ Pa after oxidizing at 500°C in air. All the specimens of both alloys without dehydration (no-dehydration) showed interface failure at the periphery, (a) in Figs. 2.3-4 and 2.3-5. Most of the dehydrated specimens showed cohesive failures as in (b), and the average bonding strength was higher than in (a). The (b) averages were 41.3 MPa and 39.1 MPa for the Co-Cr alloy and 18-8 stainless steel, similar to the average 39.2 MPa obtained previously from as-polished Co-Cr alloy specimens (section 2.1).

Here the different oxidation states of the oxides must be considered by heating at 700°C under a vacuum of $1\times10^{-4}$ Pa. The structure of the oxide layer formed by heating Co-Cr alloy and 18-8 stainless steel at 500°C in air were as follows: the outer surface of the oxide of the Co-Cr alloy was $Co_3O_4$-rich and the inner part of the oxide layer was $Cr_2O_3$-rich as shown in Fig. 2.2-8. On 18-8 stainless steel, $FeCr_2O_4$ co-existed with $Cr_2O_3$ or a solid solution of $Cr_2O_3$-$Fe_2O_3$[1]. When these alloys were heated at 700°C at $1\times10^{-4}$ Pa, the conditions determining the reduction of these oxides can be estimated thermodynamically by comparing the oxygen partial pressure in $1\times10^{-4}$ Pa with the dissociation pressure of oxide calculated from the Gibbs free energies, $\Delta G$. The dissociation pressure, $\pi O_2$, of oxide and $\Delta G$ are related by [2]:

$$\Delta G = RT\ell n\pi O_2 \quad \text{---------- (2.3-1)}$$

where $R$ is the gas constant and $T$ the absolute temperature. The values of $\log \pi O_2$ at 700℃ are calculated from the $\Delta G$ [3] shown in Table 2.3-1. The oxygen partial pressure, $P_{O2}$, at $1\times10^{-4}$ Pa is about $2.6\times10^{-10}$ atom, ($\log P_{O2}$ = -9.6), and oxides where $\log \pi O_2 > \log P_{O2}$ will be reduced. As Table 2.3-1 shown, $Co_3O_4$ on the Co-Cr alloy is reduced to CoO. If the oxidized Co-Cr alloy is heated at temperatures lower than 700°C in $1\times10^{-4}$ Pa, $Co_3O_4$ will not be reduced. However, the adsorbed water molecules are not completely removed from the oxide surface even when the $Fe_2O_3$ and $TiO_2$ are heated at 700°C or 800°C[4].

On the 18-8 stainless steel, there was no change in oxide states by heating to 700°C at $1\times10^{-4}$ Pa. As shown in Fig. 2.3-5, all specimens in (a) showed partial interface failure at the periphery while the bonding ability in (b) was superior to that in (a). Since the same oxides were formed on both specimens in (a) and (b), the difference was ascribed to adsorbed water on the oxidized surface in (a). On the Co-Cr alloy, there were differences in the oxides in (a) and (b). However, the (a) and (b) failures in Fig. 2.3-4 were similar to those in Fig. 2.3-5. Therefore, the presence or absence of adsorbed water on the oxide layer probably determines the failure types in (a) and (b) of Figs. 2.3-4 and 2.3-5. It is concluded from these results that the water adsorbed on the oxide layer decreased the bonding between the oxidized alloy surface and 4-META resin.

## 2.3-4 Conclusions

The effect of a several-molecule thick water layer adsorbed on the top of oxide surfaces on the bonding ability of 4-META resin was examined with a Co-Cr alloy and 18-8 stainless steel. The alloys were heated at 500°C in air and dehydrated by heating to 700°C at $1\times10^{-4}$ Pa in the silica glass tube. Dental adhesive resin containing 4-META was bonded to these alloy surfaces and after thermal cycle treatment the bonding strengths and failure types for the dehydrated surfaces were compared with surfaces heated at 500°C. In both alloys, the specimens oxidized at 500°C in air showed partial interface (alloy/resin) failure at the periphery. However, except for a few cases, dehydrated specimens displayed cohesive failure and the bonding strength was similar to that of the as-polished Co-Cr alloy, showing excellent bonding ability. The experimental evidence showed that the bonding ability of the 4-META resin to the dehydrated oxide layer surface was excellent when adhesion procedures were performed in an atmosphere excluding water vapor. This supports the hypothesis described in section 2.2 that adsorbed water on the oxide layer leads to a deterioration in the bonding ability of resin and oxidized alloys.

## REFERENCES

1) Miyake S: A study of oxide films on metal surface with cathode ray diffraction (Part Ⅱ) Fe, Cr, Ni, and their alloys. *Sci Paper IRCR*, **31**: 161-173, 1937.

2) Fueki K: T-ΔG diagram and its applications to high temperature oxidation of pure metals. *Denki Kagaku*, **26**: 292-297, 1958 (in Japanese).

3) Kubaschewski, O and Alcock CB: *Metallurgical thermo-chemistry (5th ed.)* Pergamon Press Ltd., Oxford, 1979, pp. 378-384.

4) Nakamae K: *Adhesion and interface chemistry*, *Nippon-Gomu-Kyoukai-shi*, **57**: 482-491, 1984 (in Japanese).

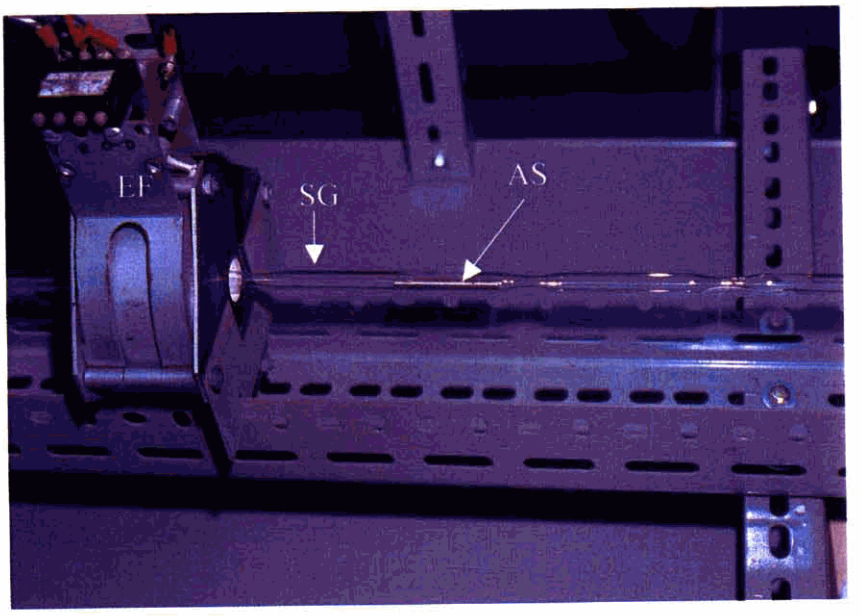


Fig. 2.3-1 Apparatus for dehydration of the oxide surface. EF: electric furnace, AS: alloy specimen, SG: silica glass tube.

Fig. 2.3-2 Alloy specimens enclosed in silica glass tubes under $1 \times 10^{-4}$ Pa after dehydration.

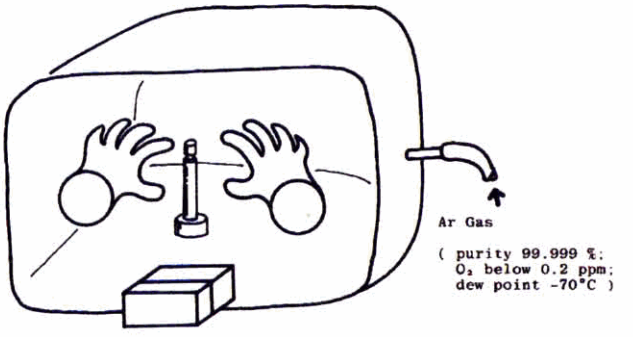


Fig. 2.3-3 Argon gas chamber for adhesion procedures.

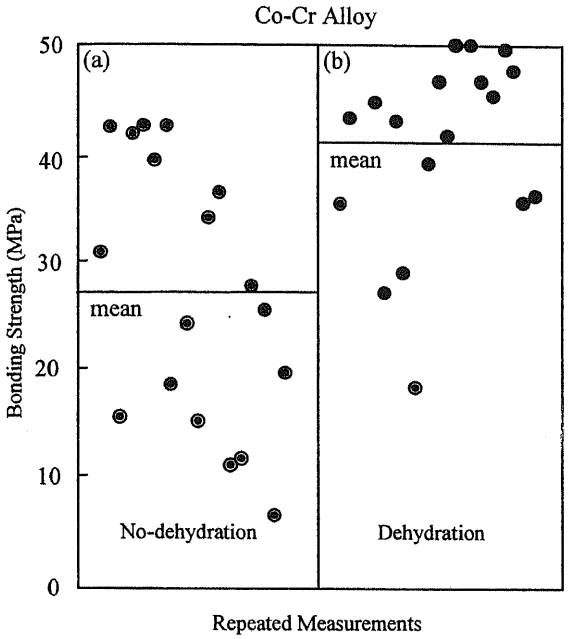


Fig. 2.3-4 Results of bonding strength measurements obtained from specimens bonded to Co-Cr alloy surfaces. All specimens were subjected to thermal cycles. (a): as-heated specimen oxidized at 500℃ in air, (b): specimen dehydrated at 700℃ in $1 \times 10^{-4}$ Pa after heating 500℃ in air. The horizontal line means indicate the average of repeated tests.

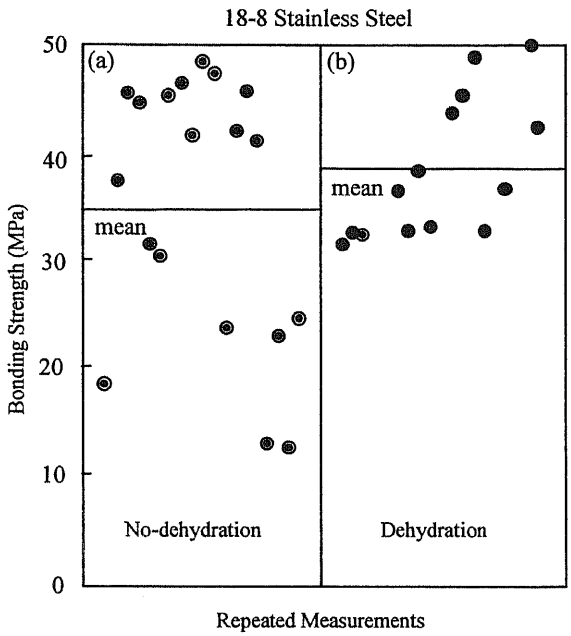


Fig. 2.3-5 Results for the 18-8 stainless steel. Conditions as in Fig. 2.3-4.

Table 2.3-1 Dissociation pressure, $\pi O_2$, of oxides and $\Delta G$ at 700℃.

| | Reaction | $\Delta G_{973}$ (cal)[6] | $\log \pi_{O_2}$ |
|---|---|---|---|
| (1) | $2<Co>+O_2=2<CoO>$ | −78,913 | −17.7 |
| (2) | $6<CoO>+O_2=2<Co_3O_4>$ | −18,712 | −4.2 |
| (3) | $4<Fe_3O_4>+O_2=6<Fe_2O_3>$ | −53,815 | −12.1 |
| (4) | $\frac{4}{3}<Cr>+O_2=\frac{2}{3}<Cr_2O_3>$ | −138,218 | −31.0 |
| (5) | $2<Fe>+O_2+2<Cr_2O_3>=2<FeCr_2O_4>$ | −108,053* | −24.3 |

*extrapolated value

## 2.4 Adhesive Ability of 4-META Adhesive Resin to the Cleaned Metal Surface Obtained by Hydrogen Gas Redaction

### 2.4-1 Introduction

As discussed in the sections 2.1 and 2.2, the adhesion of 4-META resin to the as-polished surface of Co-Cr alloy, which is covered with a passive film, was superior to that of the alloy surface oxidized at high temperatures. For passive films formed on the as-polished surface, the adhesive ability of the Ni-Cr alloy was inferior to that of the Co-Cr alloy. This shows that the adhesive ability of the 4-META resin was greatly affected by the surface state of the alloys. The state of a metal surface varies by metal type and surface treatment. On base metals, different amounts and kinds of oxides form on the surface. On precious metals which do not form oxides, the metal surface adsorbs gas and water molecules to decrease surface energy, and the adsorbed species and amounts vary by the kind of metal. Since the oxides and adsorbed gas layers exist between the adhesive and the metal substrate, it is critical to understand the roles of the adsorbed layer, oxides, and passive film on the adhesion.

The present study investigated the adhesion of 4-META resin to cleaned metal surfaces, obtained by heating the metal specimens in flowing hydrogen gas. As the cleaned metal surfaces adsorb oxygen and water molecules when the surface is exposed to air, adhesion procedures were performed in a polyethylene chamber filled with ultra-high purity argon gas without oxygen, water, or other contaminating species.

### 2.4-2 Materials and Methods

*Materials*

The pure metals and the alloy studied were gold, platinum, palladium, silver, copper, nickel, cobalt, iron and chromium of a purity better than 99.99%, and 18-8 stainless steel. The pure metal specimens (except for chromium) were made by soldering pure metal chips to 18-8 stainless steel rod for the tensile test as shown in Fig. 2.1-1 (section 2.1). The chromium specimen was made by electro-plating chromium on a mild steel rod of the same size as the 18-8 stainless steel rod. Both the rod specimens and 18-8 stainless steel circular block were metallographically polished to eliminate mechanical factors affecting the bonding strength.

The dental adhesive resin was 4-META resin. The monomer and polymer of the adhesive resin were dried to eliminate trace amounts of water: the monomer was dehydrated by a drying agent, well-dried anhydrous magnesium sulfate. The polymer was dried in a drying furnace at 70°C for 60 min and stored in a silica gel desiccator.

*Hydrogen Gas Reduction*

Figure 2.4-1 shows the apparatus for hydrogen gas reduction used to obtain the cleaned metal surfaces: the pipes were stainless steel except for the reduction tube which was made of silica glass. The silica glass tube was narrowed in several places to prevent movement of specimens and to facilitate sealing

of the specimen in the glass tube. Preparatory evacuation was done by an oil rotary pump and a diffusion pump up to $1\times10^{-4}$ Pa. The stainless steel pipes and silica glass tube were baked by a gas burner under evacuation to eliminate oxygen and water molecules adsorbed on the inner surface of the pipes.

With deoxidizing oxides of metals having a strong chemical affinity for oxygen, ultra-high purity hydrogen gas is necessary because traces of water and oxygen molecules pollute the metal surface[1]. For example, a stream of extremely dry hydrogen gas is necessary to reduce the Cr-oxide, $Cr_2O_3$ to metallic chromium by equation (2.4-1): the partial pressure ratio of water to hydrogen is as in equation (2.4-2) in terms of the standard Gibbs energy change of the reaction (2.4-1). Table 2.4-1 shows the values of the Gibbs energy change and the partial pressure ratio at 800℃, 900℃, and 1000℃.

$$Cr_2O_3 + 3(H_2) = 3(H_2O) + 2Cr \quad \text{---------- (2.4-1)}$$

$$1/3\Delta G^\circ_T = -4.574T \log(P_{H_2O} / P_{H_2})_{eq} \quad \text{---------- (2.4-2)}$$

The reduction has to be carried out in flowing hydrogen, containing less than $6.5\times10^{-4}$% water at 900℃. The hydrogen gas used to deoxidize the metal surface was ultra-high purity gas, purity better than 99.99999%; oxygen below 0.2 ppm; dew point -70°C (ca. 0.0003%). A U-shaped tube including an oxygen removal agent (Oxyout, Ohsaka Sanso Co., Ltd.) was attached between the hydrogen gas cylinder and the silica glass reduction tube and it maintained the oxygen content below 0.05 ppm. The metal specimen in the silica glass tube was heated by an electric furnace from the outside of the tube under a hydrogen gas flow of 100 mℓ/min. Deoxidation of the metal specimen for adhesion was confirmed visually by the color change of oxidized chips of metal, which oxidized by pre-heating in air and then placed in the silica glass tube. Heating time was 5 min and the heating temperatures for the reduction were 900°C for the chromium, iron, cobalt, and 18-8 stainless steel, 700°C for the copper and nickel, and 500°C for the gold, platinum, palladium, and silver. The silica glass tube was evacuated to $1\times10^{-4}$ Pa after the reduction treatment and then melted and cut by a gas burner at the narrow part to enclose the deoxidized metal specimen.

*Adhesion Procedures*

Adhesion procedures were performed in a polyethylene chamber with gloves filled with ultra-high purity argon gas (purity 99.999%; oxygen content below 0.2 ppm; dew point below -70°C) as shown in Fig. 2.3-3. The silica glass tube was broken to obtain the deoxidized metal specimen in the polyethylene chamber. Before adhesion, the monomer must be in contact with oxygen to produce TBB peroxide immediately after the addition of TBB to the monomer. Therefore the monomer preparation was performed in a chamber with ultra-dried air (dew point below -60°C) and using a dried dish and spatula to avoid contamination with water vapor during mixing. After mixing for 40 sec, the monomer dish was immediately transferred to the argon gas filled polyethylene chamber where the argon gas pressure was raised so as not to introduce air. In section 2.1, the adhesive resin layer was maintained at 50 μm by first

placing the specimen in contact with the circular block and next removing it to apply the resin. In this study the thickness of the resin layer could not be kept constant, because touching the cleaned metal surface to the circular block would contaminate it with the water molecules adsorbed on the surface of the circular block.

*Evaluation of Adhesive Ability*

The bonded specimens were stored at 37°C in a dry chamber for 24 hr after the adhesion procedure. Before testing, the specimens were thermal-cycled 20 times, 1 min in a water bath at 40°C followed by 1 min in liquid nitrogen (-196°C). The tensile test for the bonding strength measurement was performed on a testing machine with a crosshead speed of 2 mm/min.

### 2.4-3 Results and Discussion

Trace amounts of hydrogen gas remain on the metal surface though the hydrogen gas was evacuated to $10^{-4}$ Pa after the reduction procedure. Copper, gold, and silver do not adsorb hydrogen gas, however, chromium, iron, nickel, cobalt, platinum, and palladium do[2]. The cleanliness of the metal surface was not evaluated in this study. The study examined the adhesive ability of 4-META resin to the metal surface without passive and oxide films and did not evaluate the effect of adsorbed hydrogen in the metal surface.

Figure 2.4-2 shows the measured bonding strengths with failure types (Table 2.1-1 in section 2.1) after the thermal cycles. There was a wide scattering of bond strengths with 18-8 stainless steel, chromium, iron, and cobalt, and all showed cohesive failure in the resin. The bonding strength is strongly affected by factors such as thickness of the resin layer, inclusion of air in the resin, and variations in the monomer-polymer ratio. However, the adhesive ability at the metal/resin interface is superior to the cohesion of the resin when the fracture is a cohesive failure, even though the bonding strength is low. Since the appearance of the fracture rather than the bonding strength reflects the characteristics of the metal surface, the type of failure is important in evaluating the adhesive ability.

It has been shown that a passive film on an alloy containing chromium was effective in obtaining good bonding strength with 4-META resin (section 2.2). However, the present study showed that excellent bond strength was obtained on the cleaned surface without a passive film. Therefore the existence of a passive film and oxide layer at the alloy/resin interface is not essential for the alloy-resin bonding.

Adhesion with nickel exhibited the poorest adhesive ability of the base metals as all failures were interface failures at the periphery of the fracture area. Of the precious metals, the adhesion with palladium and platinum was inferior to silver and gold. The adhesive ability of the 4-META resin to the cleaned surfaces obtained by the hydrogen gas reduction method decreased in the following order on the base of both the measured bonding strength and that calculated from the interface fracture ratio: Cr = Co = Fe > Cu > Ag > Au = Ni > Pt > Pd. Platinum and palladium have the poorest adhesive ability. The best adhesive ability was with chromium, cobalt, iron, and 18-8 stainless steel. Mogi[3] had reported no adhesive ability of pure gold with 4-META resin. The bonding strengths to Cr, Ni, and Co were in order Cr > Ni >> Co,

different from the present study. The adhesive ability with metallic Ni was lower than that with metallic Cr. This is the reason why the adhesive ability of the Ni-Cr alloy was inferior to that of the Co-Cr alloy as described in section 2.2.

Mogi investigated the adhesive ability of pure metal surfaces exposed to air after metallographical polishing. Since small amounts of water molecules adsorbed on the alloy surface cause deterioration of the adhesive ability between the resin and alloy as shown in the section 2.3, the differences may be a result of characteristic differences in the adsorption ability of water molecules and other gas molecules on the metals and/or on the chemical affinity of oxygen to the metals.

### 2.4-4 Conclusions

The cleaned metal surface was obtained by hydrogen gas reduction. Excellent adhesive ability was obtained on chromium, cobalt, iron, and 18-8 stainless steel, showing that a passive or oxide film on the metals does not pay an essential role in the adhesion. Nickel showed the poorest adhesive ability of the base metals investigated in this study. The adhesive ability of platinum and palladium was not as good as gold.

## REFERENCES

1) Keii Y: *Adsorption*, Kyoritu Syuppan Ltd., Tokyo, 1965, pp. 11-61 (in Japanese).

2) Ohno H, Araki Y, Sagara M: The adhesion mechanism of dental adhesive resin to the alloy - Experimental evidence of the deterioration of bonding ability due to adsorbed water on the oxide layer -. *Dent Mater J*, **5**: 211-216, 1986.

3) Mog T: Studies on adhesion of methacrylic resin to cobalt-chromium alloy for denture base - Effects of 4-metacryloxyethyl trimellitate anhydride monomer -. *J Jpn Prosthodont Soc*, **23**: 660-676, 1979 (in Japanese).

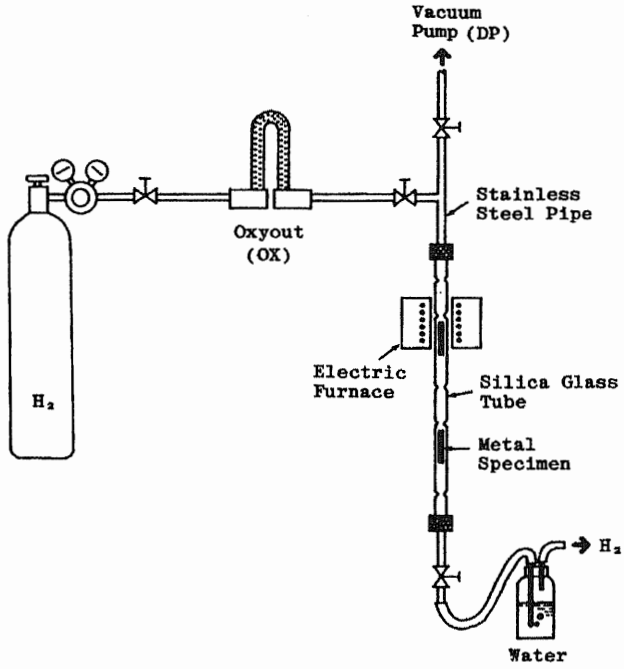


Fig. 2.4-1 Apparatus for hydrogen gas reduction: $H_2$ ; the hydrogen gas cylinder; OX; the u-shaped tube including oxygen removal agent Oxyout; DP; the oil diffusion pump.

Table 2.4-1 Values of the Gibbs energy change and partial pressure ratio of $H_2O$ to $H_2$ at different temperatures.

| °C | K | $\Delta G_T$(cal) | $(P_{H_2O}/P_{H_2})_{eq}$ |
|---|---|---|---|
| 800 | 1073 | 84,839 | $1.7\times10^{-6}$ |
| 900 | 1173 | 83,530 | $6.5\times10^{-6}$ |
| 1000 | 1273 | 82,270 | $2.0\times10^{-5}$ |

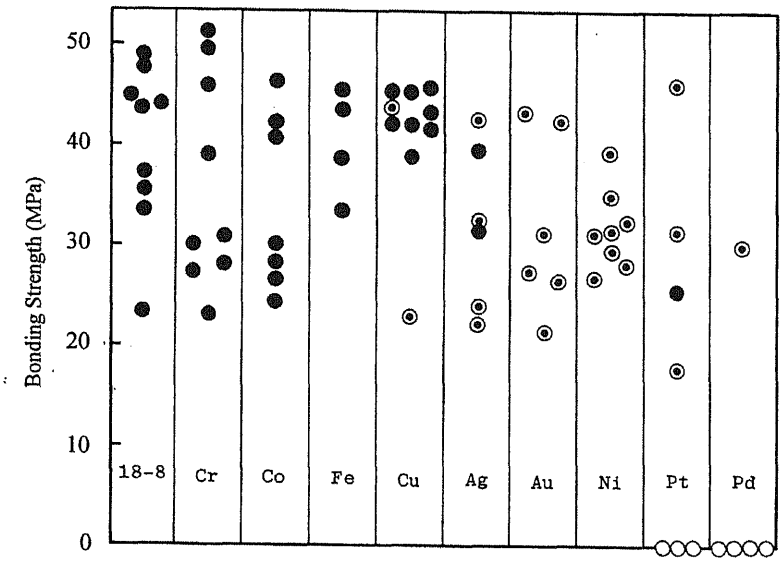


Fig. 2.4-2 Measured bonding strengths with failure type after thermal cycles (see Table 2.1-1).

Table 2.4-2 Measured and calculated bonding strengths.

| Metals and Alloy | Bonding Strength (measured)(MPa) | Interface Failure Ratio (%) | Bonding Strength* (calculated)(MPa) |
|---|---|---|---|
| 18-8 Stainless Steel | 39.7 | 0 | 43.5 |
| Cr | 36.5 | 0 | 43.5 |
| Co | 34.0 | 0 | 43.5 |
| Fe | 40.4 | 0 | 43.5 |
| Cu | 41.4 | 2 | 42.3 |
| Ag | 32.4 | 5 | 40.3 |
| Au | 29.9 | 7 | 35.7 |
| Ni | 31.5 | 25 | 28.5 |
| Pt | 17.1 | 49 | 14.1 |
| Pd | 0.6 | 86 | 0 |

* Calculated from equation (2.1-1)

# Chapter 3

# DESTRUCTION MECHANISM OF METAL-RESIN ADHESION DUE TO THE WATER

## 3.1 Destruction of Metal-Resin Adhesion due to Water Penetrating through the Resin

### 3.1-1 Introduction

Generally, joints of dental adhesive resin bonded to dental alloys weaken in wet environments though adhesion is strong in dry environments. One example is the separation or peeling at the bonded interface of metallic dentures bonded with acrylic resin, which occurs after long term use in the oral environment. Metal bridges bonded to teeth also fall off after extended use. The degradation mechanism of the adhesion interface between dental adhesive resin and alloys by water has not been established. A major problem awaiting solution is the attainment of good durability of bonding joints exposed to water. Both the permeation path of water to the adhesion interface and the water content that degrades the interface were determined in the present section.

### 3.1-2 Materials and Methods

*Permeation Path of Water to the Adhesion Interface*

Two types of specimens were made to determine whether the predominant path of water permeation to the interface is: (1) diffusion through the resin, or (2) transport along the metal/resin interface. The first type (Type A) has no exposed bond joints; the resin was a 0.2 mm PMMA film bonded with 4-META resin on an 18×18 mm metallographically polished mild steel plate with sealed bond joints as shown in Fig. 3.1-1(a). The second type (Type B) has exposed bond joints as shown in Fig. 3.1-1(b), and was bonded with three different PMMA film thicknesses, 0.1, 0.2, and 0.3 mm. Immediately after bonding with 4-META resin a 20 kg load was applied for 5 min to the two types of specimen to maintain the 4-META resin thickness of 0.05 mm. The specimens were stored in a dry chamber at 37°C for 24 hr for adequate curing before immersion in distilled water at 37°C.

*Analysis of Water Content at the Adhesion Interface*

Water content at the adhesion interface was calculated from the solution to Fick's second equation (3.1-1) [1]. The water content at the interface of the metal and a bonded resin film of thickness $\ell$ as shown in Fig. 3.1-2 is given by equation (3.1-2), assuming that there is no water flux at the metal interface:

$$\frac{\partial C_x}{\partial t} = D\frac{\partial^2 C_x}{\partial X^2} \quad \text{---------- (3.1-1)}$$

$$\frac{C(t)}{C(\infty)} = 1 - \frac{4}{\pi}\sum_{n=0}^{\infty}\frac{(-1)n}{2n+1} \times \exp\left[-D(2n+1)^2\pi^2 t/4l^2\right] \quad \text{---------- (3.1-2)}$$

Here, $C(t)$ is the concentration at the interface ($x = 0$) and $C(\infty)$ is the concentration at equilibrium; $D$ is the diffusion coefficient and $t$ is time. Since the diffusion coefficient of water molecules through PMMA depends on temperature and water content, the minimum ($C = C_\infty$), $D_{\min}$, and the maximum

($C=0$) $D_{max}$, values, of $D$ at 37°C were estimated from these values at 25°C reported in the literature [2] using the following two equations,

$$D(T)_{C=0} = a_{C=0} \exp(-b/T) \quad \text{---------- (3.1-3)}$$

$$D(C)_T = D(0)_T \exp(-kC) \quad \text{---------- (3.1-4)}$$

where $a_{C=0}$, $b$, and $k$ are constant. The constant $b$ was determined to be 4.621×103 K from the slope of the linear portion of $D$ vs. $1/T$ plot in the 25°C to 70°C temperature range reported by Kawasaki[3], assuming that $b$ was independent of water content. The constants $a$ and $k$ which were assumed independent of temperature were determined to be $7.343\times10^{-2}$ $cm^2$ $sec^{-1}$ and $3.416\times10^{1}$ based on data reported in the literature[2]. The $D_{min}(C=C_\infty)$ and $D_{max}(C=0)$ values thus obtained were $1.414\times10^{-8}$ and $2.484\times10^{-8}$ $cm^2$ $sec^{-1}$.

## 3.1-3 Results

*Permeation Path of Water to the Adhesion Interface*

Figures 3.1-3 (a) and (b) were obtained from the mild steel specimens of Type A specimens shown in Fig. 3.1-1 (a) which kept in a dry environment and in water for 5 days, as observed through the resin film. There were no changes on specimen (a), and many black spots on the specimen (b) surface after immersion. After immersion of specimens (b) for several hours, white spots appeared on the surface and they changed to brown and finally became black after 5 days. Figure 3.1-4 shows surface states of Type B specimens with three different film thicknesses, 0.15 (a), 0.25 (b), and 0.35 mm (c) after immersion for 5 days. The change in the surface appearance was more remarkable with thinner films. Both 0.15 and 0.25 mm the resin films separated completely from the metal surface while the 0.35 mm film was only partially separated. The results in Figs. 3.1-3 and 3.1-4 indicate that diffusion of water molecules to the resin/metal interface is primarily through the resin layer and not by transport along the resin/metal interface.

*Analysis of Water Content at the Adhesion Interface*

Figure 3.1-5 shows the relationship between film thickness and water content, $C(t)/C(\infty)$, at the interface, obtained from equation (3.1-2). At 0.1 days immersion, the ranges of the results calculated using the $D_{min}(C=C_\infty)$ or the $D_{max}(C=0)$ are represented by the shaded area. The relation between film thickness and water content with respect to the equilibrium water concentration of PMMA represented at other times were obtained with the average $D$ value at 37°C.

## 3.1-4 Discussion

Durability in wet surroundings is of prime importance in adhesively bonded metal structures in the biomaterials field. Many investigations[4-13] of industrial applications have studied degradation due to

moisture permeation into bonded joints. However, no such studies have been reported in the biomaterials field. 4-META resin which is comonomer with MMA, containing 5 mass% 4-META and having both hydrophilic and hydrophobic groups, bonds strongly with tooth structures[14] and dental alloys[15]. However, weakening of joints by immersion in water has been observed in some dental alloys.

Brewis et al.[9] have reported that water molecules enter joints by diffusion through the adhesive rather than by passage along the interface of the aluminum/epoxy resin. This has also been shown for bonding of aluminum alloy/polysulfone with STEM and ESCA by Ko, et al.[13], and also with adhesion of dental adhesive resin/mild steel by the experiments in the present study. The kinetics of the fracture mechanism are governed by the rate of diffusion of water through the adhesive to the interface[11, 16]. Water molecules diffuse through the PMMA and 4-META resin because the water molecule diameter is less than 0.28 nm, smaller than the interchain distance in the resin, and because the polarity of the carbonyl group in PMMA attracts water molecules. As a result PMMA has an equilibrium water concentration of approximately 2 mass%. The diffusion rate of water molecules through polymer materials may be treated as Fickian[16), 17)] or non-Fickian[12]. In the present study, the diffusion rate is calculated as Fickian.

### 3.1-5 Conclusions

Polymethyl methacrylate (PMMA) film bonded by 4-META dental adhesive resin to mild steel was used as a specimen to study the mechanism of water permeation into the adhesive interface. Water entered the interface by diffusion through the resin rather than by passage along the interface. The water content penetrated to the interface was calculated from the solution to Fick's second equation. The degradation at the interface will be discussed with respect to the water content in section 3.3.

## REFERENCES

1) Crank J: in "*The mathematics of diffusion*" 2nd ed., Clarendon Press, Oxford, 1975, p.7.

2) Takizawa A: The Society of Polymer, in " *Kohbunshi to Mizu (Polymer and Water)*" 1st ed., Saiwai Shyobou, Tokyo, 1972, p. 233 (in Japanese).

3) Kawasaki K, Sekita Y: Sorption and diffusion of water vapour in Polymethyl methacrylate. *Ohyo Butsuri (Applied Physics)*, **26**: 678-678, 1957.

4) Mostovoy S, Ripling E.J: Influence of water on stress corrosion cracking of epoxy bonds. *J Appl Polymer Sci*, **13**: 1083-1111, 1969.

5) Kerr C, Macdonald N, Orman S: Effect of hostile environments o adhesive joints. *Brit Polymer J*, **2**: 67-72, 1970.

6) Gledhill R.A, Kinloch A.J: Environmental failure of structural adhesive joints. *J Adhe*, **6**: 315-330, 1974.

7) Getting M, Baker F S Kinloch A J: Use of Auger and X-ray photoelectron spectroscopy to study the locus of failure of structural adhesive joints. *J Applied Polymer Sci*, **21**: 2375-2392, 1977.

8) Brewis D.M, Comyn J, Cope B.C, Moloney A.C: Effect of carriers on the performance of aluminium alloy joints bonded with an epoxide-polyamide adhesive. *Polymer*, **21**: 344-351, 1980.

9) Brewis D M, Comyn J, Tegg J L: The durability of some epoxide adhesive-bonded joints on exposure to moist warm air. *Int J Adhe. Adhe*, **1**:35-39, 1980.

10) Brockmann W, Hennemann O D Kollek H: Surfaced properties and adhesion in bonding aluminum alloys by adhesives. *Int J Adhes Adhe*, **Jan**: 33-40, 1982

11) Brewis D M, Comyn J Shalash R J A: The effect of moisture and temperature on the properties of an epoxide-polyamide adhesive in relation to its performance in single lap joints. *Int J Adhe Adhe,* **Oct**: 215-222, 1982.

12) Marsh L.L, Lasky R, Seraphim D.P, Springer G.S: *IBM J Res Devel*, **28**: 655, 1984.

13) Ko C U, Wightman J P: Experimental analysis of moisture intrusion into the Al/Li-polysulfone interface. *J Adhe*, **25**: 23-29,1988.

14) Nakabayashi N, Takeyama M, Kojima K, Masuhara M: Studies on dental self-curing resins, (Part 20) Adhesion mechanism of 4-META/MMA-TBB resin to dentin. *J Jpn Soc Dent Apparat Mater*, **23**: 34-39, 1982 (in Japanese).

15) Tanaka T, Nagata K, Nakabayashi N, Masuhara E: Application of 4-META on adhesive opaque resin (Part 1) Adhesive strength and the stability. *J Jpn Soc Dent Apparat Mater*, **20**: 79-84, 1979 (in Japanese).

16) Shen C, Sppringer G.S: "*Environmental Effects on Composite Materials*", Technomic Publishing, Lancaster, 1981, pp. 15-33.

17) Brewis D.M, Comyn J, Tredwell S.T: Diffusion of water in some modified phenolic adhesives. *Int J Adhe Adhe*, **7**: 30-32, 1987.

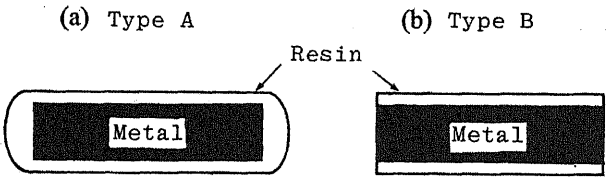


Fig. 3.1-1 Models of specimens for observation of the path of intrusion of water to the adhesion interface of the metal/resin, Type A has no joint exposed to water, Type B has exposed joints. Changes in the mild steel surface were observed through the resin film after different periods of immersion.

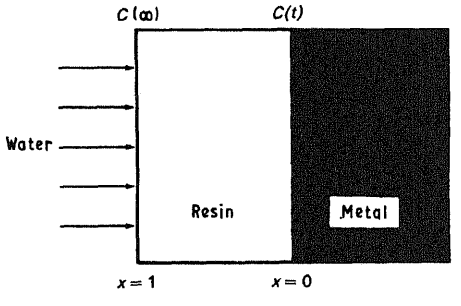


Fig. 3.1-2 Diffusion model to calculate water content at the adhesion interface.

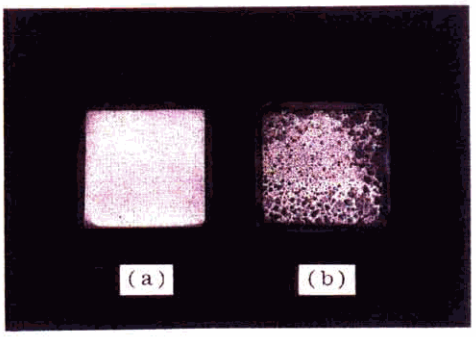


Fig. 3.1-3 Type A specimen (Fig. 3.1-1 (a)) before (a) and after (b) immersion in water at 37℃ for 5 days.

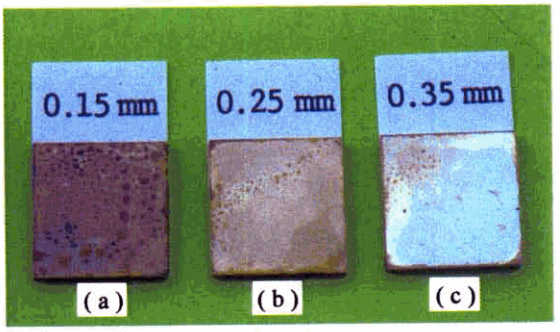


Fig. 3.1-4 Type B specimen (Fig. 3.1-1 (b)) with different resin thicknesses, 0.15 (a), 0.25 (b), and 0.35 mm (c), after immersion in water at 37℃ for 5 days.

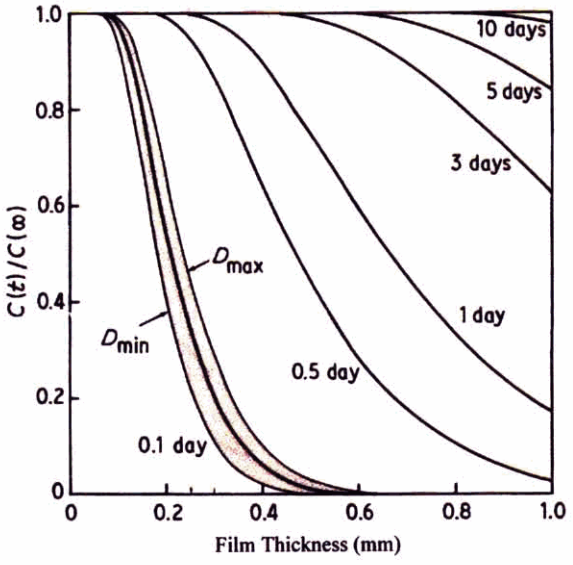


Fig. 3.1-5 Relationship between film thickness and water content at the adhesion interface with immersion periods.

## 3.2 ESCA Study on Changes in the Adhesion Interface due to Water

### 3.2-1 Introduction

In section 3.1, it was established that in the specimens bonding a polymethylmethacrylate (PMMA) film with 4-META resin to mild steel, water entered the interface by diffusion through the resin rather than by passage along the interface[1]. The present study clarifies how the structure of the adhesion interface changes with water immersion. The changes in chemical states of the mild steel surface at the adhesion interface of the PMMA film bonded with 4-META resin were studied by analytical methods, including X-ray diffraction, reflection electron diffraction, and ESCA.

### 3.2-2 Materials and Methods

*X-ray and Reflection Electron diffraction*

A 0.2 mm thick PMMA film was bonded with 0.05 mm thick 4-META resin[2] on the 18×18 mm metallographically polished mild steel plate. The bonded specimens were stored in a dry chamber at 37°C for 24 hr and then immersed in 37°C distilled water until corrosion products were observed on the mild steel surface through the transparent resin layer. Identification of the corrosion products at the adhesion interface was carried out by X-ray diffraction with a diffractometer under Fe Kα radiation with a Mn filter, 35 kV tube voltage, and 20 mA current. Products on the specimen having no diffraction pattern by the X-ray diffraction were identified with reflection high-energy electron diffraction patterns observed with an electron microscope with accelerating voltage of 100 kV.

*ESCA Analysis*

Mild steel was soldered on 18-8 stainless steel specimen holder of an ESCA (Shimadzu ESCA-850). The mild steel surface was polished metallographically and a 0.2 mm thick PMMA film was bonded to the mild steel with 0.05 mm thick 4-META resin. After storage for 24 hr in a dry atmosphere at 37℃, the specimen was immersed in distilled water for 3 days, 4 days, and 2 weeks. A PMMA block was then bonded on the PMMA film as shown in Fig. 3.2-1, to enable the imposition of large thermal stresses at the interface by thermal shock. The specimen was then sealed in a quartz glass tube filled with ultra-high purity argon gas (purity 99.999%; oxygen content below 0.2 ppm; dew point below -70°C). And the specimen in the quartz tube was subjected to thermal shock with thermal cycles from liquid nitrogen (-196°C) to water (40°C) to separate the resin layer from the mild steel surface. After the thermal shocks, the quartz glass tube was broken in a polyethylene chamber attached to the ESCA specimen chamber, filled with ultra-high purity argon gas. The ESCA specimen was introduced into the specimen chamber without exposure to air.

ESCA measurements were performed with Mg Kα radiation (1,253.6 eV) at $2\times10^{-6}$ Pa maintained by a turbo-molecular pump. The specimen surface was subjected to argon ion etching at 2 kV and 20 mA under a pressure of $5\times10^{-4}$ Pa in the spectrometer. The etching rate was 0.1 nm/sec on pure silver under this condition. The measurements and the argon ion etching were performed alternately to determine both the

amounts and chemical states of the elements with depth. The amounts of elements were calculated by considering only the photoelectron cross section.

### 3.2-3 Results

*X-ray and Reflection Electron Diffraction*

Figure 3.2-2 (a) shows X-ray diffraction patterns of the slightly brown surface of the specimen immersed in water for 2 weeks and Fig 3.2 -2 (b) is the diffraction pattern of the black surface found after 2 months immersion. Diffraction pattern (a) showed only the iron structure, while (b) showed a mixture of iron and $Fe_3O_4$. Figure 3.2-3 shows the reflection high-energy electron diffraction pattern obtained from the surface of the 2-week specimen. In Table 3.2-1, the observed lattice spacings and intensities of the diffraction pattern are shown and compared with the data for iron and iron oxide hydrate, FeO(OH). The diffraction for iron showed a ring pattern and that for FeO(OH) had a spotty pattern.

*ESCA Analysis*

Figure 3.2-4 shows the Fe $2p_{3/2}$ spectra obtained after 3 days (a) and 2 weeks (b) of water immersion. The (c) spectrum was obtained from the 2 week immersed specimen after 100×60 sec of argon ion etching in the ESCA spectrometer, showing an almost pure iron state. The surface state of the 2 weeks specimen was identified as iron oxide hydrate, FeO(OH), and the same chemical state may be assumed after 3 days immersion. Figure 3.2-5 shows the changes in concentrations (at%) of Fe, O, and C with depth, for specimens immersed for 3 (a) and 4 days (b). The carbon concentration of the 3-day specimen was higher than after 4 days of immersion, while the oxygen concentration was lower in the 3-day specimen. Figure 3.2-6 shows the Fe $2p_{3/2}$ spectra obtained at different depths after 3 (a) and 4 days (b) of water immersion with varying argon ion etching times. The peak at 707.2 eV was metallic iron, and the peak and shoulder at 710.0 and 711.2 eV indicated oxidation states. The spectra showed a mixture of metallic and oxidation states. To obtain the fraction of oxidation states of Fe, the spectrum of the oxidation states was graphically separated from the measured spectrum, and the results are shown in Fig. 3.2-7. The amount of oxidation states of Fe after 4 days immersion was higher than after 3 days.

### 3.2-4 Discussion

The bonding strength of adhesive joints is strongly influenced by water and humidity in the environment[3]. There are many investigations of industrial applications on degradation due to moisture intrusion into bonded joints: after exposure to water, the fracture path is between the adhesive and metal oxide interface, and there is a considerable increase in the iron oxide thickness[4]. For aluminium, moisture intrusion at the bonding line causes the oxide to convert to hydroxide with accompanying change in morphology and bonding strength[3, 5]. The durability in wet environments, such as the oral cavity, is also of prime importance in bonding dental adhesive materials to teeth and dental alloys.

It has been established that the water molecules reach the adhesion interface by diffusion through the

resin layer rather than by passage along the interface[2, 6, 7]. The destruction of adhesion depends on the velocity of water diffusion[3, 8, 9]. The water content at the interface has been calculated from Fick's second equation as described in the previous section. The chemical state at the adhesion interface in a short immersion time could not be determined because the PMMA film could not be separated from the mild steel substrate by thermal shock with the specimen sealed in a quartz glass tube as shown in Fig. 3.2-1.

After 3 days immersion, the water content at the adhesion interface reached close to at the equilibrium water concentration, and it was determined that iron oxide hydrate was formed at the adhesion interface after 3 days and also 2 weeks immersion. This was followed by the appearance of a black corrosion product, $Fe_3O_4$. The critical time, the change from FeO(OH) to $Fe_3O_4$, was not determined here.

Carbon is derived mainly from contamination and from the adhesive resin. The steep decreased in carbon concentration after a few minutes of argon etching shown in Fig. 3.2-5 (a) and (b) showed the extent of carbon contamination. The carbon content of the 3-day specimen was higher than that of the 4-day specimen, indicating a large amount of residual resin on the 3 days specimen. The amount of residual resin bonded with the mild steel surface decreased as destruction of the adhesion interface due to water molecules progresses.

Oxygen comes from absorbed water molecules (contamination), iron oxide hydrate, and residual resin. The high oxygen amount in the 4-day specimen showed that much oxygen was due to iron hydroxide as shown in Fig. 3.2-7 even though there was much residual resin in the 3-day specimen and absorbed water as contamination was similar for the two specimens. Side chains of 4-META bonds with hydroxyl groups on the metal surface by forming hydrogen bonds[10]. These chemical bonds may be destroyed slowly with water diffusion. This was followed by corrosion, forming iron hydroxides such as FeO(OH), resulting in a complete destruction of the adhesion interface.

### 3.2-5 Conclusions

This section discussed the mechanism destroying adhesion between 4-META and mild steel, and the action of water molecules reaching the adhesion interface. After immersion in water, the adhesive layer was separated from the metal surface. The surface was analyzed by ESCA, reflection electron diffraction, and X-ray diffraction to elucidate changes in the surfaces.

Thick black corrosion product composed of $Fe_3O_4$ was formed at the adhesion interface of the specimen after immersion for 2 months. A very thin brown product formed after immersion for 2 weeks. This included no X-ray diffraction pattern for FeO(OH) as determined by reflection electron diffraction. After 3 days immersion, no change was observed on the mild steel surface through the clear resin layer, but ESCA analysis revealed the same chemical state as in the 2-week immersion specimen.

The hydrogen bonds appeared to be destroyed with water penetrating through the resin layer. This was followed by corrosion, resulting in a complete destruction of the adhesion interface.

## REFERENCES

1) Ohno H, Endo K, Araki Y, Asakura S: Destruction of metal-resin adhesion due to water penetrating through the resin. *J Mater Sci*, **27**: 5149-5153, 1992.

2) Takeyama M, Kashibuti S, Nakabayashi N, Masuhara E: Studies on dental self-curing resins (Part 17) Adhesion of PMMA with bovine enamel or dental alloys. *J Jpn Dent Apparat Mater*, **19**: 179, 1978 (in Japanese).

3) Brockmann W, Hennemann O D Kollek H: Surfaced properties and adhesion in bonding aluminum alloys by adhesives. *Int J Adhe Adhe*, **Jan**: 33-40, 1982

4) Getting M, Baker F S Kinloch A J: Use of Auger and X-ray photoelectron spectroscopy to study the locus of failure of structural adhesive joints. *J Applied Polymer Sci*, **21**: 2375-2392, 1977.

5) Venables J D: Adhesion and durability of metal-polymer bonds. *J Mat Sci*, **19**: 2431-2453, 1984.

6) Brewis D M, Comyn J, Tegg J L: The durability of some epoxide adhesive-bonded joints on exposure to moist warm air. *Int J Adhe Adhe*, **1**: 35-39, 1980

7) Ko C U, Wightman J P: Experimental analysis of moisture intrusion into the Al/Li-polysulfone interface. *J Adhe*, **25**: 23-29,1988.

8) Gledhill R A, Kinloch A J: Environmental failure of structural adhesive joints. *J Adhe*, **6**: 315-330, 1974.

9) Brewis D M, Comyn J Shalash R J A: The effect of moisture and temperature on the properties of an epoxide-polyamide adhesive in relation to its performance in single lap joints. *Int J Adhe Adhe,* **Oct**: 215-222, 1982.

10) Masuhara E: " *A dental adhesive and its clinical applications (I)*"(Quintessence Books, Tokyo Jpn, 1982), p. 67 (in Japanese).

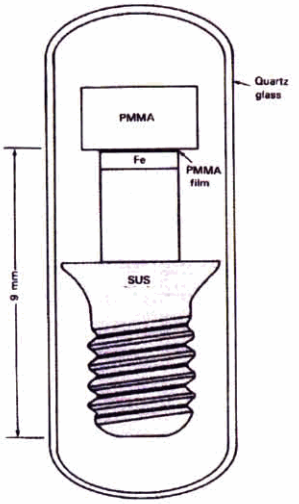


Fig. 3.2-1 ESCA specimen with soldered mild steel sealed in quartz glass tube filled with ultra-high purity argon gas.

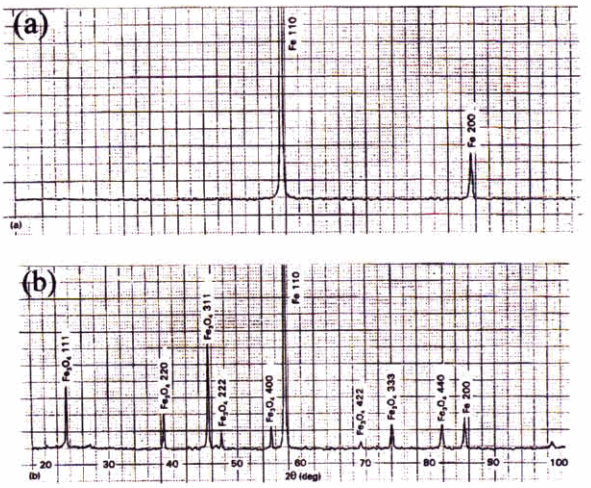


Fig. 3.2-2 X-ray diffraction patterns obtained from the water immersed specimens after 2 weeks (a) and 2 months (b).

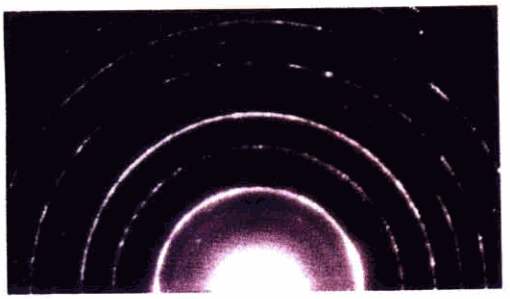

Fig. 3.2-3 Reflection high energy electron diffraction pattern obtained from the 2 week specimen.

Table 3.2-1 Observed lattice spacings and intensities with JCPDS data for iron and lepidocrocite obtained from the 2 week water immersed specimens.

| Observed values | | Reference substances | | | | | |
|---|---|---|---|---|---|---|---|
| | | Iron | | | FeO(OH) | | |
| *d* (nm) | *I* | *d* (nm) | $I/I_1$ | *hkl* | *d* (nm) | $I/I_1$ | *hkl* |
| | –[a] | | | | 0.626 | 100 | 020 |
| | –[a] | | | | 0.329 | 90 | 120 |
| 0.268 | [b] | | | | 0.279 | 10 | 011 |
| 0.252 | [b] | | | | 0.247 | 80 | 031 |
| 0.228 | [b] | | | | 0.236 | 20 | 111 |
| 0.201 | vs | 2.027 | 100 | 110 | | | |
| 0.143 | m | 1.433 | 20 | 200 | | | |
| 0.116 | s | 1.170 | 30 | 211 | | | |
| 0.101 | w | 1.013 | 10 | 220 | | | |
| 0.090 | m | 0.906 | 12 | 310 | | | |
| 0.082 | vw | 0.828 | 6 | 222 | | | |

[a] Not observed
[b] Spotty

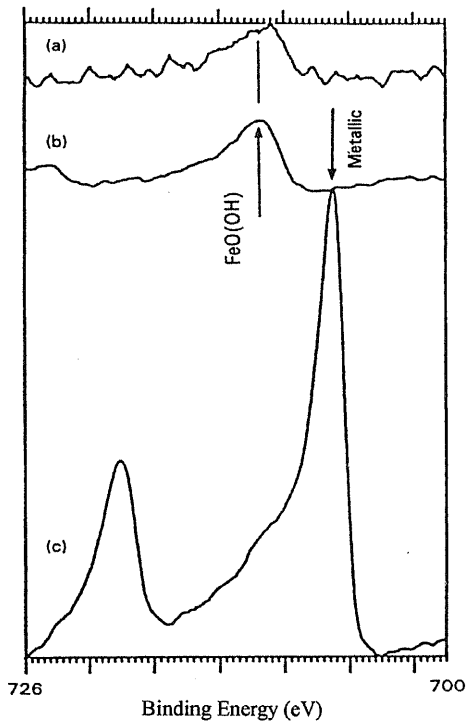


Fig. 3.2-4 The Fe 2p3/2 ESCA spectra obtained after 3 days (a) and 2 weeks (b) of water immersion; (c) shows the 2 week specimen after 100×60 sec of argon ion etching.

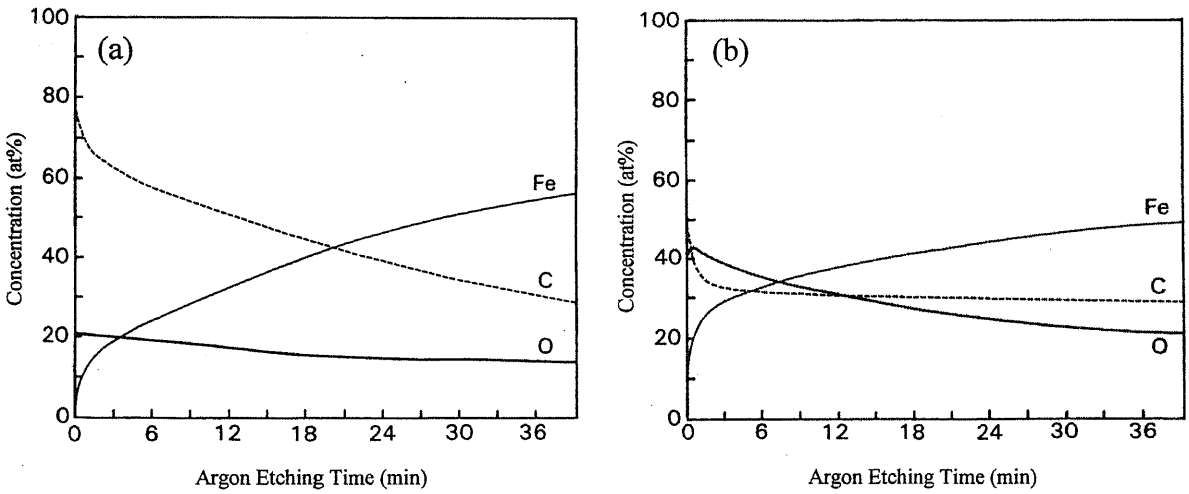


Fig. 3.2-5 Concentration variations (at%) with depth for the 3 (a) and 4 day (b) water immersed specimens.

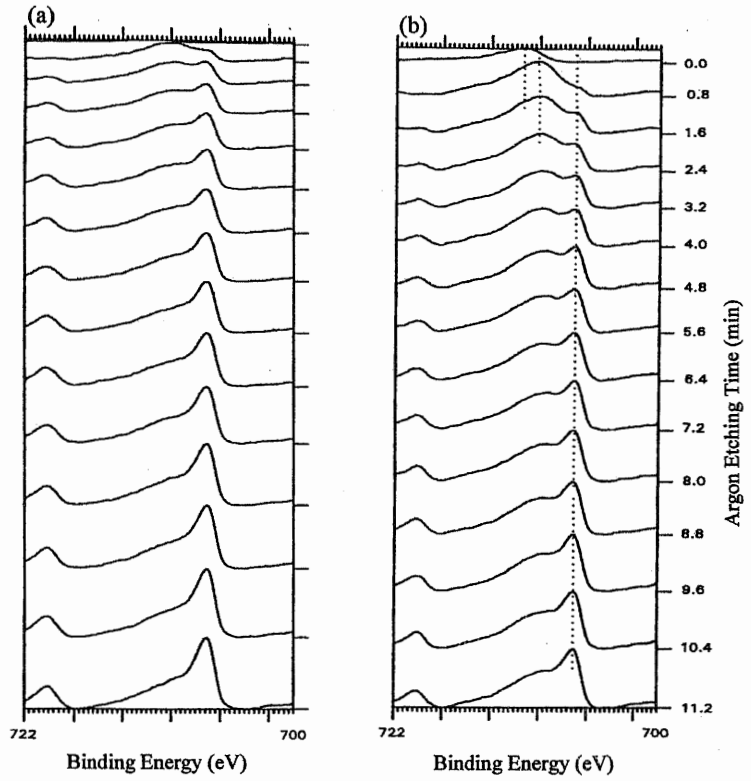


Fig. 3.2-6 The Fe 2p3/2 spectra obtained from the 3 (a) and 4 day (b) water immersed specimens after varying argon ion etching times.

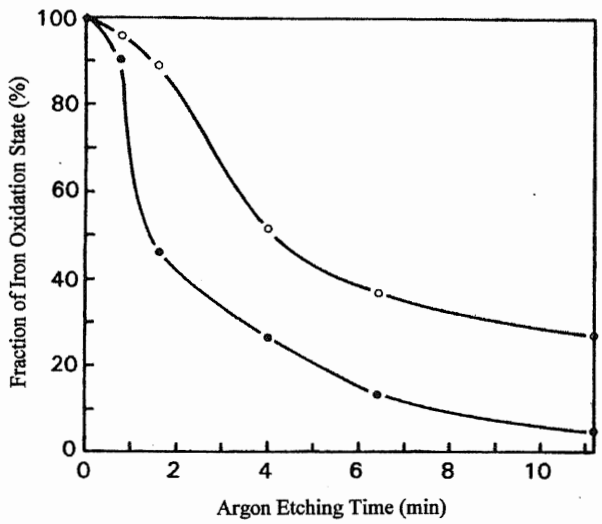


Fig. 3.2-7 Fraction of oxidation state of Fe changes with depth obtained from the (•) 3 and (○) 4-day water immersed specimens.

## 3.3 Evaluation of Water Durability at the Adhesion Interface by Separation Test of Resin Film

### 3.3-1 Introduction

Generally, joints of dental adhesive resin bonded to dental alloys weaken in a wet environment though adhesion is strong in a dry environment. Durability evaluation of the adhesion interface in water is necessary, because durability in a wet environment, such as the oral cavity, is of prime importance in the bonding of dental adhesive materials to teeth and dental alloys. It is however, necessary to establish a simple, efficient, and fast procedure of evaluation for water durability at the adhesion interface. The appropriate testing for water durability requires that the whole adhesion interface has reached the equilibrium water concentration.

With aluminum/epoxy resin[1], aluminum/Li-polysulfone[2], and mild-steel/4-META resin[3] in wet environments, water molecules enter the adhesion interface by diffusion through the adhesive resin rather than by passage along exposed bond lines. In the present study, the durability evaluation of the adhesion interface after immersion in water was performed as follows: The thin PMMA film was attached to metal specimens with 4-META resin for the water content at the interface to reach equilibrium in a short time. After water immersion, the specimen was subjected to thermal cycles from liquid nitrogen to water (40°C).

The resin film separates without degradation due to water when the resin film is thick, because the intensity of the thermal stress due to the thermal shock depends on the resin thickness. It is necessarily to determine the critical resin thickness which separates only when the adhesion interface has degraded. To determine the critical thickness, the influence of resin film thickness on the separation of the resin film with thermal shock was examined with 18-8 stainless-steel specimens which bond strongly with 4-META resin without water immersion. Mild-steel bonded resin film which is thinner than the critical resin film thickness was chosen in order to discuss the relationship between water immersion time and degradation at the adhesion interface, since adhesion interface is destroyed by water more rapidly in mild-steel than 18-8 stainless-steel. Durability of the adhesion interface to water immersion was evaluated by measurement of the separated area of resin film after the thermal cycles.

Thermal stress analysis was calculated by the three-dimensional finite element analysis.

### 3.3-2 Materials and Methods

*Separating Test by Thermal Shock Using Liquid Nitrogen*

The influence of resin film thickness on the separation of the resin film with thermal shock was investigated with the stainless-steel specimens, which bond strongly with 4-META resin without water immersion. Polymethyl methacrylate (PMMA) films of 0.2 mm to 0.7 mm thickness were made of a PMMA powder by pressing at 150°C. An 18-8 stainless-steel adherend metal plate (18×18×1.5 $mm^3$) was polished metallographically to eliminate mechanical factors that affect bonding. The PMMA film was bonded with 4-META resin to the stainless-steel plate. The bonded specimen was pressed with a 20-kgf load for five minutes to maintain a constant 0.05-mm thick 4-META resin layer, then kept in a dry chamber

at 37°C for one day. Subsequently, the specimen was subjected to 20 thermal cycles from liquid nitrogen (-196°C) to water (40°C) for 60 sec each. The separated area was traced by a profile projector. Measurements were made individually on 10 specimens.

*Degradation of Adhesion Interface by Immersion in Water*

Figure 3.3-1 shows an evaluation method of the degradation of the adhesion interface by water. A 0.2 mm thick PMMA film was bonded with 0.05 mm thick 4-META resin on the 18×18 mm metallographically polished mild-steel plate. The specimens were stored in a dry chamber at 37°C for 24 hr before immersion in 37°C distilled water. After the immersion, the specimens were subjected to 20 thermal cycles from liquid nitrogen (-195.8°C) to water (40°C), each for 60 sec. Since the resin film separates from the mild-steel surface by thermal stress when there was degradation at the adhesion interface, the separated areas were measured for each immersion time.

*Thermal Stress Analysis by the Three-dimensional Finite Element Method*

Three-dimensional finite element analysis was performed by the Integrated Structural Analysis Program (ISAP)[4]. The hexahedron elements model is composed of 8 elements along the x and y axes and 5 along the z axis for the resin layer and 10 elements along the z axis for the steel substrate as shown in Fig. 3.3-2. The coefficient of linear thermal expansion, the modulus of elasticity, and Poisson's ratio on resin and steel are listed in Table 3.3-1. A thermal load of 236°C was applied by the temperature difference between -196°C liquid nitrogen and 40°C water. Computer-aided calculations were performed for resin layers of 0.10, 0.25, and 0.50 mm thickness and 1.50 mm thick steel on a quarter of the model assuming a completely fixed resin/steel interface.

### 3.3-3 Results

*Separating Test by Thermal Shock*

Figure 3.3-3 shows the separated area versus the resin film thickness bonded to the 18-8 stainless steel without water immersion. Total interface failure occurred on specimens with resin thicker than 0.5 mm; there was critical thickness between 0.45 and 0.5 mm. After the thermal cycles, thick resin layers separated at the adhesion interface even though the resin layer was strongly adhered. To study the degradation due to water at the adhesion interface, a resin layer of 0.25 mm was selected as a resin layer which does not separate from the metal substrate if adhesion was initially strong.

*Degradation of the Adhesion Interface by Immersion in Water*

Figure 3.3-4 shows the relationship between the separated area (%) of resin films bonded to the mild-steel and immersion times (min), measured after the thermal cycles. The separated area covered only a few percent after short immersion times, below 100 min. After longer immersion times, over 200 min, the separation induced by thermal stress covered the whole metal surface, and there was a critical immersion

time for interface failure near 200 min. This indicates that failure occurs at the interface when the water content here reaches a critical value.

*Thermal Stress Analysis*

Figure 3.3-5 shows shearing stresses at the adhesion interface calculated for a quarter of the $x-y$ interface by the finite element method with a 0.5 mm thick resin layer. The abscissa shows the distance in the diagonal direction and "0" of the distance represents the center of the specimen. The thermal stress was highest at the periphery and zero at the center. Figure 3.3-6 shows maximum shearing stresses at the adhesion interface of the periphery with different thicknesses of resin. The stresses were calculated as 8 MPa for a 0.1 mm thick、16 MPa for a 0.25 mm, and 22.5 MPa for a 0.5 mm thick resin layer.

## 3.3-4 Discussion

*Evaluation Method for Water Durability at the Adhesion Interface by Thermal Shock Using Liquid Nitrogen*

The most critical factor influencing the mechanical behavior of adhesive joints is water and humidity. Water durability of adhesive structures exposed to environments like the oral cavity is very important. In general, long immersion times are need for evaluation of water durability at the adhesion interface. The present study proposed a quick evaluation method for water durability at the adhesion interface. A similar method has been reported as the separation method of oxides from alloy substrates heated at high temperature[5].

The three-dimensional finite element method showed that thermal stress increases with increasing thickness of the resin layer (Fig. 3.3-6) and showed maximum shearing stresses at the periphery of the adhesion interface (Fig. 3.3-5). The separated area versus the resin film thickness obtained from 18-8 stainless-steel specimens without water immersion showed that total interface failure occured on specimens with resin thicker than 0.5 mm (Fig. 3.3-3). The critical thermal shearing stress was calculated as 22.5 MPa for 0.5 mm thick resin. There is no difference in the critical thermal shearing stress between 18-8 stainless steel and mild-steel since thermal expansion, modulus of elasticity, and Poison's ratio are almost identical for both alloys. A resin layer of 0.25 mm was chosen in order to study the degradation of the adhesion interface by water. When the adhesion interface degraded, the adhesion is broken by lower stresses than the value for the 0.25 mm layer, 16 MPa (Fig. 3.3-6).

Traces of separating resin film after 20 thermal cycles are shown with repetition of cycles in Fig. 3.3-7; excellent (a) and poor water durability (b). Separating at the adhesion interface propagates from the periphery to a point where the thermal stress balances with the adhesive force, because the stress is largest at the periphery and zero at the center. The stress at the periphery may depend on test piece size: As shown in Fig. 3.3-5, stress decreases with decrease in specimen size. When separating appears after one cycle, the maximum stress appears at the separated point in the following cycle. Separating propagates until the balance point, where shear stress and adhesive force cross in Fig. 3.3-8.

*Degradation and Water Concentration at the Adhesion Interface*

Several authors have examined the mechanism for destruction of the adhesion interface between metal and resin due to water penetrating through the resin. With aluminum, moisture intrusion at the interface converted the surface oxide layer to hydroxide with accompanying changed in morphology and bonding strength[9-11]. For dry joints, fracture occured near the epoxy resin/metal interface while water-soaked joints showed fracturing at the interface between the adhesive and the iron oxide[12]. In the previous section, the interface between mild-steel and 4-META resin was analyzed by ESCA, reflection electron diffraction, and X-ray diffraction to elucidate structural changes. After 3 days immersion, ESCA analysis showed the corrosion product to be FeO(OH) on the mild-steel/4-META resin interface. After 2 months, a thick black corrosion product composed of $Fe_3O_4$ formed at the interface[12]

The adhesion interface of mild-steel and 4-META resin rapidly degraded in wet conditions though the interface bonds strongly in dry conditions. The separated area covered only a few per cent after short immersion times, below 100 min. After longer immersion times, over 200 min, the separation induced by thermal stress covered the whole metal surface, and there was a critical immersion time for interface failure near 200 min. This indicates that failure occurs at the interface when the water content at the interface reaches a critical value. Weakening of joints by immersion in water has been observed with some metals[6]. Brewis et al.[7] reported a linear relation between the joint strength of aluminum alloy/epoxy-de-polyamide and the water content of the joints. The water content here was the average concentration of water in the adhesive and not the water content at the interface itself. We demonstrated that the relationship between the degradation of the adhesive interface and the water content at the interface of the mild-steel/4-META adhesive resin was not linear as shown in Fig. 3.3-4. In the case of mild-steel, total interface failure occurred at immersion times longer than 200 min, demonstrating that the adhesive force was lower than 16 MPa. At 200 minutes immersion, the water content at the resin-metal interface was estimated to be 48% of the equilibrium water concentration from equation (3.1-8).

Masuhara[8] has proposed an adhesion mechanism for metal and 4-META resin where side chains of 4-META bond with hydroxyl groups on the metal surface by forming hydrogen bonds. It is considered that water molecules that permeated to the interface break the hydrogen bonds with the 4-META side chain, resulting in degradation of the interface when 48% water content was reached.

In the present study, interface separation appeared after immersion times longer than 200 min, indicating a change in the surface state of the mild-steel. Changes in the metal surface at the interface after exposure to water have been reported for cases where corrosion of the iron oxide leaded to considerable increases in the oxide thickness[9]. With aluminium, moisture permeation at the interface caused the surface oxide layer to convert to a hydroxide with accompanying changes in morphology and bonding strength[10, 11].

Further experiments were performed to determine the immersion period for white spots to appear on the steel surface. Three PMMA films of 1.0, 1.5, or 2.0 mm were bonded to mild-steel with 4-META resin in the manner described previously and the surface states were observed after immersion in water. On the

1.0 mm thick resin specimens, white spots appeared after 10 days, with 1.5 mm thick resin after 20 days, and with 2.0 mm resin after 31 days. The water content at the interface when the white spots appear on the steel surface was calculated to be 95% of the equilibrium concentration from the immersion periods and resin thickness.

Figure 3.3-9 shows the relationship between immersion period in water and film thickness with the water content at the adhesion interface at 48%, 95%, and 100% of the equilibrium water concentration. In the present study there were no changes in the surface state up to the time when 48% water content was reached. When water content was reached at 95%, white spots appeared on the mild-steel surface and they become brown and then finally black. It is therefore concluded that destruction at the interface occurs by a breakdown of chemical bonds with 48% of the equilibrium water concentration, and that this is followed by corrosion forming iron hydroxide.

### 3.3-5 Conclusions

Water durability of the adhesion interface was evaluated by measurement of the separated area of the resin film bonded with 4-META resin on metal specimens after imposing thermal stress using liquid nitrogen. The intensity of the thermal stress due to thermal shock, calculated by the three-dimensional finite element method, increased with increasing resin film thickness, indicating that the resin film separates without degradation due to water when the resin film is thick. Total interface failure occurred on specimens with resin thicker than 0.5 mm. The critical thermal shearing stress was calculated as 22.5 MPa. A resin layer of 0.25 mm was chosen in order to study the degradation of the adhesion interface by water, as a thickness where the resin layer does not separate from the metal substrate if adhesion is initially strong. When the adhesion interface degrades, the adhesion is broken by lower shear stresses than the value for 0.25 mm layers, 16 MPa. Immersion time to reach equilibrium water content was 0.5 days for a 0.25 mm resin film.

A PMMA film bonded by 4-META resin to mild-steel was used to study the degradation of the adhesion interface due to water. There is a critical immersion time for interface failure near 200 min, indicating that failure occurs at the interface when the adhesive force became lower than the value, 16 MPa. The interface was broken by water when the water content at the interface reaches 48% of the equilibrium water concentration of PMMA. Observation through the PMMA film showed no change in the mild-steel surface at 48% of the equilibrium water concentration at 95% water content many small white spots appeared on the surface. The surface color further changed to black by the formation of corrosion products.

The present method has an advantage in that water durability of the adhesion interface could be evaluated rapidly, because in a rod type specimen which is used in usual bonding tests, the water immersion time to reach the equilibrium water content at the center of the adhesion interface may need several hundred days. This method is useful to evaluate the effects of surface modification of metal substrates and adhesive monomers on the water durability of the adhesion interface.

## REFERENCES

1) Brewis D M, Comyn J, Tegg J L: The durability of some epoxide adhesive-bonded joints on exposure to moist warm air. *Int J Adhe Adhe*, **1**: 35-39, 1980.

2) Ko C U, Wightman J P: Experimental analysis of moisture intrusion into the Al/Li-polysulfone interface. *J Adhe*, **25**: 23-29,1988.

3) Ohno H, Endo K, Araki Y, Asakura S: Destruction of metal-resin adhesion due to water penetrating through the resin. *J Mater Sci*, **27**: 5149-5153, 1992.

4) *Integrated Structural Analysis Program (ISAP)*, NEC, Tokyo, 1985.

5) Deadmore D L, Lowell C E: The effect of ΔT (oxidizing temperature minus cooling temperature)on oxide spallation. *Oxidation of Metal*, **11**: 91-106,1977.

6) Mogi T: Studies on adhesion of methacrylic resin to cobalt-chromium alloy for denture base - Effects of 4-methacryloxyethyl trimellitate anhydride monomer -, *J Jpn Prosthodont Soc*, **23**: 76-92, 1979 (in Japanese).

7) Brewis D M, Comyn J Shalash R J A: The effect of moisture and temperature on the properties of an epoxide-polyamide adhesive in relation to its performance in single lap joints. *Int J Adhe Adhe,* **Oct**: 215-222, 1982.

8) Masuhara E: "*A Dental Adhesive and its Clinical Applications*", Quintessence Books, Tokyo, 1982, pp. 11-68 (in Japanese).

9) Getting M, Baker F S Kinloch A J: Use of Auger and X-ray photoelectron spectroscopy to study the locus of failure of structural adhesive joints. *J Applied Polymer Sci*, **21**: 2375-2392, 1977.

10) Brockmann W, Hennemann O D Kollek H: Surfaced properties and adhesion in bonding aluminum alloys by adhesives. *Int J Adhe Adhe*, **Jan**: 33-40, 1982.

11) Venables J D: Adhesion and durability of metal-polymer bonds. *J Mater Sci*, **19**: 2431- 2453, 1984.

12) Ohno H, Endo K, Araki Y: ESCA study on the destruction mechanism of metal-resin adhesion due to water penetrating through the resin. *J Mater Sci*, **28**: 3764-3768, 1993.

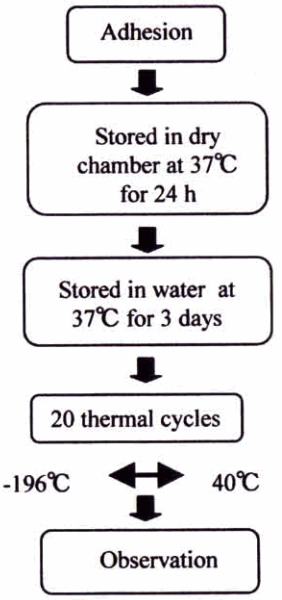


Fig. 3.3-1 Evaluation method of the degradation of the adhesion interface by water.

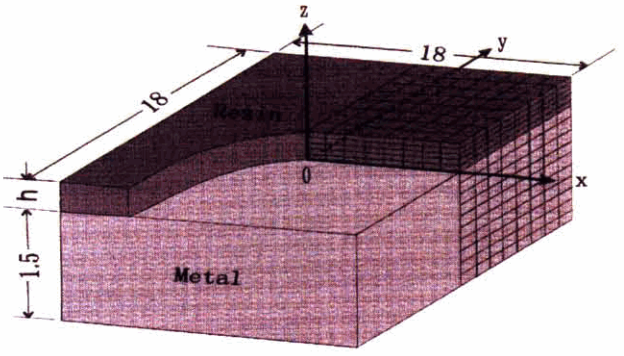


Fig. 3.3-2 Hexahedron for the three-dimensional finite element method.

Table 3.3-1 Coefficients of linear thermal expansion, modulus of elasticity, and Poisson's ratio of resin and steel.

| | coefficient of thermal expansion (/°C) | moduli of elasticity (MPa) | Poisson's ratio |
|---|---|---|---|
| Steel | $8.7\times10^{-6}$ | $2.04\times10^{5}$ | 0.29 |
| PMMA | $80\times10^{-6}$ | $0.2\times10^{5}$ | 0.32 |

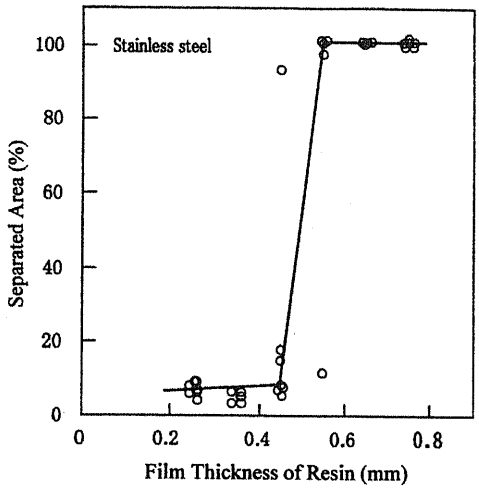


Fig. 3.3-3 Separated area of resin film bonded to 18-8 stainless steel vs. resin film thickness following thermal cycles.

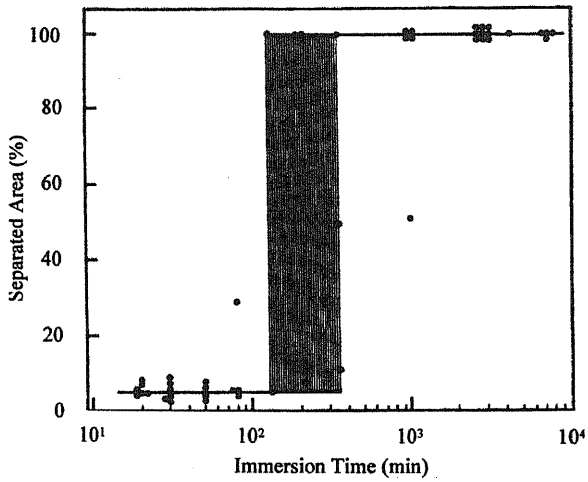


Fig. 3.3-4 Relationship between separated area of resin films bonded to mild steel vs. immersion time in water after thermal cycles.

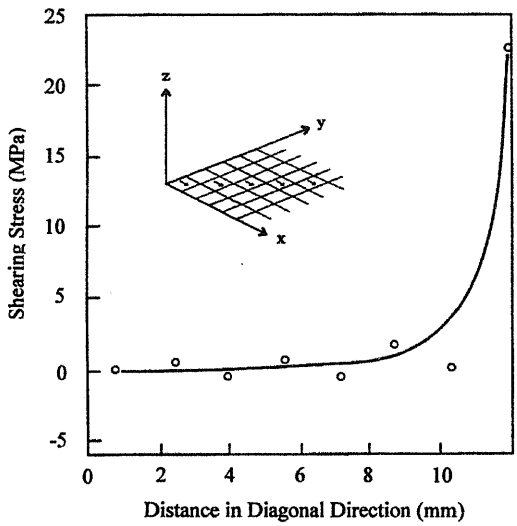


Fig. 3.3-5 Shearing stress along diagonal direction at the adhesion interface of resin with 0.5 mm thick resin layer during thermal cycle.

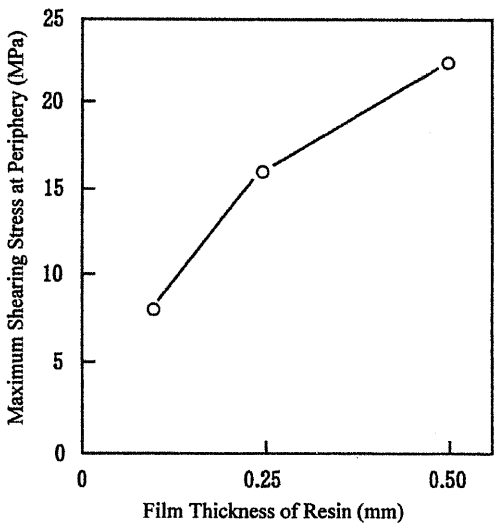


Fig. 3.3-6 Maximum shearing stress at the periphery of the adhesion interface with different resin thicknesses.

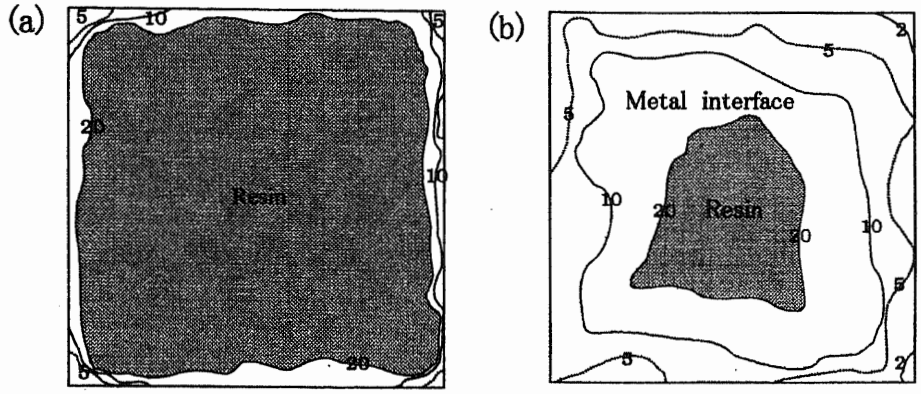


Fig. 3.3-7 Separating traces of resin films after 20 thermal cycles. Numbers indicate repetition of thermal cycles. Excellent (a) and poor water durability (b).

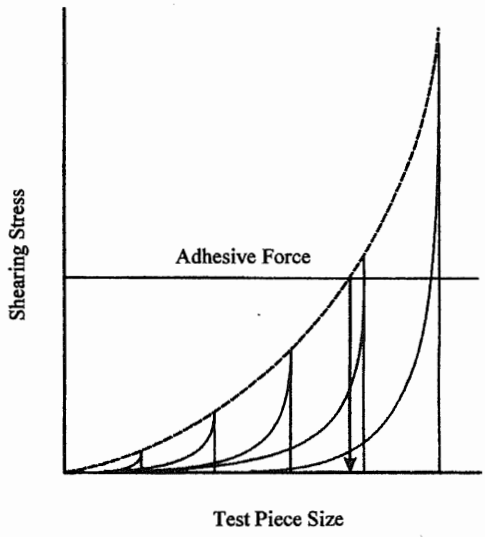


Fig. 3.3-8 Changes in maximum stress at the periphery of specimens with propagating separation of resin film.

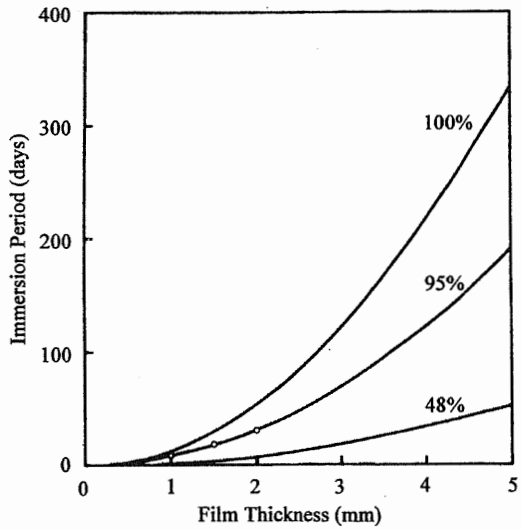


Fig. 3.3-9 Relationship between the immersion period in water and the film thickness for the water content at the adhesion interface to reach 48% (interface failure occurs), 95% (white spots appear), and 100% of the equilibrium water concentration.

# Chapter 4

# NEW SUFACE MODIFICATION FOR DENTAL ALLOYS BY Ga-Sn ALLOY

## 4.1 A New Surface Modification Method for Resin Bonding – Modification Effects on Dental Alloys –

### 4.1-1 Introduction

Adhesion of adhesive resins to dental base-metal alloys is comparatively good. However, the resins bond inadequately to dental precious metal alloys because they have low chemical affinity for the precious metals. Several surface modification methods have been developed for improvement of adhesion to dental alloys: high-temperature oxidation[1], immersion in an oxidizing agent[2], immersion in concentrated nitric acid[3,4,5], anodizing[6], electroplating with tin[7,8], SiOx coating[9], and ion coating[10]. However, these methods have drawbacks, such as complicated procedures, expensive equipment, and degradation of chemical agents.

Ohno et al.[11] have developed a simple new method of modifying adherend metal surfaces by which excellent adhesion to metals is achieved by simply applying liquid Ga-Sn alloy (named Adlloy) on the adherend metal surface. This chapter discussed the surface modification method and its effects on various dental alloys. Adhesion to three other surfaces, as-polished, oxidized at high temperature, and electroplated tin were also studied for comparison with the adhesion to the Adlloy-modified surface. Bonding strength was measured and the durability against water at the adhesion interface was evaluated.

### 4.1-2 Materials and Methods.

*Materials*

The Table 1-1 shows the compositions of the nine commercial dental alloys studied: Type IV and 14 K indicate ADA Type IV and 14 K gold alloys; Ag-Pd, Ag-Cu, Ag-Sn, and Ag-In are silver-based alloys; SUS (18-8 stainless steel), Co-Cr and Ni-Cr are base metal alloys. The resin was an adhesive dental resin containing 4-META (4-META resin).

*Surface Modification by Adlloy*

Adlloy is a 75 mass%Ga-25 mass%Sn alloy with a solidus point at approximately 20°C and liquidus point at approximately 50°C. The Adlloy is a mixture of solid (Sn) and liquid (90%Ga-10%Sn) at room temperature (25°C)[12]. Adlloy was applied and rubbed to a polished adherend alloy surface by use of a pure tin bar at 25°C. The surplus liquid Adlloy on the adherend surface was wiped off with clean paper tissue one minute after contact with the adherend surface. A new alloying layer with Ga and Sn was formed on the adherend surface.

*Surface Modification by Other Methods*

High temperature oxidation was carried out at 400°C for 5 min in air in an electric furnace. The electroplating with tin was performed in a solution of $SnSO_4$ (0.3 mol/ℓ), $H_2SO_4$ (0.5 mol/ℓ), and cresol sulfonic acid (0.3 mol/ℓ) under a current of 150 A/m$^2$ at 20°C.

*Measurement of Bonding Strength*

Five specimens, Type IV, 14K, Ag-Pd, Co-Cr, and Ni-Cr, were soldered to a 11 mm$^{\phi}$×6 mm circular disk of stainless steel as shown in Fig. 2.1-1 and three specimens, Ag-Cu, Ag-In, and SUS were formed in the same size as the stainless steel disk. Before the surface-modification procedures, all adherend metal surfaces were polished metallographically as mirror like surface to eliminate mechanical factors affecting the bonding strength.

A 5-mm diameter stainless steel rod was vertically bonded to the adherend metal surface with a constant 0.05-mm-thick adhesive layer by use of the adhesion apparatus with micrometer (Fig. 2.1-2). The bonded specimens were stored at 37°C for one day in a dry chamber for adequate cure of the adhesive. After removal of excess resin protruding from the stainless steel rod with a steel dental bur, the specimens were subjected to 20 thermal cycles from liquid nitrogen (-195.8°C) to water (40°C) alternately for 60 sec each before the tensile test. With each alloy, tensile tests of 20 test pieces were performed on a testing machine (Shimadzu, IS-5000, Kyoto, Japan) with a test speed of 2 mm/min, after insertion of a U-shaped piece in the groove of the stainless steel rod (Fig. 2.1-1). The fractured surfaces were observed with a profile projector after the test. The results were statistically analyzed by Duncan's test at a $p = 0.01$ level.

*Evaluation of the Durability of the Adhesion Interface after Immersion in Water*

Water molecules degrade the adhesion interface by diffusion through the resin rather than by passage along the interface[13, 14]. In this study the durability evaluation on the adhesion interface after immersion in water was performed on the method as described in section 3.3. Durability of the adhesion interface to water immersion was evaluated by measuring the separated area of the resin film after the thermal cycles. Measurements were made on 10 specimens for each alloy. The results were analyzed by Duncan's test at a $p = 0.01$ level.

*ESCA Analysis*

ESCA measurements were performed with Mg Kα radiation (1,253.6 eV) at $2\times10^{-6}$ Pa maintained by a turbo-molecular pump. The specimen surface was subjected to argon ion etching at 2 kV and 20 mA under a pressure of $5\times10^{-4}$ Pa in the spectrometer. The etching rate was 0.1 nm/sec on pure silver under this condition. The measurements and the argon ion etching were performed alternately to determine both the amounts and chemical states of the elements with depth. The amounts of elements were calculated by considering only the photoelectron cross section.

## 4.1-3 Results

*Bonding Strength and Failure Appearance*

Figure 4.1-1 shows the bonding strength and failure types obtained from the as-polished (a), oxidized (b), and Adlloy-modified specimens(c). Failure appearances after the tensile tests were classified in five types as shown in Table 2.1-1. The result for the tin electro-plated specimens is in (c) for the Type IV gold

alloy. Of the as-polished specimens (a), the gold (Type IV and 14K) and silver-based (Ag-Pd and Ag-Cu) alloys showed lower bonding strengths between 10 MPa and 20 MPa with a wide scattering of strengths and Type III failure. The silver-based (Ag-Sn and Ag-In) and base-metal alloys (SUS, Co-Cr, and Ni-Cr) showed mainly cohesive failures, with bonding strengths near 40 MPa, and a smaller scattering in the measured strengths.

On the high-temperature oxidized specimens (b), the gold (Type IV and 14K) and silver-based (Ag-Pd and Ag-Cu) alloys showed higher bonding strengths than the as-polished specimens ($p < 0.01$). Conversely, the silver-based (Ag-Sn and Ag-In) and base-metal (Co-Cr and Ni-Cr) alloys showed lower bonding strengths than the as-polished specimens ($p < 0.01$) and had Type III or IV failure.

On the Adlloy-modified specimens (c), high bonding strengths were obtained for the gold- (Type IV and 14K) and silver-based (Ag-Pd, Ag-Cu, and Ag-Sn) alloys with cohesive failure. The bonding strengths obtained on the Adlloy-modified specimens for silver-based (Ag-In) and base-metal (SUS, Co-Cr, and Ni-Cr) alloys were lower than those obtained on the as-polished surfaces ($p < 0.01$). All the fractured surfaces for these alloys modified by Adlloy showed a total interface failure. No difference was observed on the bonding strengths between tin-electroplated and Adlloy modified specimens of Type IV gold alloy ($p < 0.01$).

*Water Durability at Adhesion Interface*

Figure 4.1-2 shows the separated area (%) obtained from the as-polished (a), oxidized (b), and Adlloy modified-specimens (c) after immersion in water for 3 days and imposition the thermal cycles. The separated area for Type IV gold alloy electro-plated with tin is shown in (c). Large separated areas indicate low water durability.

Of the as-polished specimens (a), the separation induced by thermal stress covered the whole alloy surface for the gold-based (Type IV and 14K) and silver-based (Ag-Pd and Ag-Cu) alloys, and these showed no water durability at the adhesion interface. The Ag-Sn and Ag-In silver-based alloys showed excellent water durability. The base metal alloys (SUS, Co-Cr, and Ni-Cr) exhibited in 40 to 60% separated areas.

On the oxidized specimens (b), the water durability of the gold-and silver-based (Ag-Pd and Ag-Cu) alloys was improved by high-temperature oxidation ($p < 0.01$). However, the separated areas showed 10 to 50%. The Ag-Sn and Ag-In silver-based alloys showed lower durability than the as-polished specimens ($p < 0.01$). No statistical difference was observed on the water durability between the oxidized and as-polished specimens for base-metal alloy ($p > 0.01$). As shown in (c), the separated area of the Adlloy-modified gold- and silver-based (Ag-Pd and Ag-Cu) alloys covered only a few percent, indicating excellent water durability of the adhesion interface. However, Adlloy did not improve the water durability of the Ag-In silver-based and base-metal alloys ($p < 0.01$). Consequently, the Adlloy surface modification was effective for all the dental precious metal alloys except the Ag-In-Zn silver-based alloy.

*ESCA Measurements*

Fig. 4.1-3 shows the Au 4f spectra (a), the Ga $2p_{3/2}$ spectra (b), the Sn 3d spectra (c), and the O 1s spectra (d), obtained at different depths of the modified layer formed on a 14K gold alloy surface with Adlloy after different argon ion etching times. Before argon ion etching (0 min), Au, Ga, and Sn were found on the surface after 2 hr from application of Adlloy, which demonstrated the formation of a new alloying layer containing Ga and Sn. The Ga $2p_{3/2}$ peaks at 1,207.0 eV and 1,208.9 eV were from metallic Ga and Ga oxide. The Sn $3d_{5/2,3/2}$ spectra (485.0 and 493.2 eV) were from metallic Sn and the neighboring shoulder at the higher binding energy side was from Sn oxide. After 0.5 min argon ion etching, the Ga oxide peak at 1,208.8 eV became a shoulder of the metallic state peak at 1,207.0 eV and the Sn oxide shoulder almost disappeared. This was accompanied by a decrease in O 1s intensities. By further argon ion etching, Ga and Sn in the oxide state disappeared and only the metallic state remained; Sn disappeared after 4 min. Ga diffused deeper into the gold alloy substrate than did the Sn.

Figure 4.1-4 shows the variations in concentration (at%) of the alloying elements with depth, obtained from the 14K gold alloy. Compositions at the top surface before argon ion etching were 74%Ga, 10%Cu, 8%Au, 5%Sn, and 3%Ag. The Adlloy- modified layer was approximately 500 nm in thickness.

Figure 4.1-5 shows the change in concentration (at%) of Ga in the depth for various dental alloys after Adlloy conversion. The diffusability of Ga in the alloys were in the order: Ag-In > Ag-Pd > 14K > Type IV > Ni-Cr.

*SEM Observation*

The SEM images shown in Fig. 4.1-6 were obtained from an as-polished 14K gold alloy surface (a), 14K gold alloy surface modified by Adlloy ((b) and (c)), Ag-In silver alloy surface modified by Adlloy (d), Ni-Cr alloy surface modified by Adlloy (e), and 14K gold alloy surface electroplated with tin (f). Scratches in (a) observed on the as-polished surface were diminished after the surface modifications. On the surface modified by Adlloy, small white particles and fine needle-like crystals were formed on the 14K gold ((b) and (c)) and Ag-In silver alloys (d). However, there were no needle-like shapes on the Ni-Cr alloy surface modified by Adlloy, which was composed only of small particles (e). On the tin- electroplated surface (f) there were small irregularities with voids.

## 4.1-4 Discussion

*Bonding Strength and Water Durability at Adhesion Interface*

The as-polished base-metal alloys (SUS, Co-Cr, and Ni-Cr) and high-temperature-oxidized precious metal alloys (Type IV, 14K, Ag-Pd, and Ag-Cu) showed high bonding strengths in a dry atmosphere (Fig. 4.1-1 (a) and (b)). However, the water durability at the adhesion interface for these alloys was inadequate as shown in Fig. 4.1-2 (a) and (b). Therefore, it is emphasized that the adhesive ability of the adherend and adhesives should not be evaluated by measuring the bonding strength only under dry conditions. In the present study, the Adlloy-modified gold-based (Type IV and 14K) and silver-based (Ag-Pd and Ag-Cu)

alloys showed not only high bonding strengths but also excellent water durability at the adhesion interface, offering good potential for dental use.

*Surface States and Adhesive Ability*

With the Type IV, 14K, Ag-Pd, and Ag-Cu specimens, the high-temperature oxidized surfaces had higher bond strengths and better water durability than the as-polished surfaces. Tanaka [1] has reported that copper oxide, CuO, formed on the surface heated at 400°C for 5 min in air improve adhesive ability.

Conversely, on the Ag-Sn, Ag-In, SUS, Co-Cr, and Ni-Cr specimens, the as-polished surface showed better adhesive ability than the high temperature oxidized surface. On the as-polished surface, the Ag-Sn and Ag-In specimens were covered with very thin $SnO_2$ and $In_2O_3$ films[15]; the SUS and Ni-Cr alloy specimens were covered with a passive film of approximately 2 nm, primarily composed of $Cr^{3+}$ with minor amount of $Ni^{2+}$ [16]; Co-Cr alloy specimen was also covered with a passive film of approximately 2 nm composed of $Cr^{3+}$ and $Co^{2+}$ [17]. By high-temperature oxidation in air, the Ag-Sn specimen was covered with ZnO and $SnO_2$; the Ag-In specimen with $In_2O_3$ and ZnO; the SUS and Ni-Cr specimens with $Cr_2O_3$ and NiO; and the Co-Cr specimen with $Cr_2O_3$ and $Co_3O_4$[16].

In electroplating with tin, the surface was covered with 1 nm $SnO_2$[18]. Hotz et al. have reported good adhesive ability for tin electroplating with glass ionomer cements[19]. Yamashita et al. have also reported excellent adhesive ability with a dental adhesive resin[20]. Adhesion of 4-META resin to Type IV gold alloy modified by Adlloy was comparable with that after tin electroplating as shown in Figs. 4.1-1 (c) and 4.1-2 (c).

*Surface Modification of Adherend Alloy by Ga-Sn Alloy*

Differences of surface morphology were also indicated by the SEM images in Fig. 4.1-6; the needle-like structures on the surfaces of 14K gold and Ag-In silver alloys were not present on the Ni-Cr alloy. Ga diffused faster into these alloy substrates than into the Ni-Cr alloy, and Sn remained near the surface of the substrate, as shown in Fig. 4.1-4. The alloy surface modified by Adlloy was covered with 2-6 nm of a Ga and Sn oxide film. Metallic Ga and Sn diffused into the alloy substrate, but Ga and Sn oxides could not diffuse and remained on the surface. This thin oxide layer plays an important role in the chemical bonding of the adhesive resin to the dental precious alloys[18].

For determination of whether oxides were present at different depths, the oxides and metallic states were separated from the Ga and Sn spectra measured by ESCA as follows: The Ga $2p_{3/2}$ standard spectra of oxide, $Ga_2O_3$, and metallic states, which are indicated as 100% intensity, are shown in Fig. 4.1-7 (a). So that the area fraction of oxide and metallic states could be obtained, the metallic standard spectrum was graphically subtracted from the measured spectrum as shown in Fig. 4.1-7 (b). The observed spectrum for which the main peak was due to the metallic state was subtracted by the metallic standard spectrum. The subtracted spectrum after argon ion etching for 0.5 min, shown in Fig. 4.1-3 (b), was shown in Fig. 4.1-7 (b) with separated spectra and area fractions of the peaks. Peaks (1) and (2) are attributed to the metallic

and oxide states. Although the surface before argon ion etching was composed almost exclusively of $Ga_2O_3$, the oxide component decreased to 18% by 0.5 min of argon ion etching.

The changes in the amounts of oxide with depth, for $Ga_2O_3$ on Adlloy-modified surfaces and $SnO_2$ on tin-electroplated surfaces, were shown in Fig. 4.1-8. The surface of the 14K gold alloy modified by Adlloy was covered with a $Ga_2O_3$ layer similar in thickness to that of $SnO_2$ formed on the tin-electroplated surface. A $Ga_2O_3$ layer, thicker than that on the 14K gold alloy, was formed on the Ag-In silver-based alloy. The Ni-Cr alloy surface had no layer structure but was a mixture of metallic Ga and oxide states.

Adhesion of 4-META resin to gold alloy (Type IV and 14K) and silver-based alloy (Ag-Pd-Cu, Ag-Cu, and Ag-Sn) modified by Adlloy gave not only high bonding strengths but also excellent water durability at the adhesion interface. The adhesion ability of 4-META resin to the gold alloys modified by Adlloy was comparable with that to Type IV gold alloy electroplated with tin. Adlloy had no effect on adhesion to the Ag-In silver-based alloy or to base-metal alloys such as Ni-Cr, Co-Cr, and stainless steel.

The main factor for excellent adhesion between dental precious-metal alloys and 4-META resin was the formation of very thin Ga and/or Sn oxide layer less than 1-2 nm thick on the alloy surface. However, conversely, a thick Ga-Sn layer leaded to low bonding ability, as shown Ag-In silver-based and Ni-Cr alloys (Fig. 4.1-8). This is presumably the reason why the A-In silver-based metal alloy did not demonstrated improved adhesion after modification of the surfaces with Adlloy.

Surface modification by Adlloy has many advantages as compared with the other methods. The Adlloy method is characterized by: (1) efficiency for only precious metal alloys; (2) easy application and no special equipment; (3) short times of application; (4) high bonding strength and excellent water durability; (5) low price; (6) harmless and causing no irritation[21, 22]; (7) no degradation of Adlloy during storage. The critical point in handling Adlloy is to remove surplus liquid Adlloy from the substrate after use because surplus liquid Adlloy on the substrate surface reduces bonding strengths and water durability. Sand blasting by clean glass beads or ultrasonic cleaner, several times, are effective in removing surplus Adlloy from irregular surfaces. There are other alloys having low solidus points such as Ga-Zn (solidus point 25°C) and Ga-In (15.7°C). The effects of these alloys on the surface of dental precious metal alloys are being investigated.

### 4.1-5 Conclusions

Adhesion of 4-META resin to gold alloys (ADA Type IV and 14K) and silver-based alloy (Ag-Pd-Cu-Au, Ag-Cu, and Ag-Sn) modified by Adlloy gave not only high bonding strengths but also excellent water durability at the adhesion interface. The adhesion ability of 4-META resin to Type IV gold alloy modified by Adlloy was comparable with that to Type IV gold alloy electroplated with tin. Adlloy had no effect on adhesion to the Ag-In silver-based alloy or to base-metal alloys such as Ni-Cr, Co-Cr, and stainless steel.

The surface involved in the adhesion with adhesive resin is a Ga-rich layer. The main factor for achieving excellent adhesion between dental precious metal alloys and adhesive materials is the formation

of very thin Ga and/or Sn oxides less than 1-2 nm thick on the alloy surface, which the thin Ga oxide layer overcomes the weak adhesion ability of the unmodified precious metal surfaces. However, conversely, a thick Ga-Sn layer leads to low bonding ability. This is the reason why the Ag-In silver-based and base metal alloys did not demonstrate improved adhesion after modification of the surface with Adlloy.

## REFERENCES


1) Tanaka T, Nagata K, Takeyama M, Nakabayashi N, Masuhara E: Heat treatment of gold alloy to get adhesion with resin. *J Jpn Soc Dent Apparat Mat*, **21**: 95-102, 1980 (in Japanese).

2) Tanaka T; Fujiyama E, Shimizu H, Atsuta M: Study on surface treatment of non-precious alloys for adhesion bridge, *J Jpn Prosthodont Soc*, **27**: 706-712, 1983 (in Japanese).

3) Tanaka T, Nagata K, Nakabayashi N, Masuhara E: Application of 4-META on adhesive opaque resin. *J Jpn Soc Dent Apparat Mat*, **20**: 221-227, 1979 (in Japanese).

4) Tanaka T, Nagata K, Takeyama M, Atsuta M, Nakabayashi N, Masuhara E: 4-META opaque resin-a new resin strongly adhesive to nickel-chromium alloy. *J Dent Res*, **60**: 1697-1706, 1981.

5) Yamashita A, Yamami T: Procedures for applying adhesive resin (MMA-TBB) to crown and bridge restorations (Part 1). *J Jpn Prosthodont Soc*. **26**: 584-591, 1982 (in Japanese).

6) Yamashita A, Yamami T, Ishii M, Yamaguchi T, Uramoto T: Procedures for applying adhesive resin (MMA-TBB) to crown and bridge restorations (Part 3). *J Jpn Prosthodont Soc*, **26**: 1118-1127, 1982.

7) Yamashita A, Kondo Y, Fujita M: Adhesive strength of adhesive resin PANAVIA EX to dental alloys. *J Jpn Prosthodont Soc*, **28**: 1023-1033, 1984 (in Japanese).

8) Kondo Y, Yamashita A, Suzuki K: Pre-treatment of dental alloy for adhesive restorations. *J J Dent Mater*, **7**: 13-19, 1988 (in Japanese).

9) Musil R: Clinical verification of the Silicoater technique, results of three-years' experience. *Dent Lab*, **35**: 1709-1715, 1987.

10) Tanaka T, Hirano M, Kawahara H, Matsumura H, Atsuta M: A new ion-coating surface treatment of alloys for dental adhesive resins. *J Dent Res*, **67**: 1376-1380, 1988.

11) Ohno H, Araki Y, Endo K: An new conversion method for adhering metal surfaces to improve adherence with dental adhesive resins and poly-electrolyte cements, *Trans Int Cong Dent Mater*, **Nov**: 241-242, 1989.

12) Hansen H: *Constitution of binary alloys, 2nd ed.*, New York: McGraw-Hill Book Co, pp. 757-758, 1958.

13) Brewis D M, Comyn J, Tegg J L: The durability of some epoxide adhesive-bonded joints on exposure to moist warm air, *Int J Adhe Adhe*, **1**: 35-39, 1980.

14) Ohno H: Destruction of metal-resin adhesion due to water penetrated through the resin. *Adhe Dent*, **8**: 277- 282, 1990 (in Japanese).

15) Endo K, Araki Y, Ohno H, Matsuda K: ESCA analysis of tarnish films on dental alloys removed from the oral cavities (Parts I and II). *J J Soc Dent Mater*, **7**: 184-196, 1988 (in Japanese).

16) Ohno H, Araki Y, Endo K, Matsuda K, Sakaguti K: ESCA study on improvements in adhesive ability of dental adhesive resin to Ni-Cr alloy treated by $HNO_3$ solution. *Higashi Nippon Dent J*, **6**: 13-22, 1987.

17) Ohno H, Araki Y, Sagara M: The adhesion mechanism of dental adhesive resin to the alloy - Relationship between Co-Cr alloy surface structure analyzed by ESCA and bonding strength of adhesive resin -. *Dent Mater J*, **5**: 46-65, 1986.

18) Ohno H, Araki Y, Endo K: ESCA study on dental alloy surfaces modified by Ga-Sn alloy. *J Dent Re*, **28**: 3764-3768, 1993.

19) Hotz P, McLean J W, Sced L, Wilson A D: The bonding of glass ionomer cements to metal and tooth substrate. *Brit Dent J*, **18**: 41-47, 1977.

20) Yamashita A, Kondo Y, Fujita M: Adhesive strength of adhesive resin PANAVIA EX to dental alloys. *J Jpn Prosthodont Soc*, **28**: 1023-1033, 1984 (in Japanese).

21) Matsui S, Saruta T, Matsumoto Y, Hikage S, Nakade O, Kaku T, Endo K, Sagara M, Ohno H: Toxic activities of the Ga-Sn alloy (Adlloy-OH) on nutritional condition and dental caries development in rats. *Higashi Nippon Dent J*, **9**: 47-54, 1990 (in Japanese).

22) Hikage S, Ohno H, Sakaguti K, Iizuka Y: Cytotoxicity of Adlloy-OH (Ga-Sn alloy) for conversion of metal surface to resin bonding. *J Jpn Prosthodont Soc*, **35**: 1053-1059, 1991 (in Japanese).

(a) As-polished

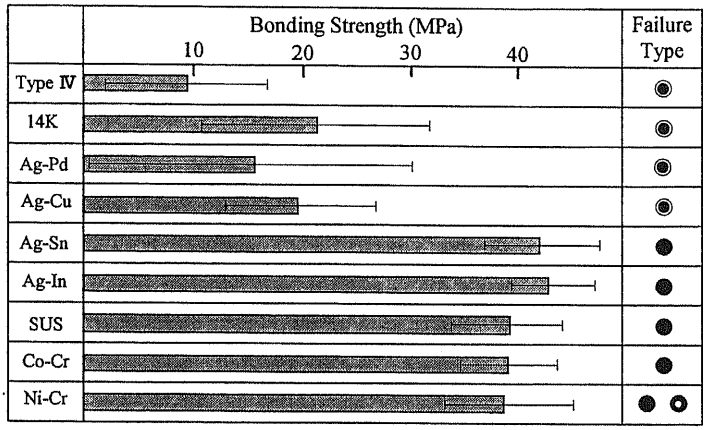


(b) High-temperature Oxidation

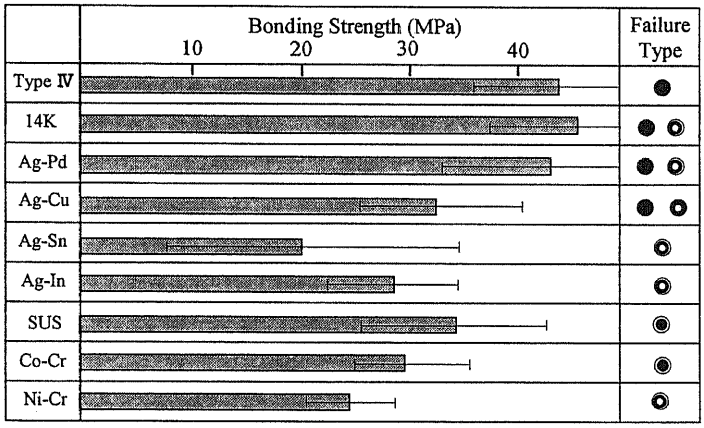


(c) Adlloy Modification

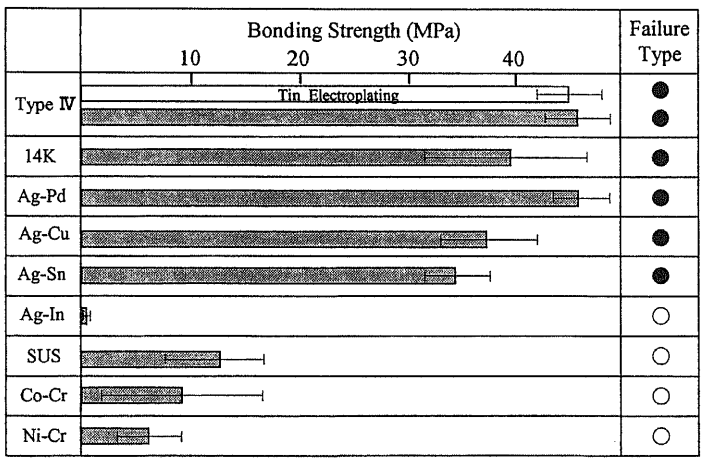


Fig. 4.1-1 Bonding strength and failure types with as-polished (a) oxidized (b), and Adlloy converted specimens (c): The notation indicates failure in the resin (cohesive failure), a mix of cohesive and interface failure, and total interface failure.

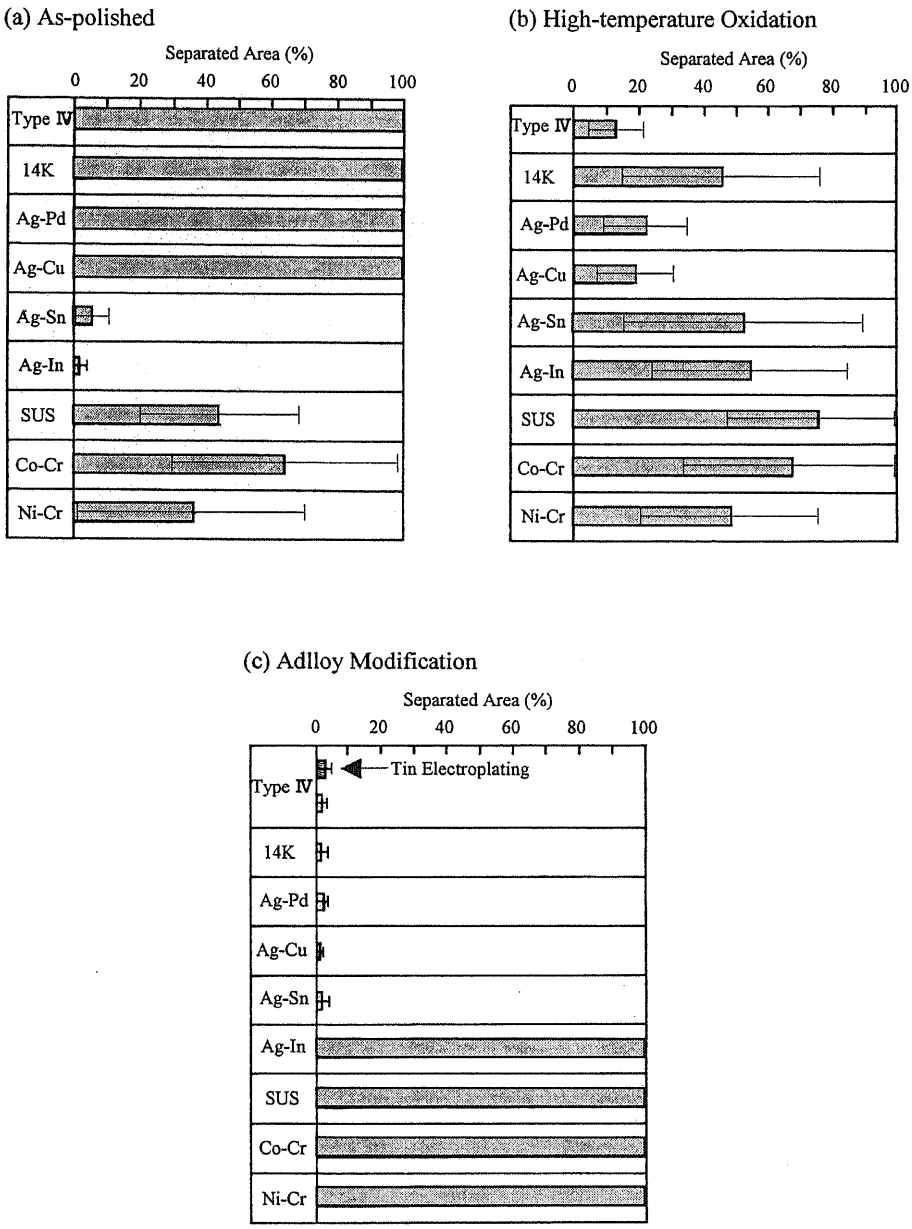


Fig. 4.1-2 Separated area (%) of obtained from as-polished (a), oxidized (b), and Adlloy-converted specimens (c) after immersion in water for three days and imposition of 20 thermal cycles from liquid nitrogen to 40 °C water. The peeled area for Type IV gold alloy electroplated with tin is shown in (c).

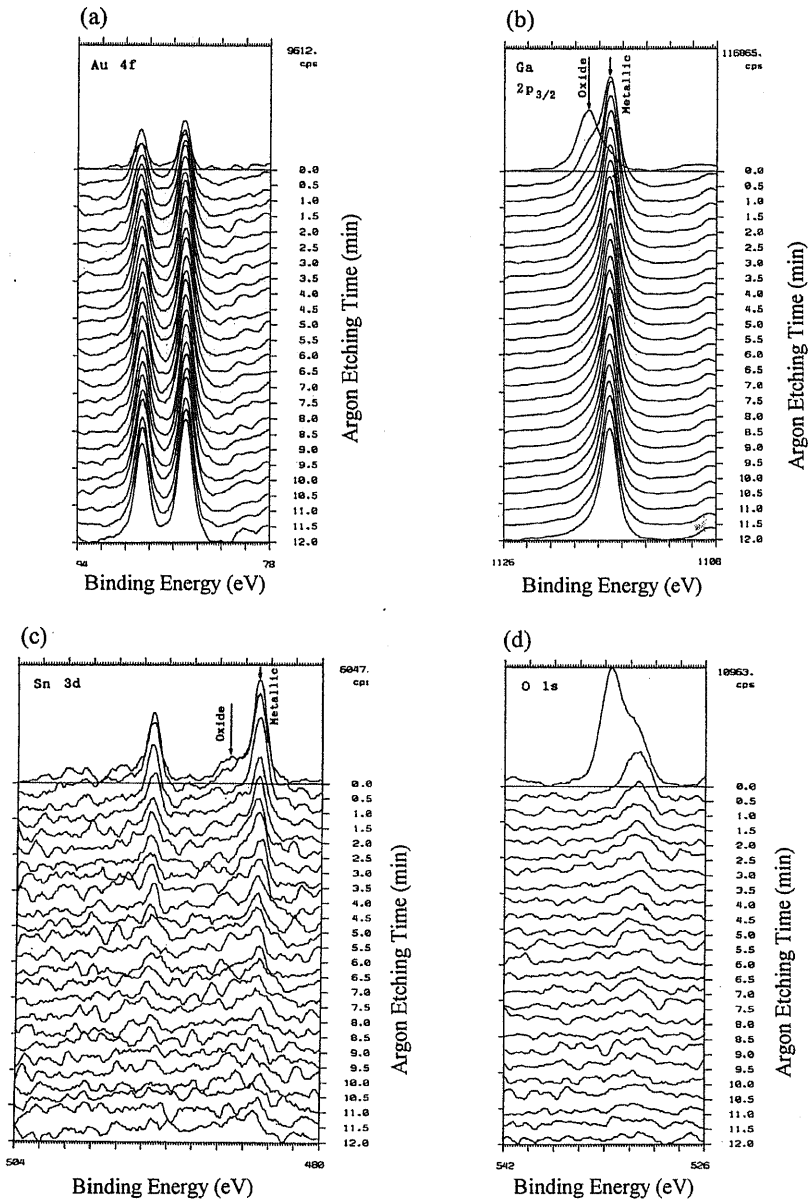


Fig. 4.1-3 ESCA spectra obtained at different depths of the modified layer formed on the 14K gold alloy surface with Adlloy after different argon-ion-etching times: Au 4f (a), Ga $2p_{3/2}$ (b), Sn 3d, and O 1s (d).

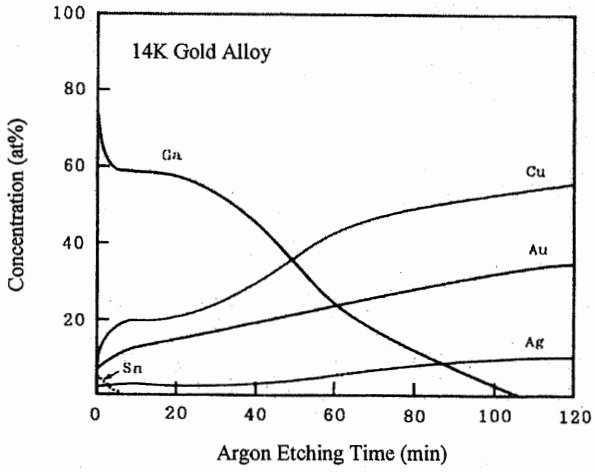


Fig. 4.1-4 Changes in concentration (at%) of alloying elements with depth, obtained from the 14K gold alloy after surface modification by Adlloy.

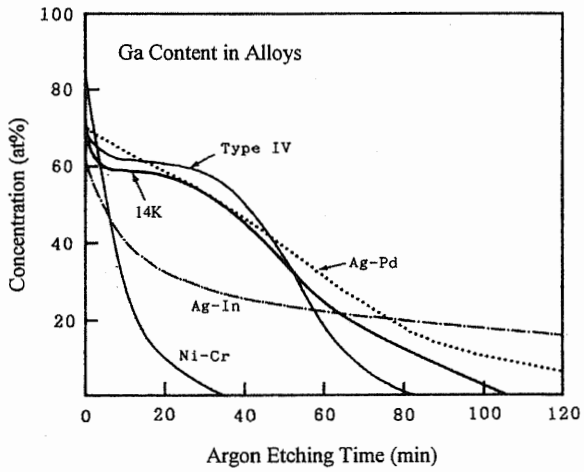


Fig.4.1-5 Changes in concentration (at%) of Ga with depth for various dental alloys after surface modification with Adlloy.

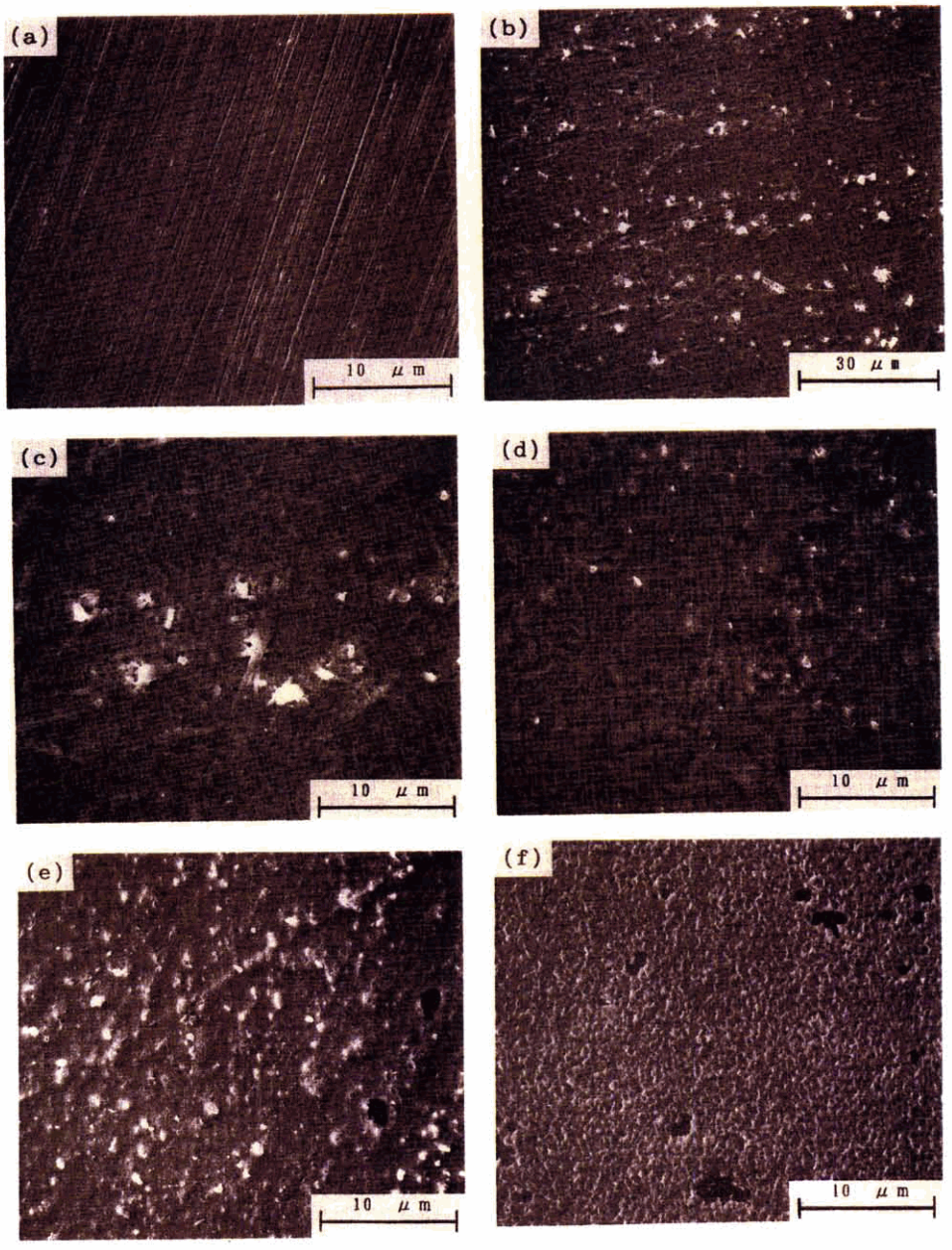


Fig. 4.1-6 SEM images obtained from as-polished 14K gold alloy surface (a), Adlloy-modified surfaces [14K gold alloy (b) and (c), Ag-In-Zn (d),And Ni-Cr (e)], and 14K gold alloy electroplated with tin (f)

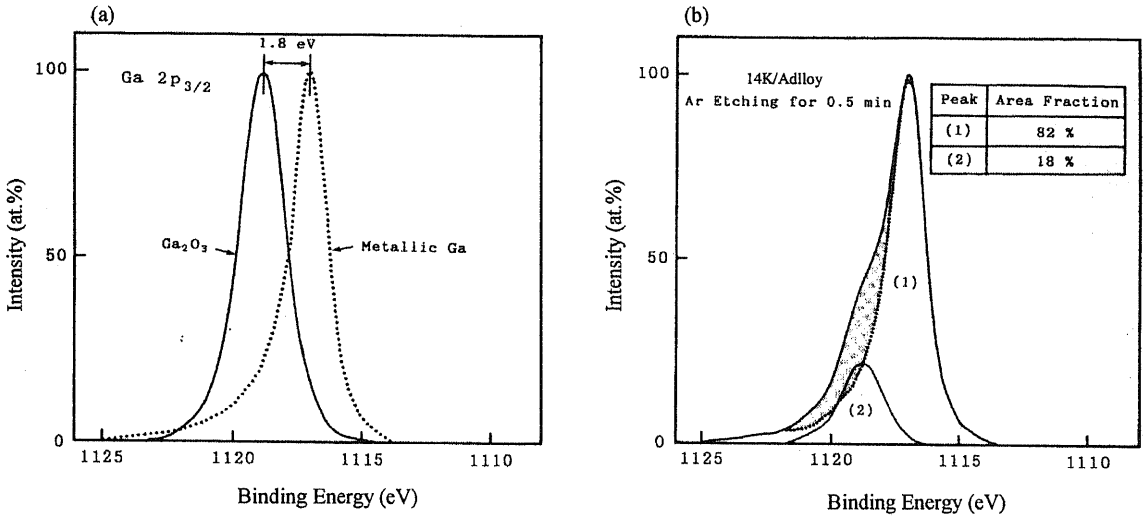


Fig.4.1-7 ESCA standard spectra (a) obtained from $Ga_2O_3$ (solid line) and metallic Ga (dotted line) and subtracted spectra (b) after 0.5 min of argon Ion etching , as shown in Fig. 4.1-3 (b). The peaks (1) and (2) are attributed to metallic and oxide states.

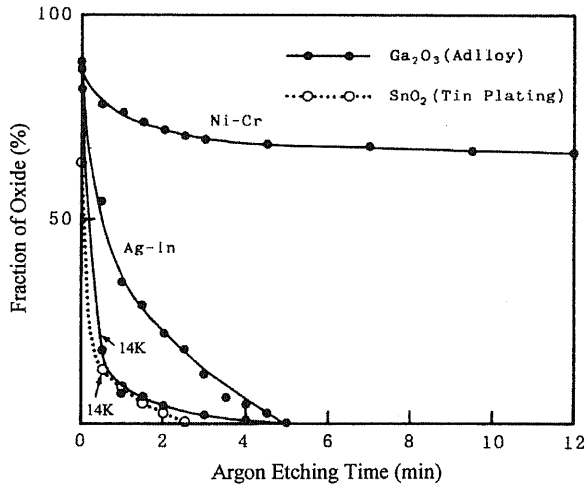


Fig.4.1-8 Changes in the fractions of oxides with depth: $Ga_2O_3$ on 14K gold alloy, Ag-In-Zn alloy, and Ni-Cr alloy surface, modified by Adlloy; $SnO_2$ on 14K gold alloy electroplated with tin.

# Chapter 5

# DEVELOPMENT OF PRECIOUS METAL ALLOYS FOR RESIN BONDING

## 5.1 Improvement of Adhesion of 4-META Resin to Precious Metal Alloys by Adding Base Metals (In, Zn, or Sn)

### 5.1-1 Introductions

Dental adhesive resin (4-META resin) does not adhere strongly to dental precious metal alloys without surface modification. Different methods of surface modification for alloys have been developed to improve their adhesive ability as described in section 4.1, but these require special equipment, have short shelf agent life, and suffer from complicated handling procedures. If dental adhesive resins could be made to bond strongly to dental precious metal alloys without surface modification, the adhesion procedures would be simplified.

In the present study, a base metal was added to a dental precious metal alloy in an attempt to develop alloys that adhere strongly to dental adhesive resins without surface modification of the alloy. The idea for the present study was derived from the experimental finding that 4-META resin bonds strongly to as-polished surfaces of silver based alloys such as Ag-Sn-Zn and Ag-In-Zn with excellent water durability at the adhesion interface[1)] and that oxides such as $Ga_2O_3$ and $SnO_2$ play an important role in improving the adhesive ability of the alloys as described in the previous section 4.1. This excellent adhesive ability may be caused by the effect of the base metals (In, Zn, and Sn) because the 4-META resin does not adhere strongly to pure silver[2)]. Nor does 4-META resin adhere strongly to pure gold[2)]. It was assumed that alloying base metals (In, Zn, and Sn) with precious metal alloys having poor adhesive ability to adhesive resins could improve the adhesive ability of the dental precious metal alloys without the need for surface modification.

First, binary Au, Pd, Ag, or Cu based alloys containing In, Zn, or Sn were made to determine what base metals are effective in improving adhesion. The efficacy of the added elements was evaluated from the water durability of the adhesion interface and the bonding strength. As oxides on the alloy surface play a very important role in the adhesion with 4-META[3)], the alloys were analyzed by ESCA. Next, new dental precious metal alloys for resin bonding were developed on the basis of the results of the binary alloy experiments. The adhesive ability of these alloys was evaluated by their water durability.

### 5.1-2 Experimental Methods

*Materials*

Binary Au, Ag, Cu, or Pd based alloys containing In, Zn, or Sn up to 35 mass% were made to study the effects of added base metals on adhesive ability. To make these alloys, metals of purity higher than 99.9% were melted in an alumina crucible covered with graphite using a high frequency induction furnace in an argon gas atmosphere. Weight loss by the melting was less than 0.02%. The dental adhesive used in the present study was 4-META resin.

*Water durability at the adhesion interface*

Evaluation of water durability at the adhesion interface was[4] performed with a separating test after thermal shocks using liquid nitrogen as described in section 3.3.

*Bonding strength*

With alloys melting above 700°C, the tensile test piece was soldered to a 11 mm$^{\phi}$×6 mm circular disk of stainless steel as shown in Fig. 2.1-1. Alloys melting below 700°C were cast in the same size as the stainless steel disk. The adhesion surface was metallographically polished to eliminate possible mechanical factors affecting the bonding strength. An adhesion apparatus with a micrometer[5] (Fig. 2.1-2) was used for two purposes: to attach the 5 mm$^{\phi}$ stainless rod vertically to the alloy surface and also to maintain a constant 50-μm thick 4-META resin layer. The effect of excess resin at the adhesion area on the bonding strength was eliminated by attaching Scotch Tape with a 5 mm diameter hole to the precious metal alloy surface. The tensile test of the bonding strength measurement was carried out after keeping the specimen at 37°C for 24 hr. Before the tensile test, the specimens were subjected to the thermal cycling described above. The test was performed on a testing machine (Shimadzu Auto-Graph, Shimadzu Co. Ltd., Kyoto, Japan) with a cross head speed of 2 mm/min. Measurements were made individually on 5 specimens at each condition.

*Surface analysis of alloys by ESCA*

Binary alloys of Au with 20 mass%In, 20%Zn, or 20%Sn were made. Alloy specimens for ESCA analysis were 4 mm in diameter with the surfaces metallographically polished to a mirror-like finish with sandpaper and buffed with a wet abrasive of aluminum oxide powder. The ESCA measurements were performed with an electron spectrometer with Al Kα radiation (1,486.6 eV) under a pressure of $2\times10^{-6}$ Pa evacuated with a turbo-molecular pump as same conditions described in section 2.2.

## 5.1 3 Results

*Adhesive ability to binary alloys*

Figure 5.1-1 shows the mean values of separated area (%) as the results of the water durability tests at the adhesion interface, obtained from Au-based binary alloys containing In, Zn, or Sn. Lager separating areas (%) indicate lower water durability. Addition of In was the most effective method to improve the adhesive ability of gold, resulting in water durability improvements with more than 15%In. Figure 5.1-2 shows the relationship between bonding strength and added In amounts with the Au-In alloys. No fracture appeared at the interface between the stainless rod and 4-META resin. The marks indicate the fracture appearance after the tensile test as shown in Table 2.1-1. The figure shows that the adhesive ability decreases in the order ●>◉>○. The mean values of bonding strengths increased and the interface failure at the periphery decreased with higher amounts of In. The failures with 20%In were only cohesive failures. The results of bonding strength measurements coincided with the water durability at the interface.

Figure 5.1-3 shows the separated areas (%) obtained from the Ag-based binary alloys containing In, Zn, or Sn. The water durability was improved with more than 20%Zn. Bonding strength increased with increasing Zn content as shown in Fig. 5.1-4, finally exhibiting only cohesive failure with 20%Zn added. Figure 5.1-5 shows the separated areas (%) obtained from the Cu-based binary alloys containing In, Zn, or Sn, showing that the water durability was remarkably improved by small amounts of base metal. Figure 5.1-6 shows the bonding strength of Cu-In alloys, demonstrating that the Cu-based alloy was involved only in cohesive failures. Although the tensile tests of pure copper also showed only cohesive failure, the separated area (%) here was about 50%. The adhesive ability of 4-META resin to pure copper is poor in humid environments, indicating low water durability at the interface. There was no effect of base metal addition with Pd that displayed 100% separating. The characteristic of Pd was improved by adding In in the equi-atomic alloy PdCu as shown in Fig. 5.1-7.

*Oxides on the alloy surface*

The ESCA spectra obtained from the Au-In, Au-Zn, and Au-Sn alloys before and after argon ion etching with standard spectra are shown in Figs. 5.1-8 to 5.1-10. Figure 5.1-8 shows In 3d spectra obtained from (a) the as-polished Au-In alloy surface before argon ion etching, (b) $In_2O_3$, and (c) the Au-In alloy surface after argon ion etching indicating the metallic state. The structure of the oxide on the adhesion surface in (a) was a mixture of In and $In_2O_3$. Figure 5.1-9 shows Zn LMM auger spectra obtained from (a) the as-polished Au-Zn alloy surface before argon ion etching, (b) ZnO, and (c) the Au-Zn alloy surface after argon ion etching. The structure of the oxide on the adhesion surface (a) was a mixture of Zn and ZnO. Figure 5.1-10 shows Sn 3d spectra obtained from (a) the as-polished Au-Sn alloy surface before argon ion etching, (b) $SnO_2$ and (c) SnO as standards, and also (d) the Au-Sn alloy surface after argon ion etching. The oxide on the adhesion surface (a) was a mixture of Sn and SnO rather than $SnO_2$.

Figure 5.1-11 shows concentration variations of In in the depth direction for 95Au-5In (mass%), 90Au-10In, 85Au-15In, and 80Au-20In alloys. Figure 5.1-12 shows a set of O 1s spectra obtained from the surface without argon ion etching for pure gold (a) and Au-In binary alloys containing 5 (b), 10 (c), 15 (d), and 20 (e) mass% In. The O 1s peak was at 532.8 eV for pure gold (a) and at 531.9 eV for the Au- 15In alloy (d). With increasing In concentration, the intensity of the lower binding energy increased, indicating that the shoulder at 530.0 eV was due to $In_2O_3$. The chemical shifts of the higher binding energy peak of the Au-15In alloy and pure gold were 1.9 eV and 2.8 eV with reference to the $In_2O_3$ state.

*Design of gold alloy*

Table 5.1-1 shows the alloy compositions designed on the basis of the results mentioned above. A commercial gold alloy (Alloy No.6) was chosen as the starting alloy. The composition of the experimental 18K gold alloy (Alloy No.3) was determined as follows; firstly, the amounts of base metals added to 100 g of Alloy No.6 were calculated. Since this alloy contained 75g Au and 16.2g Cu, the amount of In added was calculated to be 12.06g (15%Au + 5%Cu). The amount of Zn was also calculated to be 1.76 g (20%Ag).

Then the composition of Alloy No.3 (Au 75g, Ag 8.8g, Cu 16.2g, In 12.06g, Zn 1.76g) was calculated. The compositions of Alloys Nos. 1, 2, 4, 5, and 7 were obtained by modifying Alloy No.3.

*Design of Au-Ag-Pd alloy*

The composition of the experimental Ag-Pd-Cu-Au alloy (Alloy No.9) was determined in addition to the experimental 18K gold alloy. A commercial Ag-Pd-Cu-Au alloy (Alloy No.11) was chosen as the starting alloy. The composition of Alloy No.9 was obtained by adding In equivalent to 15% of Au content, Zn equivalent to 20% of Ag content, In equivalent to 5% of Cu, and In equivalent to 15% of Pd content coexisting with Cu. The compositions of Alloys Nos. 8, 10, and 12 to 16 were obtained by modifying Alloy No.9.

*Adhesive ability of experimental alloys*

The water durability at the adhesive interface is shown in Table 5.1-1. Alloys No.6 and 11 without addition of In, Zn, and Sn, resulted in total separating, showing no water durability. Adding In, Zn, and Sn effectively improved the adhesive ability of the gold alloys. The water durability for Ag-Pd-Cu-Au alloys was not improved by the addition of small amounts of In, Zn, or Sn. Good water durability of the Ag-Pd-Cu-Au alloys was obtained by adding total amounts of In and Zn above 15% (Nos. 8 and 9) or a large amount of Zn (Nos. 10 and 12).

## 5.1-4 Discussion

*Evaluation of adhesive ability*

The most critical factors influencing the mechanical behavior of adhesive joints are water and humidity. The water durability of adhesive structures exposed to environments like the oral cavity is very important. In general, long immersion times are needed for evaluation of water durability at the adhesive interface. The adhesive ability was evaluated by separating and tensile tests in the present study. With the separating test, a thin PMMA film was attached to metal specimens with 4-META resin in order for the water content at the interface to reach equilibrium in a short time. The separating test is effective as a quick evaluation method for the water durability at the adhesive interface[4].

Observation of the fracture appearance after the tensile test is also effective for evaluating the adhesive ability because the appearance reflects the characteristics of the metal surface. A weak chemical bond of 4-META to the alloy surface leads to total interface failure. An increased area of interface failure at the periphery indicates a decrease in bonding strength as shown in Fig. 2.1-7.

*Adhesive Ability of Designed Dental Precious Metal Alloys*

The silver-based alloys, Ag-Zn-Sn and Ag-In- Zn, showed mainly cohesive failures with tensile bonding strengths near 40 MPa and excellent water durability by the separating test[1], although using silver as the main component in the silver-based alloys gave poor adhesive ability with 4-META[2]. It was

considered that the effect of the base metals could be the reason for the excellent adhesive ability, and on this basis dental precious metal alloys for resin bonding without alloy surface modification were developed.

The adhesive ability of Au was improved by adding 15%In, Ag was improved with 20%Zn, Cu was improved with small amounts of In, Zn, or Sn, and Pd was improved with 15%In coexisting Cu equivalent to equi-atomic% of Pd. The compositions of dental precious metal alloys for resin bonding were designed on the basis of these results.

*Adhesive Ability Affected by Adding Base Metals*

Oxides on dental precious metal alloys play very important roles in the adhesion with 4-META. The adhesive ability of adhesive resin to alloys depends on both the kinds and amount of oxides on the alloy surface. The ESCA study showed formation of $In_2O_3$, ZnO, and SnO on the binary gold alloys, the Au-In alloy, the Au-Zn alloy, and the Au-Sn alloy (Figs. 5.1-8, 5.1-9, and 5.1-10). The thickness of the oxide layers formed on these binary gold alloys was below the escape depth of the photoelectron (1 nm). The same oxides were formed on the silver-based alloys. With precious metal alloys containing two and three base metals, oxides forming preferentially on the alloy surface depend on the activity coefficients of oxygen and base metal, concentration of oxygen and solute metal, and the Gibbs' standard free energy of formation[6].

The chemical bonds of 4-META with oxides on gold alloys containing In, Zn, Sn, or Si were described on the basis of theoretical considerations[7] of acid-base interactions presented by Bolger et al[8]. Bolger's theory considers electrostatic interaction between acids or bases of polymer and hydroxyl groups on the metal surface on the basis of measured values of the isoelectric point of oxides and the acid dissociation constants of adhesive monomers. The chemical interaction of 4-META with $In_2O_3$ was considered to be ionic[7]. Hydrogen bonding was assumed with $SiO_2$[7].

The effect of In addition to Au on the water durability at the adhesion interface has been demonstrated as shown in Fig. 5.1-1. Larger separated areas (%) indicate lower water durability. Adding In was the most effective to improve the adhesive ability of gold, and water durability improved by addition of more than 15 mass%In.

There was no effect of base metal addition with Pd that displayed 100% separating. This emphasizes that although Pd plays an important role in inhibiting sulfide formation of Ag-based alloys[9], Pd also hinders resin bonding. This characteristic appears to be due to Pd easily absorbing hydrogen, resulting in an alteration of the characteristics of the hydroxyl groups adsorbed at the top of the metal surface. The characteristics of Pd were improved by adding In to the equi-atomic alloy PdCu as shown in Fig. 5.1-7. The reason why the adhesion ability of Pd improved with the coexisting Cu is unknown.

*Chemical States of Oxygen*

Figure 5.1-12 shows O 1s spectra from the surface, without argon ion etching, pure gold and Au-based binary alloys containing 5, 10, and 20 mass%In. To clarify the changes in the oxygen chemical state, the

data analysis system in the ESCA spectrometer was used to separate the oxygen states on the O 1s spectra by assuming that the spectra could be approximated by a Gaussian function. Figure 5.1-13 shows the O 1s spectra obtained from the Au-15In alloy: (a) shows the separated spectra of O 1s, obtained from the spectrum without argon ion etching: The O 1s spectrum could be separated into three components indicated by the dotted lines. The solid line, the observed spectrum, agreed well with the chained line that is a composite of the three components. Among the O 1s spectra component Ⅰ was the same chemical state as the oxygen in $In_2O_3$ as noted for Fig. 5.1-12. Figure 5.1-13 (b) shows the separated spectra of O 1s, obtained from the spectrum after argon ion etching for 0.05 min. The oxygen state indicated at 531.9 eV (Ⅱ) was decreased remarkably by the argon ion etching. It could be surmised that the oxygen of components Ⅱ and Ⅲ were present in the upper part of component Ⅰ oxygen because the oxygen due to Ⅱ and Ⅲ was decreased remarkably by the very limited argon ion etching.

To decrease the surface energy due to free valence of metal atoms at the solid surface, the surface is stabilized (decreasing free energy) by arranging the atoms into particular positions and by adsorbing molecules. Metal surfaces immediately adsorb oxygen and water vapor if exposed to the air. With reactive metals there is initially some chemisorption that soon gives way to chemical reactions and the formation of oxides or hydroxides. There may be rearrangement of the surface atoms of the metal during the early stages of oxide growth[4]. Therefore, the surface is not directly exposed to air because it is covered with -OH groups or a layer of $H_2O$, while the base metal bonds with oxygen to form oxide. Table 5.1-2 shows binding energy (eV) and area fraction (%) of oxygen chemical states, obtained from pure gold and Au-15In (mass%) alloy (Fig. 5.1-13). Since the Ⅱ and Ⅲ components were removed by argon ion etching, component Ⅰ increased from 27% to 54%. With argon ion etching, component Ⅱ decreased from 55% to 35% and component Ⅲ decreased from 18% to 11%: The decrease in the amount of component Ⅱ was bigger than that of component Ⅲ, indicating that component Ⅱ is on top of component Ⅲ.

Figure 5.1-14 shows the atomic distribution of Au (white) and In (black) at the adhesion surface, the surface before argon ion etching, obtained from the quantitative analysis shown in Fig. 5.1-11: (a) Au-5In alloy having poor adhesive ability, and (b) Au-15In alloy having excellent adhesive ability. The atomic% of Au and In at the top surface were 90Au-10In on (a) and 56Au-44In on (b). Indium atoms bond with oxygen to form $In_2O_3$, and to obtain excellent adhesive ability it is necessary that the alloy surface is covered with the In-oxide. The poor adhesive ability of the alloy containing only small amounts of In or pure gold as shown in Fig. 5.1-1 was due to chemisorbed $H_2O$ molecules and insufficient indium oxide on the alloy surface. The atomic distribution shown in Fig. 5.1-14 does not show the top surface, but indicates the mean atom distribution in the photoelectron mean free path. However, the distance related to adhesion was nearly equal to the photoelectron mean free path by ESCA because adhesion depends on atomic interactions which are determined by atoms less than 1 nm from the top surface[10]. To obtain excellent adhesion of 4-META resin with a gold alloy, there must be no chemisorbed $H_2O$ molecules on the alloy surface and the oxide element with chemical affinity for 4-META must cover at least 50% of the alloy surface as shown in Fig. 5.1-14 (b).

## 5.1-5 Conclusions

The present study developed dental precious metal alloys having excellent adhesive ability to 4-META resin without alloy surface modification. This was attempted because Ag-based alloys containing In, Zn, and/or Sn have excellent adhesive ability with 4-META, although pure silver does not adhere strongly to 4-META resin. The water durability and bonding strength of 4-META resin to binary alloys of Au, Ag, Cu, or Pd containing In, Zn, or Sn were studied to determine the kinds and amounts of base metals that may be added to the dental precious metal alloys. Gold binary alloys containing In, Zn, or Sn were analyzed by ESCA, showing that $In_2O_3$, ZnO, and SnO formed on the binary gold alloys. The adhesive ability of adhesive resin to alloys depends on the kind of oxide and should be affected with the amount of oxide on the alloy surface.

With In in Au based alloys, the $In_2O_3$ on the alloy surface plays a very important role in the adhesion with 4-META. The ESCA O 1s spectra were separated to clarify the changes in the oxygen chemical states. The adhesive ability was discussed in terms of the separated oxygen states, oxygen due to $In_2O_3$, chemisorbed and physisorbed water molecules. It was established that to obtain excellent adhesion, the element of an oxide having chemical affinity for 4-META must cover at least 50% of the alloy surface. The poor adhesive ability of 4-META resin to pure gold is considered to be caused by chemisorbed $H_2O$ molecules on the surface.

The adhesion ability of the binary alloy was improved by adding In equivalent to 15% of Au content, Zn equivalent to 20% of Ag content, and also In, Zn, or Sn equivalent to 5% of Cu content. There was no addition effect of base metals for Pd. However, 15% of In addition was effective with Pd based alloys containing an equal-atomic ratio of Cu and Pd. Dental precious metal alloys for resin bonding without alloy surface modification were developed on the basis of the results detailed above. Alloy constituents should ultimately be determined on the basis of factors such as corrosion behavior, mechanical properties, aging characteristics, and castability.

## REFERENCES

1) Ohno H, Araki Y, Endo K: A new method for promoting adhesion between precious metal alloys and dental adhesives, *J Dent Res*, **71**: 1326-1331, 1992.

2) Mogi T: Studies on adhesion of methacrylic resin to cobalt-chromium alloy for denture base - Effects of 4-methacryloxyethyl trimellitate anhydride monomer -, *J Jpn Prosthodont Soc*, **23**: 660-676, 1979 (in Japanese).

3) Konishi Y, Ohno H, Hirai T, Koshino H, Ishijima T, Endo K: Adhesion of heat-curing resin to precious metal alloy denture - Surface modification method and adhesive ability -, *J Jpn Prosthodont Soc*, **41**: 357-362,1997.

4) Ohno H, Araki Y, Endo K, Yamane Y, Kawashima I: Evaluation of water durability at adhesion interface by peeling test of resin film, *Dent Mat J*, **15**: 183-192, 1996.

5) Ohno H, Araki Y, Sagara M: The adhesion mechanism of dental adhesive resin to the alloy, *Dent Mat J*,

**5**: 46-65, 1986.

6) Bohm G, Kahlweit M: On internal oxidation of metallic alloys, *Acta Meta*, **12**: 641-648, 1964.

7) Yamane Y, Ohno H, Endo K: Mechanism of adhesion between 4-META resin and alloys based on Bolger's acid-base interaction. *Dent Mater J*, **20**: 63-74, 2001.

8) Bolger JC, Michaels AS: Molecular structure and electrostatic interactions at polymer-solid interfaces, *Interface conversion for polymer coating*, Ed. by Weiss P and Cheever GD, Elsevier Publishing Co. New York, 1968, pp. 3-60.

9) Endo K, Ohno H, Matsuda K, Araki Y: Electrochemical and surface studies on the passivity of a dental Pd-based casting alloy in alkaline sulphide solution. *Corro Sci*, **45**: 1491-1504, 2003.

10) Nishiyama Y: Design of surface (Modification of surface, ed. By Japan Chemical Soc), *Kagaku-Sousètsu*, No. 44, 1984, pp. 1-6, (in Japanese).

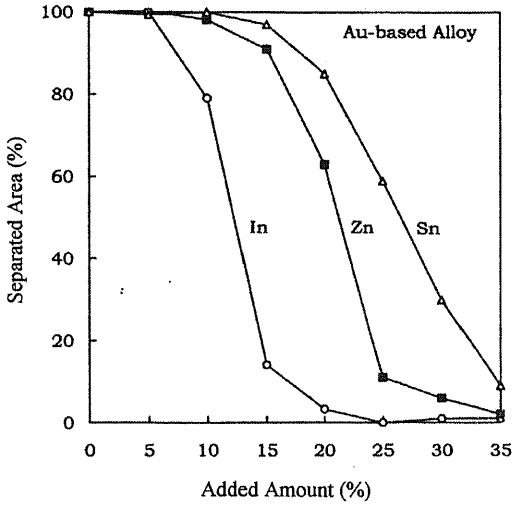


Fig. 5.1-1 Separated area (%) of Au-based binary alloys containing In, Zn, or Sn.

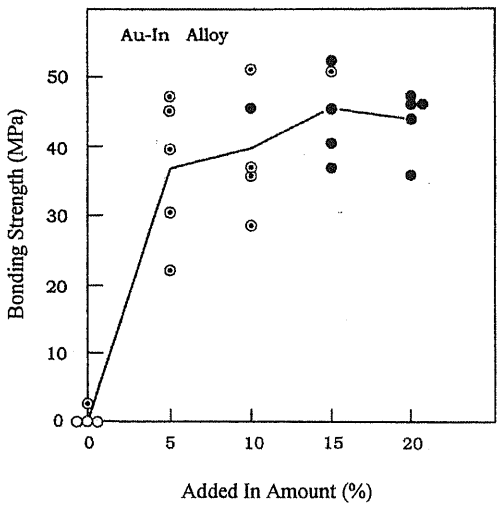


Fig. 5.1-2 Bonding strength versus In amounts with Au-In alloys.

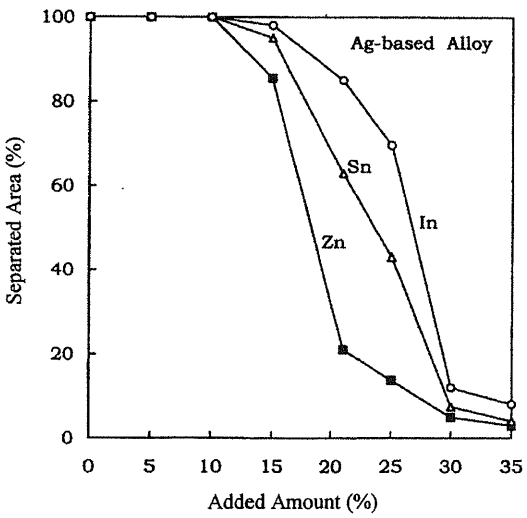


Fig. 5.1-3 Separated area (%) of Ag-based binary alloys containing In, Zn, or Sn.

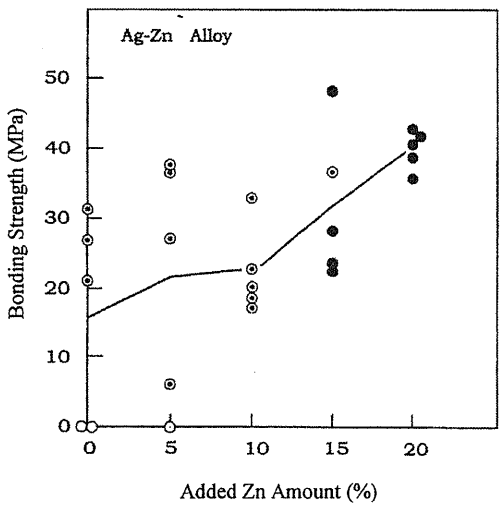


Fig. 5.1-4 Bonding strength versus Zn amounts with Ag-Zn alloys.

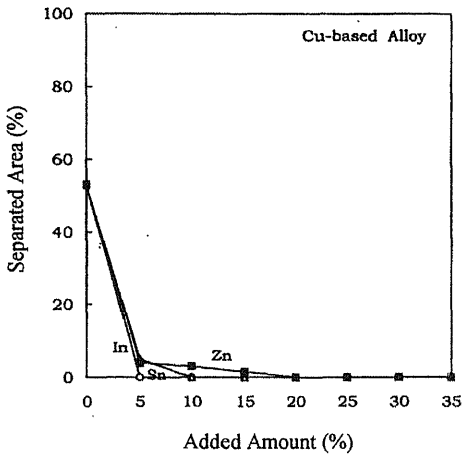


Fig. 5.1-5 Separated area (%) of Cu-based binary alloys containing In, Zn, or Sn.

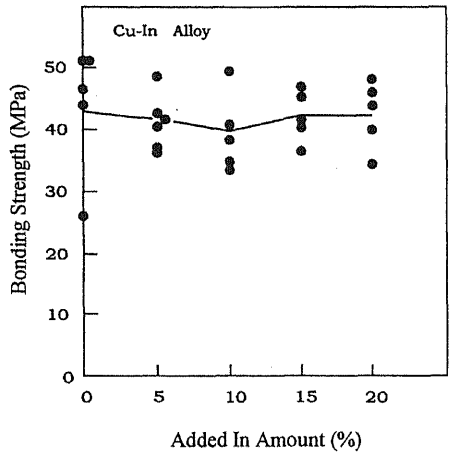


Fig. 5.1-6 Bonding strength versus In amounts with Cu-In alloys.

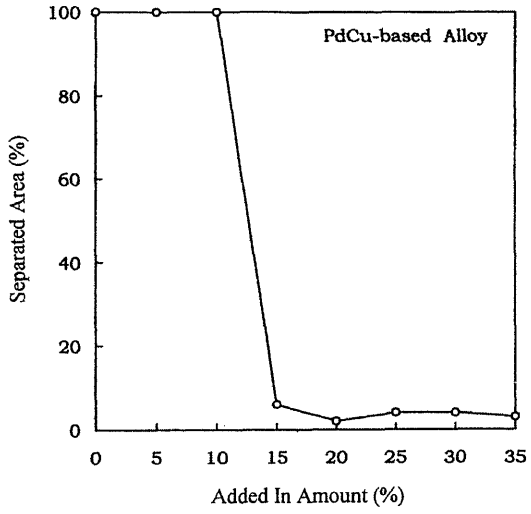


Fig. 5.1-7 Separated area (%) of PdCu based alloy containing In.

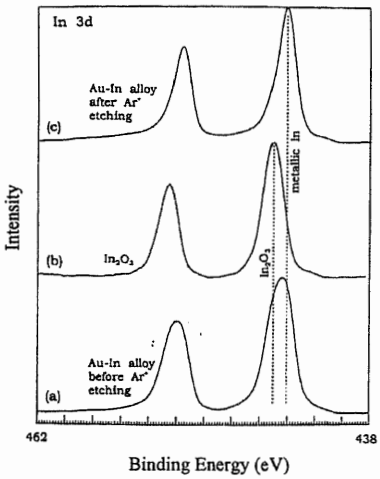


Fig. 5.1-8 In 3d spectra obtained from (a) as-polished Au-In alloy surface before argon ion etching, (b) $In_2O_3$, and (c) Au-In alloy surface after argon ion etching.

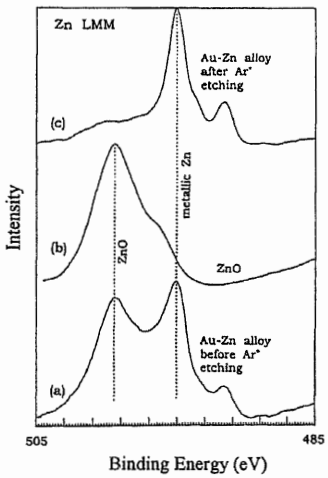


Fig. 5.1-9 Zn LMM auger spectra obtained from (a) as-polished Au-Zn alloy surface before argon ion etching, (b) ZnO, and (c) Au-Zn alloy surface after argon ion etching.

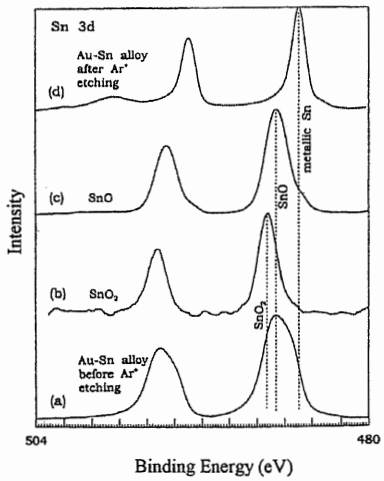


Fig. 5.1-10 Sn 3d spectra obtained from (a) as-polished Au-Sn alloy surface before argon ion etching, (b) $SnO_2$, (c) SnO, and (d) Au-Sn alloy surface after argon ion etching.

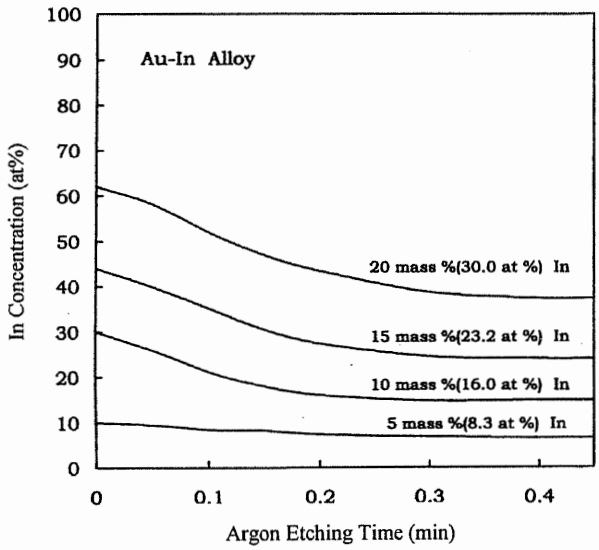


Fig. 5.1-11 Concentration variations of In in the depth direction for 95Au-5In (mass%), 90Au-10In, 85Au-15In, and 80Au-20In alloys.

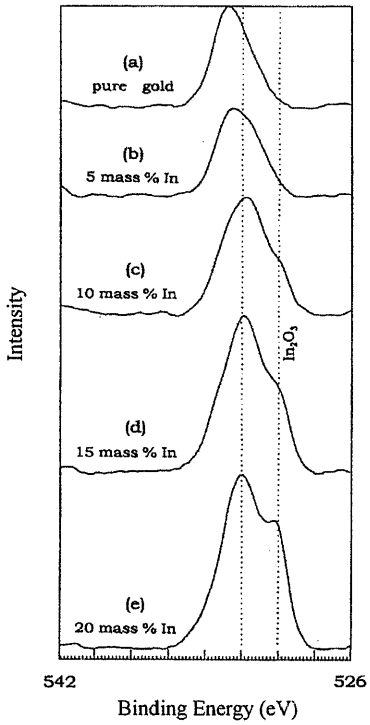


Fig. 5.1-12 O 1s spectra from the surface, without argon ion etching, pure gold and Au-based binary alloys containing 5, 10, 15, and 20 mass% In.

Table 5.1-1 Compositions (mass%) of experimental alloys for resin bonding and water durability at the adhesion interface (Separated Area (%)).

| Alloy No. | Au | Pd | Ag | Cu | In | Zn | Sn | Separated Area (%) |
|---|---|---|---|---|---|---|---|---|
| No. 1 | 58.0 | – | 10.0 | 12.0 | 20.0 | – | – | 0 |
| No. 2 | 61.4 | – | 7.2 | 13.3 | 16.1 | 2.0 | – | 0 |
| No. 3 | 65.8 | – | 7.7 | 14.2 | 10.6 | 1.7 | – | 0 |
| No. 4 | 65.0 | – | 8.0 | 15.0 | 5.0 | 2.0 | 5.0 | 0 |
| No. 5 | 70.0 | – | 8.0 | 15.0 | – | 2.0 | 5.0 | 0 |
| No. 6 | 75.0 | – | 8.8 | 16.2 | – | – | – | 100 |
| No. 7 | 77.0 | – | 5.0 | 15.0 | 3.0 | – | – | 0 |
| No. 8 | 9.8 | 16.3 | 44.7 | 8.1 | 7.7 | 13.0 | – | 0 |
| No. 9 | 10.3 | 17.2 | 47.3 | 11.2 | 4.6 | 9.4 | – | 0 |
| No.10 | 12.0 | 15.0 | 40.0 | 8.0 | – | 25.0 | – | 0 |
| No.11 | 12.0 | 20.0 | 55.0 | 13.0 | – | – | – | 100 |
| No.12 | 12.0 | 20.0 | 40.0 | 8.0 | – | 20.0 | – | 0 |
| No.13 | 12.0 | 20.0 | 45.0 | 15.0 | – | 8.0 | – | 25 |
| No.14 | 12.0 | 20.0 | 40.0 | 18.0 | 3.0 | – | 2.0 | 17 |
| No.15 | 12.0 | 20.0 | 45.0 | 18.0 | 3.0 | 2.0 | – | 24 |
| No.16 | 20.0 | 20.0 | 40.0 | 18.0 | 2.0 | – | – | 57 |

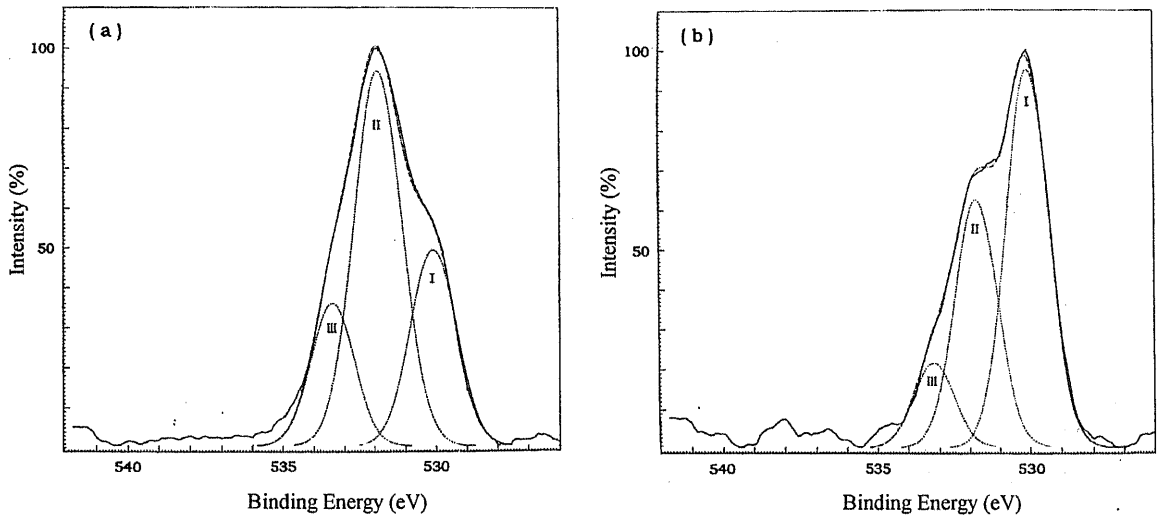


Fig. 5.1-13 (a): Separated O 1s spectra obtained from Au-15In (mass%) alloy without argon ion etching in (b): Separated O 1s spectra obtained from Au-15In alloy after argon ion etching for 0.05 min.

Table 5.1-2 Binding energy (eV) and area fraction (%) of oxygen chemical states.

| | argon ion etching | oxygen chemical states | | |
|---|---|---|---|---|
| | | I ($In_2O_3$) | II | III |
| pure gold | without | – | 532.1 eV (34%) | 533.6 eV (66%) |
| 85Au-15In alloy | without | 530.1 eV (27%) | 531.9 eV (55%) | 533.4 eV (18%) |
| 85Au-15In alloy | with | 530.1 eV (54%) | 531.8 eV (35%) | 533.2 eV (11%) |

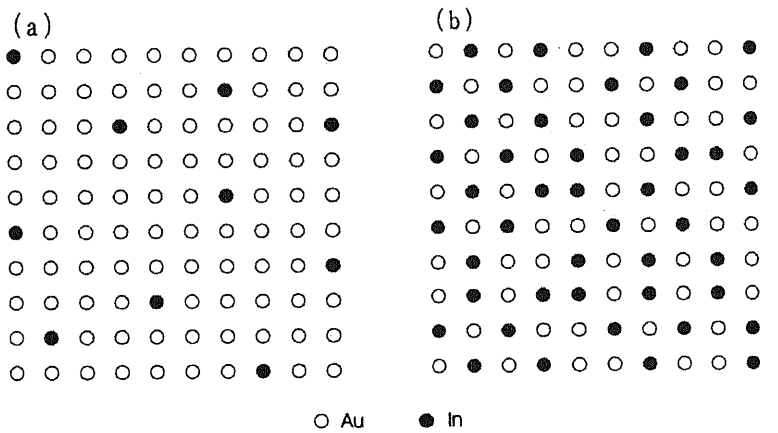


Fig. 5.1-14 Atomic distribution of Au (white) and In (black), from the quantitative analysis in Fig. 5.1-11; (a) Au-5In (mass%) alloy with poor adhesive ability and (b) Au-15In (mass%) alloy with excellent adhesive ability.

# Chapter 6

# NEW MECHANICAL RETENTION METHOD FOR RESIN AND GOLD ALLOY BONDING

## 6.1 New Mechanical Retention Method for Resin and Gold Alloy Bonding

### 6.1-1 Introduction

Adhesion of a resin containing 4-META to base metal alloys is relatively good. However, bonding of resins to dental precious metal alloys is inadequate because of the low chemical affinity of 4-META to precious metals. Several surface modification methods have been developed for improving precious metal alloy-resin bonding, such as high-temperature oxidation[1)], electroplating with tin[2)], silane-coating[3)], ion-coating[4)], priming with an adhesive bonding promoter (metal primer)[5)], and application of a liquid 75 mass%Ga-25%Sn alloy (Adlloy)[6)]. Before surface modification by these methods, the precious metal alloys were usually subjected to sandblasting with aluminum oxide to increase the surface area for adhesion and to enhance the mechanical retention of the resin[1-5)]. Creation of a porous structure on a precious metal alloy surface before surface modification for enhancing chemical bonding appears to be effective for increasing mechanical retention and establishing an excellent adhesion interface.

In dental precious metal alloys containing Cu, external and internal oxidation zones composed of Cu oxides, CuO and/or $Cu_2O$, were formed on the alloy surface with heating at a high temperature in air[7)]. A sponge-like structure was formed on the alloy surface after removing the internal oxidation particles with an acid solution. It was thought that this sponge-like structure would enhance mechanical bonding. However, there have been no reports of any previous attempts to improve adhesion between dental adhesive resins and gold alloys by creating a sponge-like structure on the alloy surface. In the present study, we investigated the bonding of 4-META resins to a porous 14K gold alloy surface created by high-temperature oxidation treatment and subsequent pickling. The effect of surface modification using an adhesive metal primer on the bonding strength of 4-META resin to the porous alloy surface was also examined.

### 6.1-2 Materials and Methods

*Materials*

A 14K gold alloy containing 59 mass%Au, 3%Pd, 14%Ag, and 24%Cu was used in the present experiments. The metals, more than 99.99% pure, were weighed to give a 100-g alloy sample and then melted in an argon atmosphere. The melting was done in an alumina crucible covered with a graphite tube using a high-frequency induction furnace. Weight loss during melting was less than 0.01%.

Two types of resin were used for bonding in order to examine the effects of mechanical and chemical factors on bonding strength. One was a 4-META resin, which is used clinically as a dental adhesive resin. The other was an experimental self-cured resin without 4-META, which was prepared by combining a PMMA powder provided with the 4-META resin product with a MMA liquid supplied with a commercial self-cured resin product (Unifast Ⅱ, GC, Tokyo, Japan). A thiophosphate-type metal primer (M-Primer Ⅱ, GC, Tokyo, Japan ) as shown in Fig. 6.1-1, which has been found to be effective in enhancing adhesion of resin to a gold-rich metal surface[8-9)], was used in combination with 4-META resin to strengthen the

chemical bonding between 4-META resin and the porous alloy surface.

*Analysis of High-temperature Oxidation Zone, Pickled Alloy Surface, and Resin Impregnation in the Sponge-like Structure*

The alloys were cast in 3 mm×3 mm×10 mm ingots to prepare specimens for morphological observations and X-ray microanalysis of the oxidation zones. The cast specimens were polished metallographically to a mirror-like finish using silicon carbide paper (#240, #400, and #600) followed by alumina paste (3 μm and 0.05 μm ), and then oxidized at 800℃ in air in a clean electric furnace for 60 min. The oxidized specimens were subsequently pickled in a thioglycolic acid solution to remove the external and internal oxides on the alloy surface, washed in an ultrasonic bath with distilled water, and dried in a current of air. The oxidized specimens were mounted with the use of a hard resin (Epomet, Buehler, Lake Bluff, IL) to prevent the edges from becoming rounded during polishing. For the pickled specimens, 4-META resin was first applied to the porous surface and then the specimens were mounted with the hard resin. The section perpendicular to the oxidized surface was polished metallographically as described previously. Impregnation of 4-META resin in the sponge-like structure was confirmed by Laser-Raman spectroscopy. Raman spectra were obtained using a Raman spectrophotometer (NR-1800, JASCO, Tokyo, Japan) equipped with a charge-coupled device detector (CCD). The excitation wavelength of 514.5 nm was obtained from an Ar ion laser (Innova 70 spectrum, Coherent, Santa Clara, USA). The laser power delivered at the specimen point was no more than 20 mW.

A 30-40 nm carbon film was deposited on the polished alloy surface to provide electrical conductivity for observation by scanning electron microscope (SEM) and an electron probe X-ray micro-analyzer (X-650, Hitachi, Tokyo, Japan).

Since Cu in the gold alloy becomes an oxide with high-temperature oxidation, the surface changes to a more precious metal rich-composition. The alloy surface of the pickled specimens was analyzed by ESCA as described in section 2.2.

*Measurement of Bonding Strength*

The gold alloy was cast into cylindrical specimens, 11 mm in diameter and 6 mm in height. The alloy surface was metallographically polished as described previously to eliminate the possibility of initial mechanical factors affecting the bonding strength, and then oxidized, pickled, and washed as described previously. Alloy specimens for bonding strength measurements were cast in the same size as the stainless steel disk (Fig. 2.1-1). The U-shaped piece was applied to the groove in the stainless steel rod for the testing. An adhesion apparatus equipped with a micrometer (Fig. 2.1-2) was used to attach a 5-mm diameter stainless steel rod vertically to the alloy surface and to maintain a constant 50-μm-thick layer of 4-META resin[11]. The effect of excess resin in the adhesion area on bonding strength was eliminated by attaching Scotch Tape (3M, USA) with a hole of 5 mm in diameter on the alloy surface. A tensile bonding strength test was carried out after keeping the specimen at 37°C in a dry condition for 24 hr. A testing

machine (Auto-Graph, Shimadzu, Kyoto, Japan) with a crosshead speed of 2 mm/min was used for the tensile bond tests[11]. Measurements were carried out individually on 10 specimens under each set of conditions. The bonding strengths were analyzed by one-way ANOVA and Fisher' PLSD test at the 0.05 level of significance.

Bonding strength measurements were carried out to determine the effects of three factors (mechanical, chemical, and mechanical plus chemical) on adhesion between the alloy and resin. The effect of mechanical and chemical contributions to bonding strength was examined by bonding a stainless steel rod with 4-META resin to the sponge-like gold alloy surface structure after applying the M-Primer Ⅱ. The mechanical component of the bonding was examined by applying the experimental self-cured resin without 4-META to the sponge-like alloy surface structure and then bonding a stainless steel rod with 4-META resin immediately after application of the experimental self-cured resin on the alloy surface. The effect of the porous surface structure on the bonding strength of 4-META resin was examined using the alloy specimen with flat surface. The flat surface specimen with identical alloy composition to the porous alloy specimen was made as follows; the washed and dried alloy surface after pickling was pressed with a glass plate under a load of 2,000 kg to make a flat surface. Next, the pressed alloy surface was slightly polished by hand using a polishing cloth with alumina slurry (0.05 μm) to make a mirror-like finish of the alloy surface, and the specimen was then washed with distilled water and dried in a current of air. A stainless steel rod was then bonded with 4-META resin on the flat alloy surface after applying the M-Primer Ⅱ.

### 6.1-3 Results

*Analysis of High-temperature Oxidation Zone, Pickled Alloy Surface, and Resin Impregnation in the Sponge-like Structure*

The images shown in Fig. 6.1-2 are a secondary electron image (a) and characteristic X-ray images of Au Lα (b) and Cu Kα (c) perpendicular to the oxidized surface obtained from the 14K gold alloy containing only Cu as a base metal, after oxidizing at 800°C in air for 60 min. The X-ray images showed that an external oxidation zone was formed on the alloy surface and that internal oxidation particles composed of copper oxide precipitated in the alloy matrix from the alloy surface to 30 μm in depth. Each internal oxidation particle was isolated two-dimensionally, but actually the particles were connected three-dimensionally with the external oxidation zone, as described in the next paragraph.

The images shown in Fig. 6.1-3 are a secondary electron image (a) and X-ray images of Au Lα (b) and Cu Kα (c) obtained from a specimen treated by oxidation and then pickling perpendicular to the alloy surface. The X-ray image of Cu Kα (c) shows that the external and internal oxidation particles were almost completely removed with pickling and that the alloy matrix near the alloy surface was depleted in Cu. The results of ESCA analysis revealed that the surface composition of the gold alloy after high-temperature oxidation followed by pickling changed from 59 mass%Au-3%Pd-14%Ag- 24%Cu to 88.4%Au-2.2%Pd-8.7%Ag-0.7%Cu. Figure 6.1-4 shows a secondary electron images obtained from the surface after pickling, oxidized at 800°C in air for 1 hr (a) and 10 hrs (b). The pore size of the specimen

heated for 10 hours was larger than that of the specimen heated for one hour. If the resin was able to impregnate into the sponge-like structure, stronger mechanical bonding could be expected.

The images shown in Fig. 6.1-5 are a secondary electron image (a) and X-ray image of C Kα (b) obtained from a pickled 14K gold alloy specimen bonded with 4-META resin. The X-ray image shows that the resin has impregnated the internal oxidation pores. Figure 6.1-6 shows Raman spectra obtained from the filling in the internal oxidation pore and a poly methylmethacrylate (PMMA) plate. The laser-irradiated area of the alloy specimen was shown in a CCD image inserted in Fig. 6.1-6. Both spectra exhibited a peak at 2,955 $cm^{-1}$ due to C-H stretching, indicating that the internal pore was filled with applied 4-META resin (95%PMMA, 5%4-META). Figure 6.1-7 shows a secondary electron image of the resin side of the resin-alloy bond structure after the alloy substrate had been removed with aqua regia. Many fine resin tags can be seen in this SEM image, showing that the resin had penetrated into the pores that had formed on the alloy surface after pickling.

*Measurement of Bonding Strength*

Figure 6.1-8 shows the tensile bonding strength of resins to the alloy specimens with porous and flat surfaces. The bonding strengths of the self-cured resin without 4-META to the porous specimens ranged from 14 MPa to 24 MPa (19±1 (mean±SD) MPa). SEM examination indicated that partial interfacial failure had occurred, but resin remained in the pores on the alloy surface. The bonding strength of 4-META resin to the flat specimen applied with M-Primer Ⅱ was 24±2 MPa. SEM examination revealed a mixed mode fracture in this case, with partial interfacial failure on the alloy surface and cohesive failure in the 4-META resin. The mean bonding strength of 4-META resin to the porous specimens applied with M-Primer Ⅱ was 38±3 MPa, with totally cohesive failure in the 4-META resin observed by SEM. As shown in Fig. 6.1-8, statistical analysis demonstrated that the bonding strength of 4-META resin to the porous specimen was significantly higher than that of 4-META resin to the flat specimen ($*p<0.05$), indicating that the porous structure created by the high-temperature oxidation and the subsequent pickling was effective for increasing bonding strength when the adhesive resin containing 4-META was used in combination with M-Primer Ⅱ.

## 6.1-4 Discussion

*Formation of a Sponge-like Structure on the Alloy Surface*

It was previously shown from characteristic X-ray images and state analysis by an electron probe microanalysis that the oxidation zone of a dental 14K gold alloy containing Cu, which forms after high-temperature oxidation by heating at 800°C in air, that the external oxidation zone was composed of two copper oxide layers, an outer layer of CuO and an inner layer of $Cu_2O$, and the internal oxide particles were composed of only $Cu_2O$[7].

Oxygen must be appreciably soluble in an alloy for the internal oxidation of an alloying element[12]. In a gold alloy, the solubility of oxygen is very small, and the gold alloys used in the present study did not satisfy this condition for internal oxidation. However, oxide precipitation has been observed at the grain

boundaries in gold alloys. As shown in Fig. 6.1-9, the oxide formed along the grain boundaries acts as a diffusion path that permits the penetration of $O^{2-}$ into the bulk alloy matrix, resulting in internal oxidation predominantly along the grain boundaries[13-14].

The morphology of the internal oxidation zone of the dental gold alloys was found in these previous studies to change markedly according to the kind of base metals in the composition: Ni, In, or Cr with Cu. The external oxidation zone and internal oxidation particles composed of copper oxide in the present 14K gold alloy were removed by pickling in a thioglycolic acid solution, resulting in the formation of a porous alloy surface. However, NiO, $In_2O_3$, and $Cr_2O_3$ with Cu oxide in the internal oxidation zone could not be removed from other oxidized gold alloys by pickling, and remained in the alloy matrix near the surface because the internal oxides were well-developed and fine needle-like in shape[15]. This suggests that a gold alloy containing only Cu as a base metal is a suitable alloy for forming interconnected internal oxide deposits, resulting in the formation of a sponge-like structure on the oxidized alloy surface after pickling.

The shape and distribution of the internal oxidation particles depend not only on the kind and amount of base metals but also on various other factors, including oxidation temperature, heating time, oxygen pressure, grain size of the alloy, and extent of grain growth during heat treatment. The oxidation process of dental gold alloys in air follows a parabolic law[7]. It was found that with increasing Cu content in a 14K gold alloy, the internal oxidation zone became well developed on the alloy surface[16]. However, the resistance of the 14K gold alloy to corrosion and tarnish decreased with increased Cu content[17]. The optimal Cu content should be further addressed to develop a 14K gold alloy for resin bonding, which forms a sponge-like structure on the surface without reducing the corrosion and tarnish resistance. Although grain-refining elements, Ir or Rh, are generally incorporated in commercial dental gold casting alloys, these elements were not added to the 14K gold alloy used in the present study. As adding these elements affects the sponge-like structure on the alloy surface, it is necessary to continue further research on the effects of these elements.

*Effect of a Sponge-like Structure on the Alloy Surface on Bonding Strength*

Bonding strength refers to the force required for separating two parts, and it consists of two factors: mechanical bonding and chemical adhesion. Mechanical bonding is an anchoring effect that is related to the surface roughness of the alloy surface. Therefore, both mechanical and chemical factors are essential to create stable bonding. Since the chemical affinity of 4-META was high enough to base metal alloys but it was quite low to gold-rich alloys, in the present study a thiophosphate-type metal primer (M-Primer Ⅱ) was applied to the pickled alloy surface in order to enhance the chemical adhesion. The bonding strength of 4-META resin to the porous 14K gold alloy surface treatment with M-primer Ⅱ was 38±3 (mean±SD) MPa, which was much higher than that of 4-META resin to the surfaces of gold alloys after high-temperature oxidation treatment (25 MPa)[1] and to the surface of Sn ion-sputtered type Ⅳ gold alloy (21-27MPa)[4].

Joints of dental adhesive resin bonded to dental alloys weaken in wet environments, though adhesion

is strong in dry environments[18-20]. One example is the separation or peeling that occurs after long-term use in the oral environment. When the water molecules have destroyed the chemical bond, the bonding strength is lowered to a level that is sustained by the mechanical retention. As mechanical bonding would play an important role in maintenance of the bond structure in this situation, increased mechanical retention is essential for durability of the adhesion interface. It is speculated from the results shown in Fig. 6.1-8 that the pores formed by dissolution of the internal oxidation particles are effective for increasing mechanical retention and establishing a reliable bonding.

## REFERENCES

1) Tanaka T, Nagata K, Takeyama M, Nakabayashi N, Masuhara E. Heat treatment of gold alloy to get adhesion with resin. *J Jpn Soc Dent Apparat Mater*, **21**: 95-102, 1980 (in Japanese).

2) Yamashita A, Kondo Y, Fujita M. Adhesive strength of adhesive resin PANAVIA EX to dental alloys. *J Jpn Prosthodont Soc*, **28**: 1023-1033, 1984 (in Japanese).

3) Musil R. Clinical verification of the silicoater technique. Results of three-years' experience. *Dent Lab*, **35**: 1709-1715, 1987.

4) Tanaka T, Hirano M, Matsumura H, Atsuta M. A new ion-coating surface treatment of alloys for dental adhesive resins. *J Dent Res*, **67**: 1376-1380, 1988 .

5) Atsuta M, Matsumura H, Tanaka T. Bonding fixed prosthodontic composite resin and precious metal alloys with the use of a vinyl-thiol primer and an adhesive opaque resin. *J Prosthodont Dent*, **67**: 296-300, 1992.

6) Ohno H, Araki Y, Endo K. A new method for promoting adhesion between precious metal alloys and dental adhesives. *J Dent Res*, **71**: 1326-1331, 1992.

7) Ohno H. Studies on high-temperature oxidation of precious metal alloys for dental use (Part I ). *J Jpn Soc Dent Apparat Mater*, **17**: 297-312, 1976 (in Japanese).

8) Imai Y. New modification methods of metals for resin bonding. *Hotetsu Rinsho*, **Special Issue**: 265-267, 1991 (in Japanese).

9) Ohno H, Yamane Y, Endo K, Araki Y, Kawashima I. Evaluation of water durability at adhesion interfaces between 4-META resin and precious metal alloys modified with two adhesive metal primers. *J Jpn Soc Dent Product*, **11**: 35-41, 1996 (in Japanese).

10) Ohno H, Endo K, Tanabe M. Quantitative analysis of extremely small samples by ESCA. *Shimadzu Rev*, **47**: 97-101, 1990 (in Japanese).

11) Ohno H, Araki Y, Sagara M. The adhesion mechanism of dental adhesive resin to the alloy. *Dent Mater J*, **5**: 46-65, 1986.

12) Meijering JL. Internal oxidation in alloys. *Adv Mater Res*, **5**: 1-81, 1971.

13) Ohno H, Miyakawa O, Watanabe K, Shiokawa N. The structure of oxide formed by high-temperature oxidation of commercial gold alloys for porcelain-metal bonding. *J Dent Res*, **61**: 1255-1261, 1982.

14) Ohno H, Kanzawa Y. Internal oxidation in gold alloys containing small amounts of Fe and Sn. *J Mater*

*Sci*, **18**: 919-929, 1983.

15) Sagara M, Ohno H. Gold alloys for resin bonding including small amounts of base metals – Structural changes of alloy surface by the high-temperature oxidation. *Dent Mater J*, **18**: 366-384, 1999.

16) Ohno H, Endo K, Araki Y, Kawashima I, Yamane Y, Zheng JH, Xu ST. Strengthen of adhesive ability between resin and precious metal alloys by internal oxidation - Effects of adding base metals on sponge-like structure. *J J Soc Dent Mater*, **19** (Special issure): 129, 2000 (in Japanese).

17) Lang BR, Bernier SH, Giday Z, Asgar K. Tarnish and corrosion of precious metal alloys. *J Prosthodont Dent*, **48**: 245-252, 1982.

18) Brewis DM, Comyn J, Tegg JL. The durability of some epoxide adhesive-bonded joints on exposure to moist warm air. *Int J Adhe Adhe*, **1**: 35-39, 1980.

19) Ko CU, Wightman JP. Experimental analysis of moisture intrusion into the Al/Li-polysulfone interface. *J Adhe*, **25**: 23-29, 1988.

20) Ohno H, Endo K, Araki Y, Asakura S. Destruction of metal-resin adhesion due to water penetrating through the resin. *J Mater Sci*, **27**: 5149-5153, 1992.

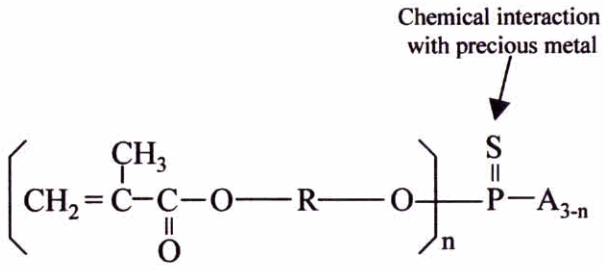


Fig. 6.1-1 Thiophosphate-type metal primer (M-Primer)

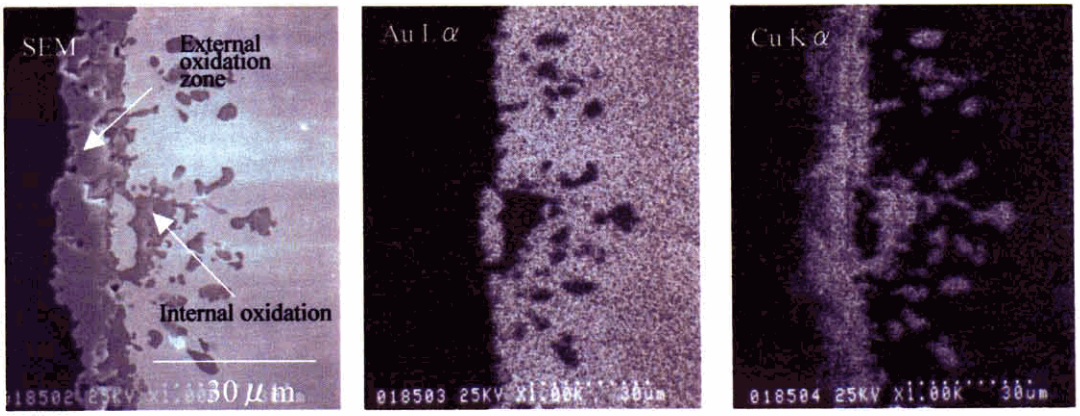


Fig. 6.1-2 Secondary electron image (a) and characteristic X-ray images of Au L $\alpha$ (b) and Cu K $\alpha$ (c), obtained from a 14K gold alloy specimen after oxidizing at 800℃ in air for 60 min, perpendicular to the oxidized surface.


Fig. 6.1-3 Secondary electron image (a) and X-ray images of Au L $\alpha$ (b) and Cu K $\alpha$ (c) obtained from a specimen treated by oxidation and pickling.

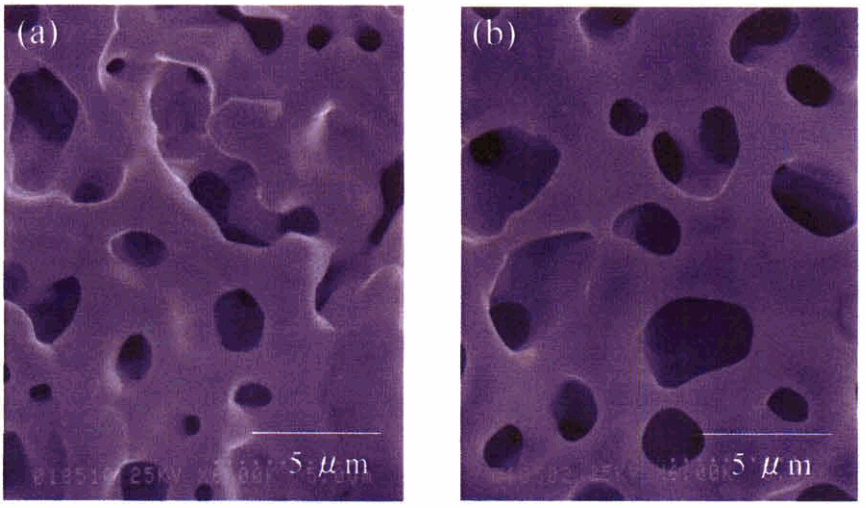


Fig.6.1-4 Secondary electron image obtained from the surface after pickling, oxidized at 800℃ in air for 1 hr (a) and for 10 hrs (b).

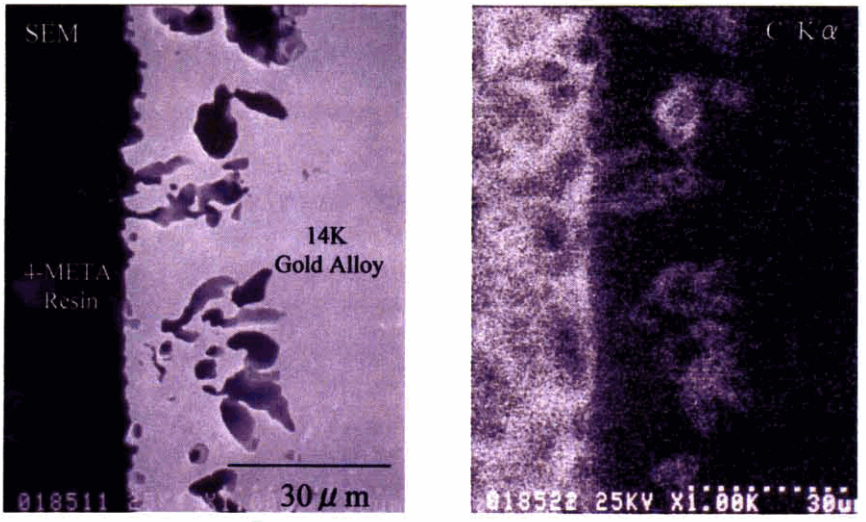


Fig. 6.1-5 Secondary electron image (a) and X-ray image of C K $\alpha$ (b) obtained from a specimen treated by oxidation and pickling followed by bonding with 4-META resin;

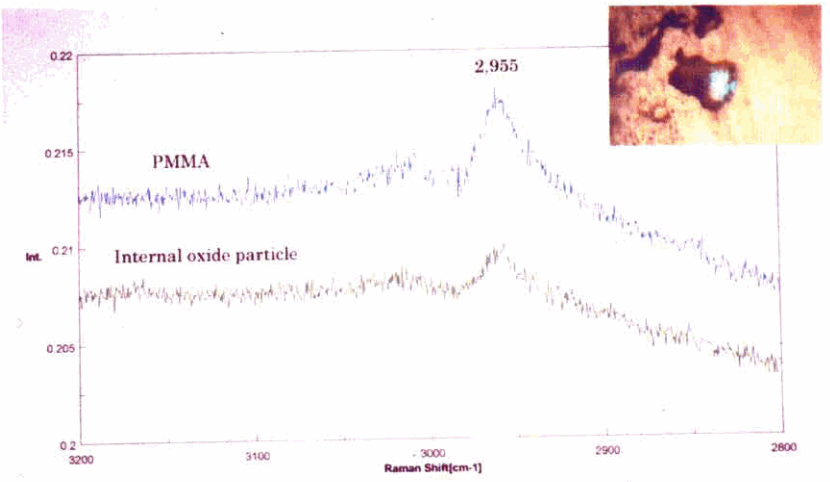


Fig. 6.1-6 Raman spectra obtained from the filling in the internal oxidation pore and a polymethylmethacrylate (PMMA) plate.

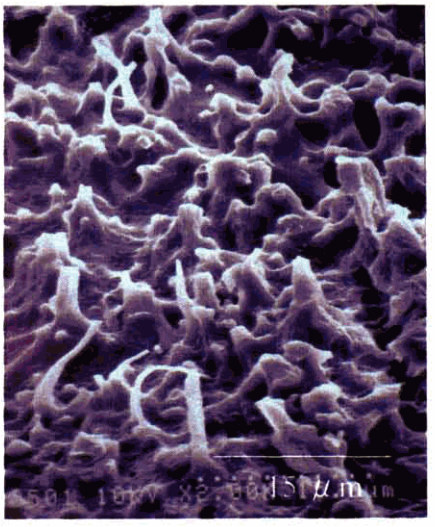

Fig. 6.1-7 Secondary electron image obtained from the resin side of the resin-alloy bond structure after removal the alloy substrate with aqua regia.

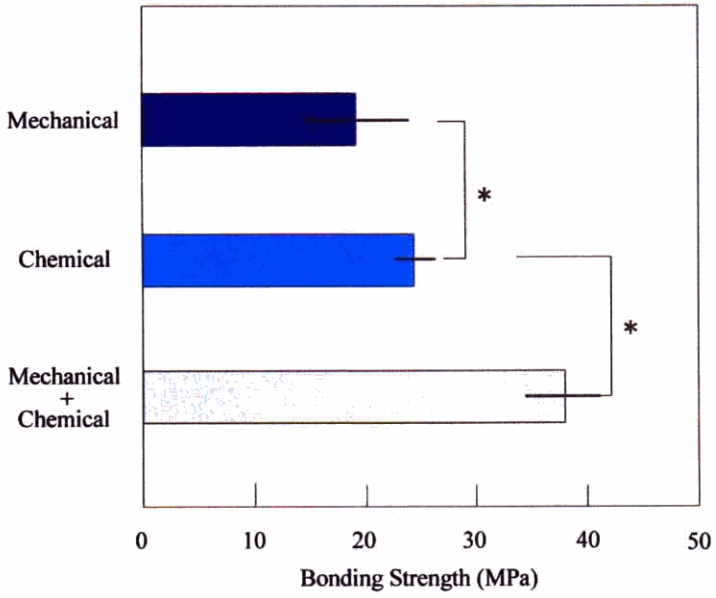


Fig. 6.1-8 Tensile bonding strength of self-curing resins to the alloy specimens with porous and flat surfaces. Each column represents mean ±SD (10 specimens per each group). The stared groups (*) indicate significant differences between the groups ($p < 0.05$ by one way ANOVA).

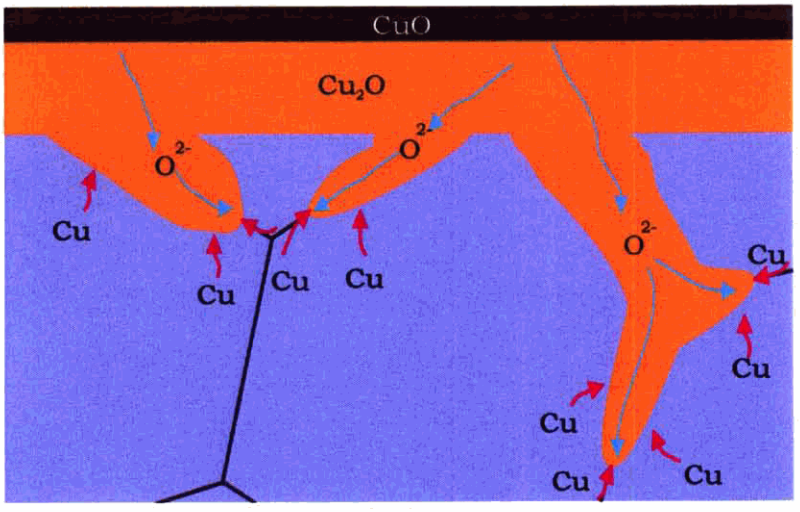


Fig. 6.1-9 Mechanism of formation of a porous structure on alloy surface by high-temperature oxidation.

# Chapter 7

# CONCLUSIONS

# CONCLUSIONS

In 1978, a dental adhesive containing 4-META was developed to meet several requirements: strong bonding to tooth substances and dental materials, simple handling procedures, insolubility in saliva, no deterioration at the adhesion interface under oral humid conditions, and non-toxicity to and no harmful effects on the human body. In this dissertation, the results of experiments on adhesion of dental alloys and 4-META dental adhesive resin with respect to the surface structures of alloys as adherend were presented and discussed.

The results of experiments on the bonding ability of 4-META resin to base metals such as Co-Cr, Ni-Cr, and 18-8 stainless steel were presented in chapter 2. Bonding ability was evaluated by bonding strength measurements and observations of the fracture appearance. The 4-META resin showed comparatively good adhesion to as-polished alloys covered with passive films. The bonding strength of 4-META resin to as-polished alloy surfaces was found to be greater than that to oxidized surfaces heated at 300°C or 500°C. Thermal cycles that used liquid nitrogen showed clear differences in the alloy surface states affecting the adhesion.

The relationships between the bonding strengths and the alloy surface structures analyzed by ESCA and reflection electron diffraction were discussed. The structure of the as-polished Co-Cr alloy surface was an amorphous 2-3 nm thick passive film made of a monolayer of six –OH and/or $H_2O$ coordinated around $Cr^{3+}$ and $Co^{2+}$ or $Co^{3+}$ metal ions. On the alloy surfaces oxidized at 300°C and 500°C, $Co_3O_4$ was predominantly formed with a several-molecule-thick layer of adsorbed water at the top of the oxide surface. The presence of the water molecules was thought to be the reason why adhesion to surfaces oxidized at high temperatures was inferior to that of the as-polished surfaces. This speculation was supported by the results of an experiment in which the several-molecule-thick layer of adsorbed water on the oxidized surface was removed.

On the as-polished surfaces, the adhesive ability of a Ni-Cr alloy was inferior to that of a Co-Cr alloy. Treatment of the as-polished Ni-Cr alloy surface with concentrated $HNO_3$ solution resulted in excellent adhesion, comparable to that of the Co-Cr alloy, and adhesion was maintained even after thermal cycling. Both as-polished and $HNO_3$-treated Ni-Cr alloys were analyzed by ESCA to determine the reason for the superior adhesive ability of the alloy surface treated with $HNO_3$ solution. The Ni content on the alloy surface was decreased by elution of Ni to the $HNO_3$ solution. As a result of Ni elution, Cr that has good chemical affinity to 4-META resin, concentrated on the alloy surface.

Water durability at the adhesion interface is critically important for adhesive structures used in humid environments like the oral cavity because environmental water and humidity influence the mechanical properties of the adhesive joints. Chapter 3 discussed a basic study on degradation due to water at the adhesion interface carried out to determine the mechanism of degradation of adhesion between mild steel and 4-META dental adhesive resin. It was found that water entered the interface by diffusion through the resin layer. The water content at the interface was calculated by Fick's law of diffusion and it was possible

to evaluate the degradation with respect to the water content at the interface. The water induced corrosion of the mild steel that resulted in complete destruction of the adhesion interface. Electron diffraction and ESCA analysis demonstrated that FeO(OH) was formed at the adhesion interface after immersion for 2 days. The amount of hydroxide increased steadily and hydroxide finally changed to $Fe_2O_3$.

Evaluation of water durability at the adhesion interface was also discussed in chapter 3. Water durability at adhesion interfaces was investigated by measurement of the separated areas of thin resin films bonded with 4-META resin on metal surfaces after imposing thermal stress using liquid nitrogen. In the case of 18-8 stainless-steel specimens that bonded strongly with 4-META resin, total interface failure occurred in specimens with resin thicker than 0.55 mm in dry conditions. A resin layer of 0.25 mm was chosen to study degradation of the adhesion interface by water because a thin PMMA film was bonded on dental alloys to allow water saturation at the adhesion interface after a short immersion time. Thermal stress at the adhesion interface was calculated by a computer-aided finite element method. Shear stress was calculated to be 16 MPa for a 0.25-mm thick resin layer. When degradation of the adhesion interface occurred due to immersion in water, the thin resin film separated from the metal substrate due to thermal stress.

Water molecules rapidly degraded the mild-steel interface with 4-META resin. The relationship between water immersion time and degradation at the adhesion interface was examined together with the amount of water that penetrated though the resin to the interface. When the water content at the adhesion interface reached 48% of the equilibrium water concentration of PMMA, destruction occurred at the interface due to breakdown of chemical bonds between hydroxyl groups on the metal surface and side chains of 4-META. This may be the first report in which degradation of the adhesion interface based on the water content at the interface is discussed. The method used in the present study is useful for quick evaluation of water durability at the adhesion interface.

The water durability of the adhesion interface between 4-META resin and precious metal alloys was inadequate. Thus, a simple and easy method of surface modification to improve adhesion with a precious metal alloy was needed. Therefore a simple new method to promote adhesion between precious metal alloys and dental adhesives was developed (Japanese patent No. 63-153853 and US patent No. 5,049,076). The new method of modifying an adherend metal surface with a liquid Ga-Sn alloy was described in chapter 4. The liquid Ga-Sn alloy-modified gold alloys (Type IV and 14K) and silver-based alloys (Ag-Pd and Ag-Cu) showed not only high bonding strengths but also excellent water durability at the adhesion interface. Adhesion to the tin-electroplated specimens was comparable with that to the Ga-Sn alloy-modified specimens. Surface modification by the Ga-Sn alloy, however, did not affect adhesion to Ag-In-Zn and base metal alloys (SUS, Co-Cr, and Ni-Cr).

The reason why the modification was only effective with some precious metal alloys and not with Ag-In-Zn and base metal alloys was also discussed based on the results of analysis of the Ga-Sn alloy-modified surface by ESCA: a new alloying layer containing Ga and Sn was formed on the precious metal alloys. The main factor responsible for the excellent adhesion was the formation of a very thin layer

of $Ga_2O_3$ and $SnO_2$, less than 1-2 nm, on the alloy surface. A thicker modified layer, as formed on the Ag-In-Zn alloy, led to poor bonding ability. The Ga-Sn alloy was not alloyed with Ni-Cr alloy, resulting in poor bonding ability with 4-META resin.

In chapter 5, results of experiments using new dental precious metal alloys for resin bonding without alloy surface modification that had been developed by adding base metals (In, Zn, or Sn) were presented and discussed. Binary alloys of Au, Ag, Cu, or Pd containing In, Zn, or Sn were first studied for water durability and bonding strength with 4-META resin. The adhesion ability of the binary alloys was improved by adding In equivalent to 15% of Au content, Zn equivalent to 20% of Ag content, and In, Zn, or Sn equivalent to 5% of Cu content. There was no additional effect of the base metals on Pd, but addition of 15% In improved adhesion with Pd-based alloys containing equi-atomic percents of Cu and Pd. The alloy surfaces were analyzed by ESCA and it was found that oxides such as $In_2O_3$, ZnO, and SnO played an important role in improving the adhesive ability of the alloys. The reason for the improved adhesion of the Au-In alloy was investigated by ESCA. The O 1s spectrum could be separated into three oxygen chemical states, $In_2O_3$, chemisorbed $H_2O$, and physisorbed $H_2O$. The amount of chemisorbed $H_2O$ decreased markedly with the increase in the amount of In. It was thought that the poor adhesive ability of the pure gold and alloys containing only small amounts of In was due to the chemisorbed $H_2O$ molecules and insufficient indium oxide on the alloy surface. It was concluded that excellent adhesion requires coverage of at least 50% of the alloy surface with an oxide that has chemical affinity for 4-META.

We investigated the bonding of 4-META resins to a porous 14K gold alloy surface created by high-temperature oxidation treatment and subsequent pickling. The method, described in chapter 6, was to improve adhesion between dental adhesive resins and a 14K gold alloy by creating a sponge-like structure on the alloy surface that enhanced mechanical bonding (Japanese patent 2000-93436). The internal oxidation particles of Cu oxides precipitated on a 14K gold alloy surface after high-temperature oxidation at 800℃ in air were removed by pickling with an acid solution to create a sponge-like structure on the alloy surface. A PMMA resin containing 4-META as an adhesive monomer and a self-cured resin without 4-META were used to examine the effects of mechanical and chemical factors on bonding strength. A thiophosphate-type metal primer was used in combination with 4-META resin to strengthen the chemical bonding of 4-META resin to the porous alloy surface because 4-META has poor adhesive ability for precious metals. The surfaces of the alloy specimens treated by oxidation, pickling, and bonding with 4-META resin were analyzed using an electron probe X-ray microanalyzer. SEM observation showed many resin tags on the resin side of the bonding structure after removal of the gold alloy matrix with aqua regia. The bonding strength of 4-META resin to the porous alloy surface was $38 \pm 3$ (mean $\pm$ SD) MPa, whereas that to a flat alloy surface with the same composition was $19 \pm 1$ MPa. The bonding strength of a self-cured resin without 4-META to the porous alloy surface was $24 \pm 2$ MPa. A high bonding strength was obtained when 4-META resin was bonded to the porous 14K gold alloy that had been surface-treated with a thiophosphate-type metal primer.

There are two major problems to be solved, water and stress at the adhesion interface, in order to

establish a durable and stable adhesion structure. Water durability at the adhesion interface is critically important for adhesive structures used in humid environments such as the oral cavity because environmental water and humidity influence the mechanical properties of the adhesive joints. Stress introduced at the adhesion interface caused by polymerization shrinkage will cause separation of resin from the interface. When water molecules and/or stress at the interface have destroyed the chemical bond, the bonding strength is lowered to a level that is sustained by mechanical retention. Since mechanical bonding plays an important role in maintenance of the bond structure in this situation, increased mechanical retention is essential for durability of the adhesion interface. Use of monomers expanding on polymerization greatly reduces the stress induced at the interface. Although such monomers have already been synthesized, none of them can be used for dental applications due to toxic compounds contained in the monomers such as polymerization initiators. Development of a safe dental adhesive resin with less shrinkage on polymerization is needed.

## ACKNOWLDGMENTS

The author wishes to thank Profs. Kazuyoshi Sekine, Masaki Shiratori, Masao Tomoi, Hiroshi Fukutomi, Hideo Ohtani, and Assoc. Prof. Atsushi Chiba, Yokohama National University, for valuable suggestions and discussions and is also grateful to Assoc. Prof. Kazuhiko Endo, Health Sciences University of Hokkaido, and Prof. Yoshima Araki, Iwate Medical University, for their generous support as coworkers.

## REFERENCES

This dissertation was based on the original articles listed below:

(1) Ohno H, Araki Y, Sagara M: The adhesion mechanism of dental adhesive resin to the alloy - Relationship between Co-Cr alloy surface structure analyzed by ESCA and bonding strength of adhesive resin -. *Dent Mater J*, **5**: 46-65, 1986.

(2) Ohno H, Araki Y, Sagara M, Yamane Y: The adhesion mechanism of dental adhesive resin to the alloy - Experimental evidence of the deterioration of bonding ability due to adsorbed water on the oxide layer -. *Dent Mater J*, **5**: 211-216,1986.

(3) Ohno H, Araki Y, Endo K, Kawashima I: The adhesion mechanism of dental adhesive resin to the alloy - Adhesive ability of dental adhesive resin to the cleaned metal surface obtained by hydrogen gas reduction method -. *Dent Mater J*, **8**: 1-8, 1989.

(4) Ohno H, Araki Y, Endo K: A new method for promoting adhesion between precious metal alloys and dental adhesives. *J Dent Res*, **71**: 1326-1331, 1992.

(5) Ohno H, Araki Y, Endo K: ESCA study on dental alloy surfaces modified by Ga-Sn alloy. *J Dent Res*, **71**: 1332-1337, 1992.

(6) Ohno H, Endo K, Araki Y, Asakura S: Destruction of metal-resin adhesion due to water penetrating through the resin. *J Mater Sci*, **27**: 5149-5153, 1992.

(7) Ohno H, Endo K, Araki Y, Asakura S: ESCA study on the destruction mechanism of metal-resin

adhesion due to water penetrating through the resin. *J Mater Sci*, **28**: 3764-3768, 1993.

(8) Ohno H, Araki Y, Endo K, Yamane Y, Kawashima I: Evaluation of water durability at adhesion interface by peeling test of resin film. *Dent Mater J*, **15**: 183-192, 1996.

(9) Ohno H, Yamane Y, Endo K, Araki Y, Iizuka Y: Adhesion of adhesive resin to dental precious metal alloys (Part Ⅰ) New precious metal alloys with base metals for resin bonding. *Dent Mater J*, **17**: 275-284, 1998.

(10) Ohno H, Yamane Y, Endo K, Araki Y, Iizuka Y: Adhesion of adhesive resin to dental precious metal alloys (Part Ⅱ) The relationship between surface structure of Au-In alloys and adhesive ability with 4-META resin. *Dent Mater J*, **17**: 285-293, 1998.

(11) Ohno H, Endo K, Yamane Y, Kawashima I: XPS study on the weakest zone in the adhesion structure between resin containing 4-META and precious metal alloys treated with different surface modification methods. *Dent Mater J*, **20**: 90-102, 2001.

(12) Ohno H, Endo K, Hashimoto H: New mechanical retention method for resin and gold alloy bonding. *Dent Mater*, **20**: 330-337, 2004.

(13) Ohno H, Endo K, Haneda K, Tamura M, Hikita K: Mechanism by which porous structure is formed on the surface of gold alloy containing only Cu as base metal. *Dent Mater J*, **24**: 503-507, 2005.

This dissertation referred the original articles listed below:

(1) Ohno H, Ichikawa T, Shiokawa N, Ino S, Iwasaki H: ESCA study on the mechanism of adherence of metal to silica glass. *J Mater Sci*, **16**: 1381-1390, 1981.

(2) Ohno H, Miyakawa O, Watanabe K, Shiokawa N: The structure of oxide formed by high-temperature oxidation commercial of gold alloys for porcelain bonding. *J Dent Res*, **61**: 1255-1261,1982.

(3) Ohno H, Kanzawa Y, Yamane Y: ESCA study on the oxidized surface of a gold alloys for porcelain-metal bonding. *Dent Mater J*, **2**: 59-67,1983

(4) Ohno H, Kanzawa Y, Kawashima I, Shiokawa N: Structure of high-temperature oxidation zones of gold alloys for porcelain bonding containing small amounts of In and Sn. *J Dent Res*, **62**: 774-779, 1983.

(5) Ohno H, Kanzawa Y, Takanohashi S: State analysis of iron oxides formed on gold alloys for porcelain-metal bonding by an X-ray micro-analyzer. *Dent Mater J*, **2**: 179-191, 1983.

(6) Ohno H, Kanzawa Y: Internal oxidation in gold alloys containing small amounts of Fe and Sn. *J Mater Sci*, **18**: 919-929, 1983.

(7) Ohno H, Kanzawa Y, Kawashima I: Structural study of oxidation zones on the gold alloys for porcelain bonding containing small amounts of In and Fe. *Dent Mater J*, **3**: 36-48,1984.

(8) Ohno H, Kanzawa Y: Structural Changes in the Oxidation Zones of Gold Alloys for Porcelain Bonding Containing Small Amounts of Fe and Sn. *J Dent Res*, **64**: 67-73,1985.

(9) Ohno H, Araki Y, Endo K, Kawashima I, Yamane Y, Sagara M: Adhesive ability of a dental adhesive resin (4-META/MMA-TBB) to as-polished, $HNO_3$ treated, and oxidized surfaces of the Ni-Cr alloy. *Higashi Nippon Dent J*, **6**: 1-12,1987.

(10) Ohno H, Araki Y, Endo K, Matsuda K, Sakaguti K: ESCA study on improvements in adhesive ability of dental adhesive resin to Ni-Cr alloy treated by $HNO_3$ solution. *Higashi Nippon Dent J*, **6**: 13-22,1987.

(11) Ohno H: A new conversion method of metal surfaces for resin bonding - Conversion effects for pure metals in dental precious metal alloys-. *Dent in Jpn*, **27**: 101-108,1990.

(12) Ohno H, Yamane Y, Endo K, Araki Y, Kawashima I: Evaluation of water durability at adhesion interface between 4-META resin and precious metal alloys modified with two adhesive metal primers. *J Jpn Soc Dent Product*, **10**: 35-41, 1996.

(13) Kemas A Z T, Ohno H, Narita T, Ishikawa I: Determination of stress and distortion of a metal/resin composite using Scanning Acoustic Microscope. *Jpn Soc Non-destructive Inspection Conference*, **Mar 24-26**: 167-172,1996.

(14) Ohno H, Yamane Y, Endo K, Araki Y, Kawashima K: Evaluation of water durability at adhesion interfaces between 4-META resin and precious metal alloys modified with two adhesive metal primers. *J Jpn Soc Dent Product*, **10**: 35-41,1996.

(15) Sagara M, Ohno H: Gold Alloys for resin bonding small amount base metals -Structural changes of alloy surface by the high-temperature oxidation-. *Dent Mater J*, **18**: 366-384, 1999.

(16) Yamane Y, Ohno H, Endo K: Mechanism of adhesion between 4-META resin and alloys based on Bolger's acid-base interaction. *Dent Mater J*, **20**: 63-74, 2001.

(17) Haneda K, Ohno H, Endo K, Tamura M, Kawashima I: Effect of surface modification using an adhesive metal primer on the bond strength of 4-META resin to a porous gold alloy surface. *J Jpn Soc Dent Product*, **19**: 31-37, 2005.